SECURITY CLASSIFICATION OF THIS PAGE *(When Data Entered)*

REPORT DOCUMENTATION PAGE

READ INSTRUCTIONS BEFORE COMPLETING FORM

1. REPORT NUMBER: AFWAL-TR-84-3066	2. GOVT ACCESSION NO.
3. RECIPIENT'S CATALOG NUMBER	
4. TITLE *(and Subtitle)*: INITIAL QUALITY OF ADVANCED JOINING CONCEPTS	5. TYPE OF REPORT & PERIOD COVERED: Final Report, June 1980 - December 1983
	6. PERFORMING ORG. REPORT NUMBER
7. AUTHOR(s): W.R. GARVER, D.Y. LEE, and K.M. KOEPSEL	8. CONTRACT OR GRANT NUMBER(s): F33615-80C-3226
9. PERFORMING ORGANIZATION NAME AND ADDRESS: General Dynamics/Fort Worth Division, P.O. Box 748, Ft. Worth, TX 76101	10. PROGRAM ELEMENT, PROJECT, TASK AREA & WORK UNIT NUMBERS: P.E. 62201F, 24010145
11. CONTROLLING OFFICE NAME AND ADDRESS: Flight Dynamics Laboratory (FIBE), Air Force Wright Aeronautical Laboratories, Wright-Patterson AFB OH 45433	12. REPORT DATE: 12 December 1984
	13. NUMBER OF PAGES: 161
14. MONITORING AGENCY NAME & ADDRESS *(if different from Controlling Office)*	15. SECURITY CLASS. *(of this report)*: Unclassified
	15a. DECLASSIFICATION/DOWNGRADING SCHEDULE

16. DISTRIBUTION STATEMENT *(of this Report)*

Approval for public release; distribution unlimited.

17. DISTRIBUTION STATEMENT *(of the abstract entered in Block 20, if different from Report)*

18. SUPPLEMENTARY NOTES

19. KEY WORDS *(Continue on reverse side if necessary and identify by block number)*

Initial Quality, Adhesive Bonding, Casting, Joining, Fatigue, Fractography, Spectrum Loading, Equivalent Initial Flaw Size, A357 Aluminum

20. ABSTRACT *(Continue on reverse side if necessary and identify by block number)*

The initial fatigue quality of three types of aircraft construction were studied. The three types included conventional mechanically-fastened joints, adhesively-bonded joints, and monolithic aluminum castings. The objectives are to obtain data for setting initial flaw assumptions for U.S. Air Force damage tolerance specifications, and to develop a methodology for comparing the relative merit of competing structural concepts. Two hundred test elements representing these joining concepts were prepared and tested under realistic

DD FORM 1 JAN 73 1473 EDITION OF 1 NOV 65 IS OBSOLETE

UNCLASSIFIED

SECURITY CLASSIFICATION OF THIS PAGE *(When Data Entered)*

20. Abstract (cont)

spectrum load histories. Nondestructive inspections were performed on all specimens, but no correlation to crack growth performance was found. Crack growth data were obtained by fractographic examination and analyzed using the equivalent initial flaw size (EIFS) concept. Statistical distributions, representing the variation in EIFS and in crack growth rate, were obtained. Adhesively-bonded structure was found to give the best overall combination of benefits. The scatter in crack growth was highest in castings, which limits reliability at high stresses. An improved methodology was developed for comparing structural performance and efficiency. The methods include consideration of initial material and manufacturing quality, and can be used to quantify reliability at any confidence level and service time.

AFWAL-TR-84-3066

INITIAL QUALITY OF ADVANCED JOINING CONCEPTS

W. R. GARVER, D. Y. LEE, and K. M. KOEPSEL
GENERAL DYNAMICS/FORT WORTH DIVISION
P. O. BOX 748
FORT WORTH, TEXAS 76101

12 DECEMBER 1984

FINAL REPORT FOR PERIOD JUNE 1980 – DECEMBER 1983

APPROVED FOR PUBLIC RELEASE; DISTRIBUTION UNLIMITED.

FLIGHT DYNAMICS LABORATORY
AIR FORCE WRIGHT AERONAUTICAL LABORATORIES
AIR FORCE SYSTEMS COMMAND
WRIGHT PATTERSON AIR FORCE BASE, OHIO 45433

NOTICE

When Government drawings, specifications, or other data are used for any purpose other than in connection with a definitely related Government procurement operation, the U S Government thereby incurs no responsibility nor any obligation whatsoever; and the fact that the Government may have formulated, furnished, or in any way supplied the said drawings, specifications, or other data, is not to be regarded by implication or otherwise as in any manner licensing the holder or any other person or corporation, or conveying any rights or permission to manufacture use, or sell any patented invention that may in any way be related thereto.

This report has been reviewed by the Office of Public Affairs (ASD/PA) and is releasable to the National Technical Information Service (NTIS). At NTIS, it will be available to the general public, including foreign nations.

This technical report has been reviewed and is approved for publication.

JOHN M. POTTER, Project Engineer
Fatigue, Fracture & Reliab Group
Structural Integrity Branch

FRANK D. ADAMS, Chief
Structural Integrity Branch
Structures & Dynamics Division

FOR THE COMMANDER

ROGER J. HEGSTROM, Colonel, USAF
Chief, Structures and Dynamics Division

"If your address has changed, if you wish to be removed from our mailing list, or if the addressee is no longer employed by your organization, please notify AFWAL/FIBE, WPAFB OH 45433-6553 to help us maintain a current mailing list."

Copies of this report should not be returned unless return is required by security considerations, contractual obligations, or notice on a specific document.

SUMMARY

This report summarizes a research program aimed at achieving two goals:

1. To collect data for use in specifying initial flaw size assumptions for crack-growth-based structural analyses for two types of advanced structural (joining) concepts.

2. To provide a methodology to enable designers to compare the relative merits of structural concepts with respect to the fracture-based philosophy of design.

An initial survey was conducted, using the F-16 fighter airframe, to determine the most attractive alternate structural concepts to replace conventional mechanically-fastened 2024 aluminum structure. Adhesive bonding with FM-73 epoxy and premium A357-T61 aluminum castings were chosen for study. Specific applications in the F-16 were chosen for modeling in the remainder of the program. These included a fuselage skin splice for adhesively bonded structure and a unitized version of the fin substructure for premium aluminum castings.

To achieve the stated goals, a test program was carried out wherein two hundred test specimens were tested using flight-by-flight loading spectra for the equivalent of two service lifetimes or until failure. Crack growth data were obtained directly from striations on the fracture surface following testing. Testing was preceded by two types of nondestructive inspection for each of the structural concepts, including conventionally-fastened baseline specimens.

Adopting the equivalent initial flaw size concept, data obtained from crack growth observations for each set of test specimens were used to determine initial manufactured fatigue quality and structural performance. The initial flaw sizes characteristic of each of the structural concepts were found to be well below the initial flaw size assumptions contained in USAF durability and damage tolerance specifications. The nondestructive test methods utilized, including eddy current, x-radiography, and ultrasonic C-scans, could not detect actual flaws correlating to equivalent initial flaws.

Considering structural performance, weight, cost, ease of inspection, and reliability, adhesive bonding was found to be the most attractive structural joining concept of those tested. Interestingly, we found that further improved performance could be obtained using unscrimmed adhesive, rather than conventional scrimmed adhesive. Unitized construction via A357-61 aluminum castings gave slightly better mean structural performance and much lower cost than conventional construction. However, the scatter in crack initiation and growth was much larger than in the other types of construction; so high reliability required lower operating stress levels than conventional 2024 construction. A correlation between defects in castings and crack initiation was found.

A general design tradeoff methodology for crack-growth-critical structure was developed, incorporating testing and analysis as carried out in this program. It is statistically based, utilizing the equivalent initial flaw size concept. Loading spectrum, spectrum stress level, and initial manufactured quality, as well as joining concept type, are included in the methodology.

FOREWORD

This report was prepared by General Dynamics/Fort Worth Division, Fort Worth, Texas, for the Structural Integrity Branch, Structures and Dynamics Division, Air Force Wright Aeronautical Laboratories, Wright-Patterson Air Force Base, Ohio, under Contract F33615-80-C-3226. Mr. John M. Potter, of AFWAL/FIBE, was the Project Engineer.

General Dynamics/Fort Worth Division was the sole contractor responsible for the performance of this program. Dr. W. R. Garver served as Program Manager and Principal Investigator. Dr. B. G. W. Yee was Management Focal Point. Coauthor K. M. Koepsel collected and processed all fracture surface crack growth data with additional contributions in spectrum development and data analysis. Dr. D. Y. Lee also helped to interpret the data and coauthored this report.

Many individuals at General Dynamics contributed to this program. S. M. Forness and P. D. Hudson provided specialized load histories and analytical crack growth predictions. Dr. J. Romanko and Dr. K. Liechti provided basic material data and theoretical guidance for the crack growth predictions in adhesively bonded specimens. Finite element stress intensity factor calculations for partially cracked adhesive layers were supplied by NASA/Langley through the efforts of D. S. Johnson and J. Whitcomb. D. Gordon and J. R. Bell of General Dynamics performed all nondestructive examinations of the test specimens. D. Bruner helped with specimen preparations and R. Nay performed all spectrum testing. The authors also wish to acknowledge M. Thomas, Dr. S. Manning, L. Koepsel, J. Norris, and R. Haile for their contributions and John Potter of AFWAL/FIBE who contributed helpful discussions and guidance.

This report is the Final Technical Report for this program, covering all work during the period June 1980 through December, 1983.

TABLE OF CONTENTS

TABLE OF CONTENTS (Continued)

LIST OF FIGURES

LIST OF FIGURES (Continued)

LIST OF FIGURES (Continued)

LIST OF FIGURES (Continued)

LIST OF TABLES

LIST OF TABLES (Continued)

SECTION I

INTRODUCTION

The current Air Force Structural Integrity (MIL-STD-1530A, Ref. [1]) design specifications require that an aircraft be designed to meet both damage tolerance (MIL-A-83444, Ref. [2]) and durability (MIL-A-8866B, Ref. [3]) requirements. These specifications require that the initial quality of aircraft primary structure must be such that there is no catastrophic failure nor widespread damage accumulation within one design service life. Design of airframes to meet these specifications has proceeded using a combination of fracture mechanics-based concepts for cyclic crack growth, along with assumptions for initial crack-like flaws which may exist undetected prior to service.

The selection of the initial flaw size and geometry to be used for design is one of the more important tasks in implementing the damage tolerance and durability requirements. The flaw sizes and geometries currently specified in MIL-A-83444 have been developed primarily for conventional built-up structure consisting of mechanically-fastened components. Little exists currently which could be used to quantify, in fracture mechanics terms, either the failure processes or the initial quality of advanced materials and joining concepts. One of the goals of this program is to provide data for two types of alternate joining concepts that can be used to base assumptions of initial flaw size and geometry for these joining concepts for direct use within the current Air Force durability specifications.

A second goal of this program is to provide the designer with a realistic way to assess design tradeoffs for competing structural joining concepts, within the framework

of the fracture-based philosophy of design. The concept of the equivalent initial flaw size (EIFS) has been used in previous investigations [4,5] to compare the durability and initial quality of conventionally-fastened joints. The concept provides quantitative data which has been successfully used to reveal the effect on durability of changes in fastener type or fit [4,6]. However, it is not clear whether the EIFS concept, by itself, can provide a useful criterion for comparing the relative merits of advanced and conventional joining concepts at the design level. Therefore, this program also seeks to provide information which can be readily used by the designer to quantitatively assess the benefits of competing structural concepts.

SECTION II

EXPERIMENTAL PROCEDURES

2.1 SELECTION OF ADVANCED JOINING CONCEPTS

Two applications of advanced joining concepts were selected to serve as prototypes for this program. These are: (a) adhesive bonding of the F-16 upper center fuselage skins and bulkheads - fuselage station 341.8 (Figure 1), and (b) monolithic casting to replace built-up structure in the F-16 vertical tail understructure (Figure 2). The details of the procedures and rationale for the above selection were presented in the Phase I Report of this program [7].

In general, adhesive bonding provides a good combination of cost and weight benefits. Previous investigations [8-12] have suggested that adhesive bonding could have additional benefits of increased durability, reduced corrosion, and improved fuel sealing in integral fuel tanks compared to mechanically-fastened structure. Monolithic casting is one type of unitized construction which has significant advantages over conventional built-up structure, especially in cost savings due to reduced material, machining, and assembly costs [13-15].

2.2 SPECTRUM TEST ELEMENTS

In addition to the two advanced joining concepts selected for this program (i.e., adhesive bonding and monolithic casting), a third test element configuration representing conventional construction was also chosen as a baseline for the adhesively bonded test element.

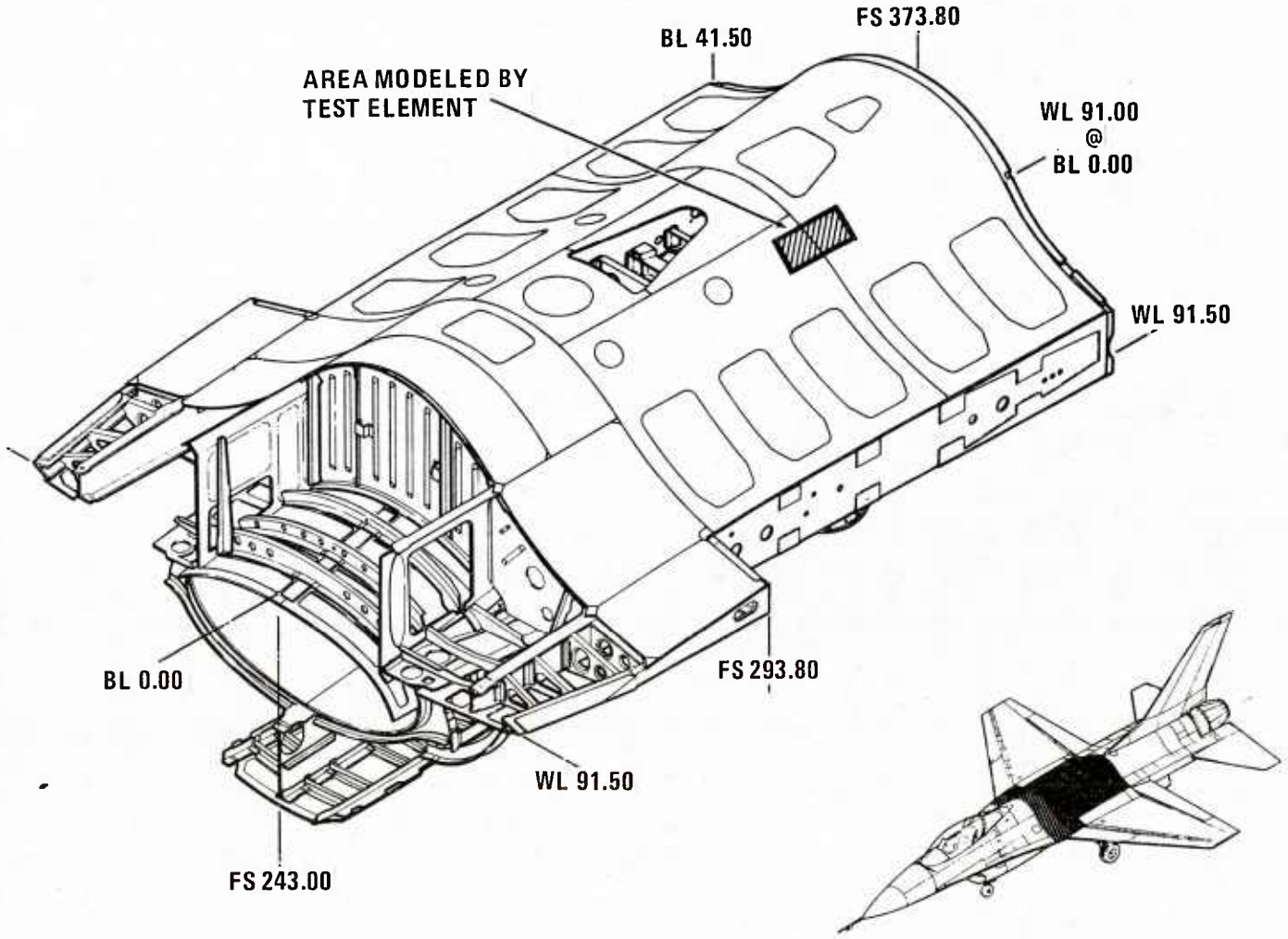

Figure 1. Location of F-16 Fuselage Skin/Bulkhead Splice Used on Prototype for Adhesive Bonding

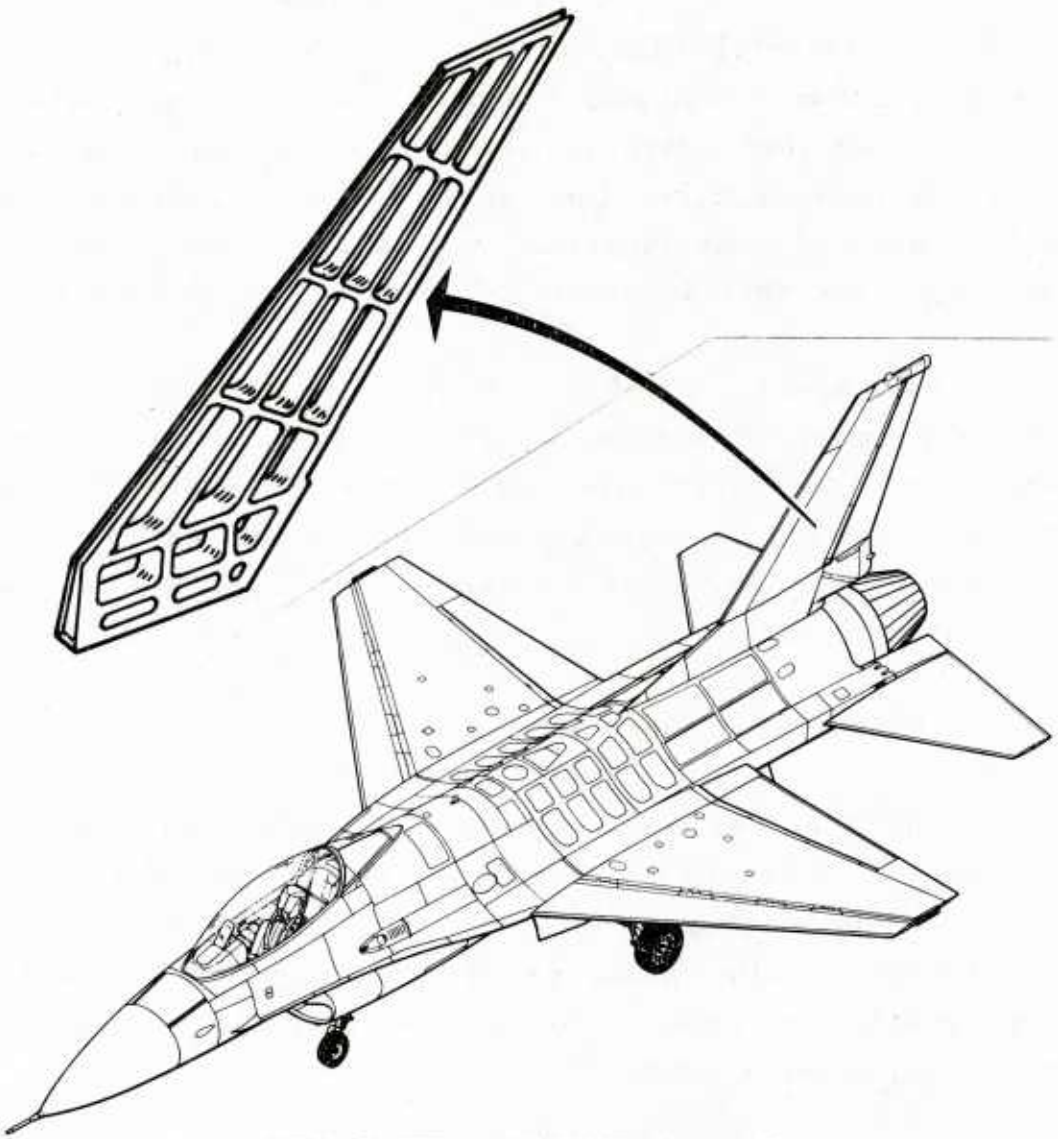

Figure 2. F-16 Vertical Tail Understructure

2.2.1 Mechanically-Fastened Specimens

The design for a conventionally-constructed test element models the F-16 upper fuselage skin/bulkhead splice at fuselage station 348.1. The F-16 bulkhead at this station is NC machined from 5.50-inch 2124-T851 aluminum plate. Skins are chem-milled, machined, and formed from

0.25-inch 2024-T81 aluminum sheet. The design for a test element, shown in Figures 3 and 4, uses identical materials, with the doubler (detail (A) of Figure 3) utilized in the short transverse direction, as in the F-16 bulkhead. Also, the specimen configuration is nearly identical to one developed for this location in the F-16 development program.

For spectrum fatigue testing, two variants of the conventionally fastened baseline (Type B) specimen were employed. The first type was assembled with faying surface sealant, which is typical of all mechanically fastened joints in the F-16, while the second type was assembled without sealant.

2.2.2 Adhesively Bonded Specimens

The specimen geometry for an adhesively bonded test element was selected as an analogy to the baseline specimen. The specimen configuration is shown in Figure 5. It is a single-strap joint geometry such as might be typical for aerodynamic surfaces. The tee is included as a means of providing lateral constraint during testing.

The adhesive chosen for this program was American Cyanamid FM-73M, which is a 250^{o}F cure adhesive containing dacron scrim fibers and small rubber particles in a modified epoxy matrix. One variant of the adhesively bonded (Type A) specimen was manufactured using FM-73M (scrimmed) adhesive film while a second variant was made using FM-73U (an unscrimmed version of FM-73).

For the preparation of test specimens, 0.125 inch thick 7075-T61 aluminum sheets (unclad) were phosphoric acid anodized and primed at Vought Corporation in Grand Prairie,

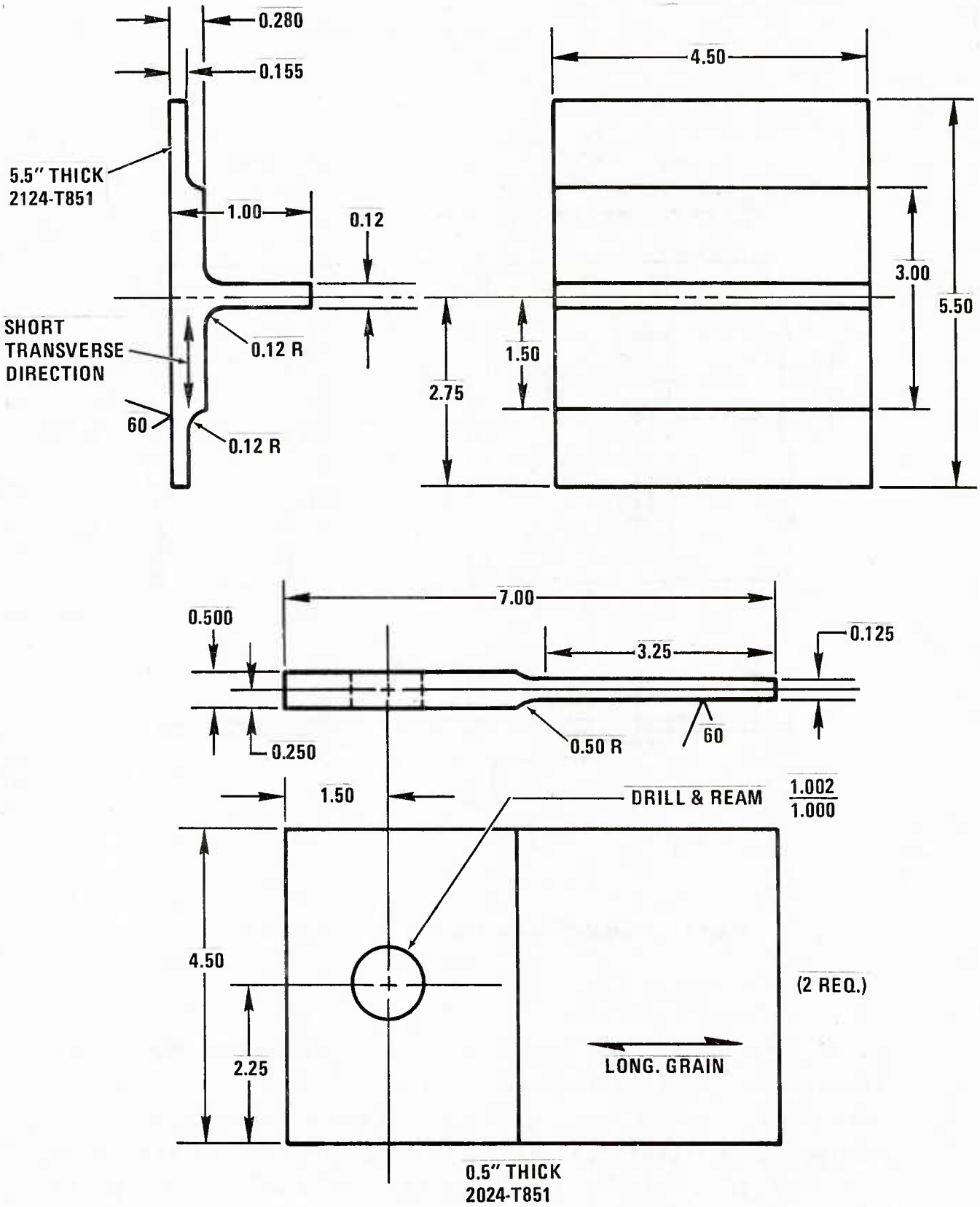

Figure 3. Details for Conventionally-Fastened Center Fuselage Skin Splice Test Element

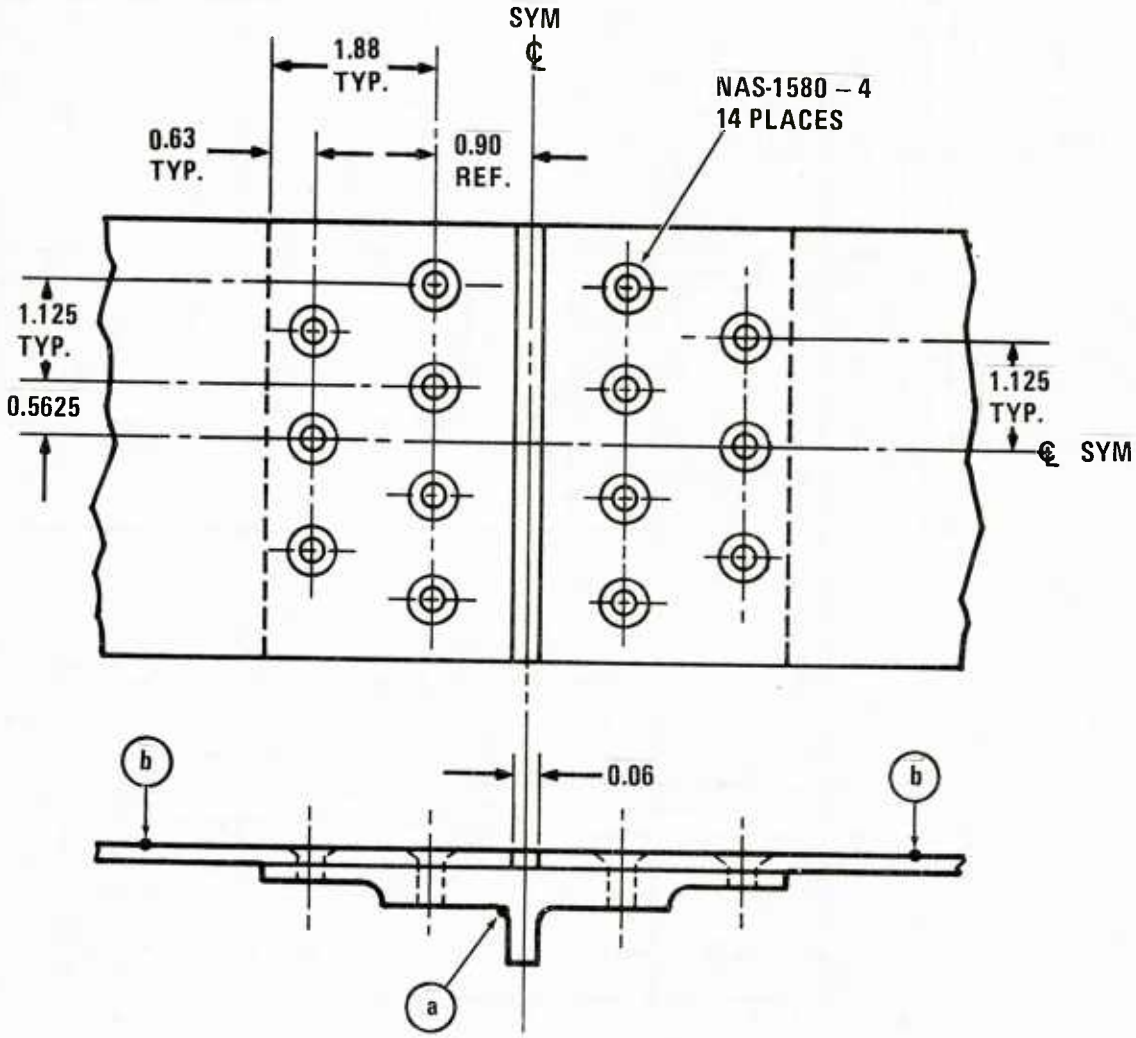

Figure 4. Fastener Pattern for Conventionally-Fastened Test Element

Texas, using BR 127-A primer. The adherends were then transferred to GD/FWD, laid up, and bonded. Bonding was performed in large bonding presses using a cure cycle recommended by American Cyanamid. Sheets were heated from room temperature to 250°F in sixty minutes (at approximately 3°F/min), held for one hour at a pressure of 40 ± 5 psi, then cooled to room temperature.

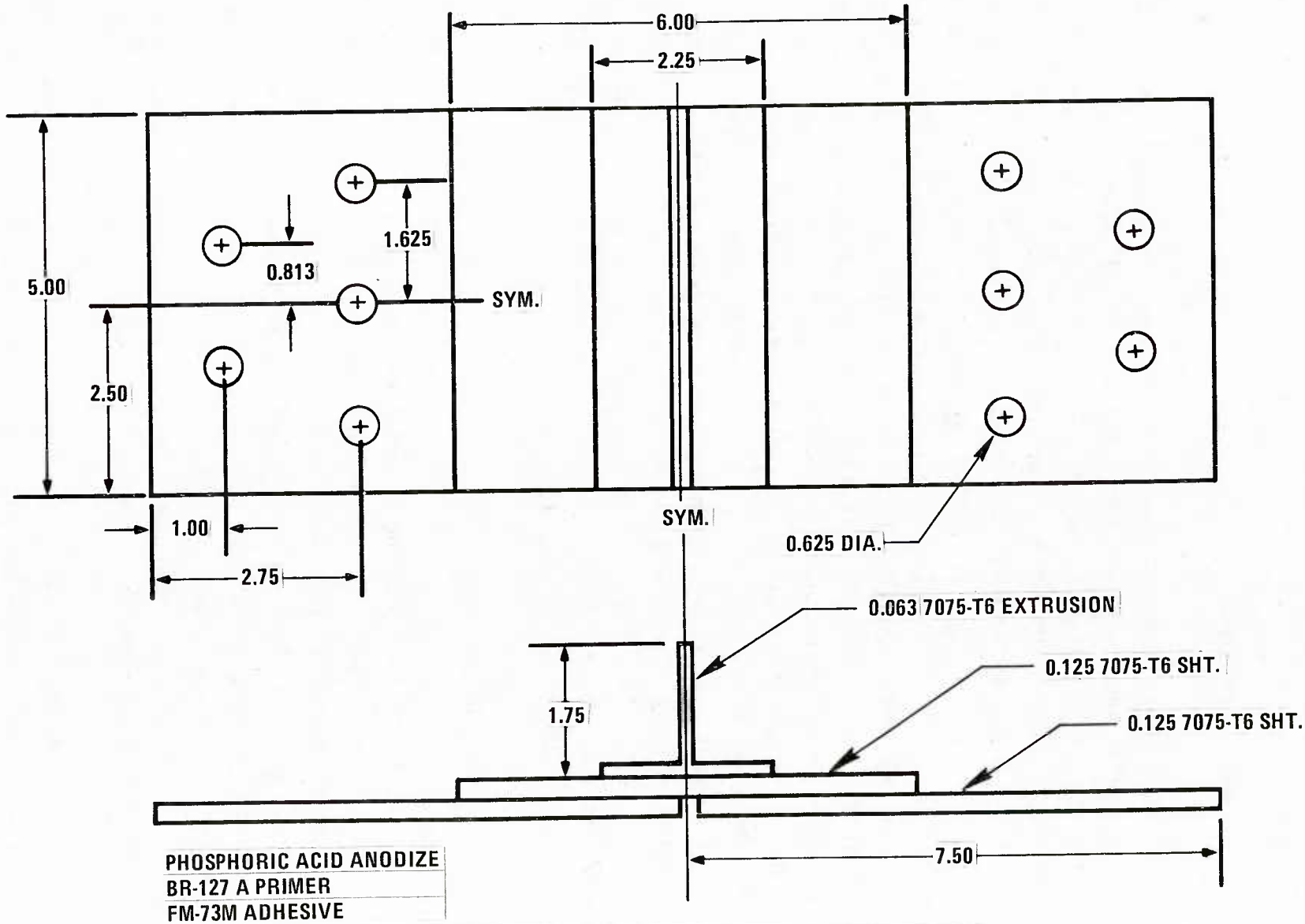

Figure 5. Adhesively Bonded Center Fuselage Skin Splice Test Element

2.2.3 Cast Specimens

The cast (Type C) test element was designed to model a point near the root of the front spar flange in the F-16 vertical tail understructure. The F-16 vertical tail understructure supports graphite-epoxy composite skins, attached with mechanical fasteners. Nominal bearing stress in the critical spar flange fastener hole is about 4/3 the nominal gross tensile stress in the flange. The test specimens were designed to have an identical ratio of bearing stress to gross stress. Bearing loads in the test specimen were introduced through mechanical fasteners from a contiguous graphite-epoxy composite strap. The cast portion of the test elements, shown in Figure 6, was A357-T61 aluminum cast at Anacast Foundry in Fort Worth, Texas. The graphite-epoxy composite straps, shown in Figure 7, were fabricated at GD/FWD. Castings and straps were co-drilled and attached using blind fasteners (0.188-inch-diameter NAS 6203), as shown in Figure 8.

2.3 LOAD HISTORY DEVELOPMENT

Each of the joining concepts proposed in Phase I was tested during Phase II of the program. Load histories were developed for the airframe location on which each joining concept was modeled in order to provide realistic stress histories during testing. The load histories also needed to provide elements that facilitate fractographic tracking to keep the testing costs reasonable and allow tracking of crack growth for small cracks.

The vertical tail root of the F-16 was used as the model for the integrally-cast joining concept in this program. The upper-fuselage skin/bulkhead splice at F.S. 341.8

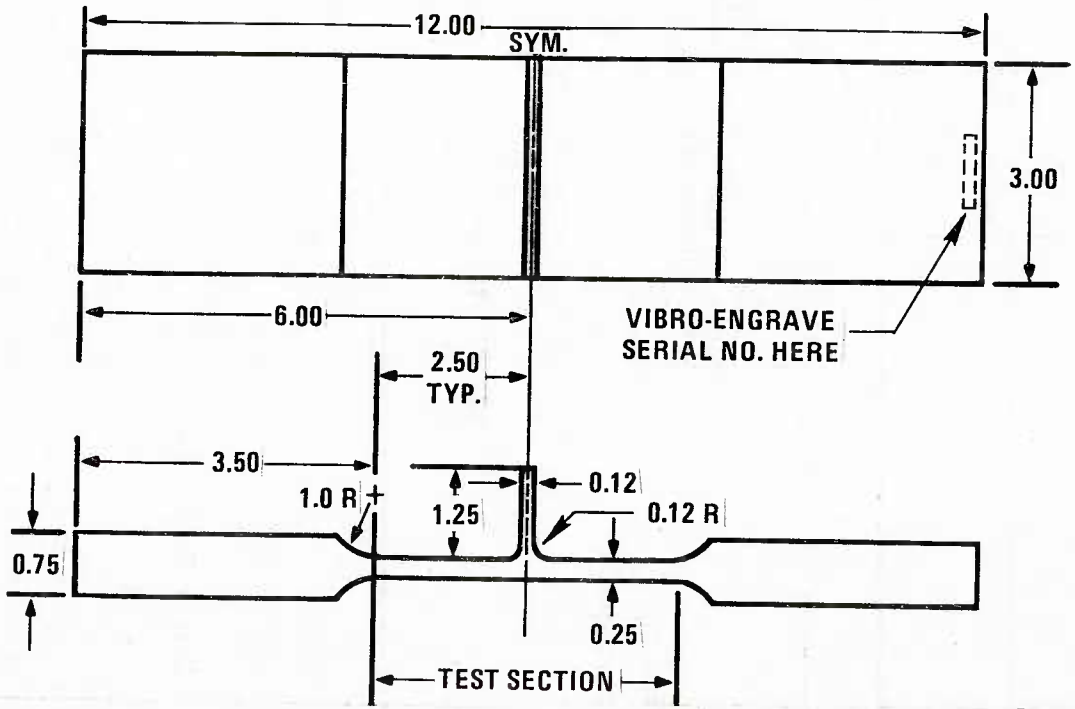

NOTES:

1. MATERIAL TO BE A357-T61 PER MIL-A-21180, CLASS 1, EXCEPT ELONGATION TO BE 4%
2. TOLERANCE ± 0.03 (Dimensions in Inches)
3. AS-CAST SURFACE FINISH 350 μIN.
4. BREAK ALL SHARP EDGES
5. MISMATCH 0.01 MAX
6. WAVINESS TOLERANCE 0.010 IN./IN.
7. STRAIGHTEN TO WITHIN 0.030 PRIOR TO INSPECTION
8. PENETRANT INSPECT PER NDTS 1101, ZONE 6
9. X-RAY INSPECT TO MIL-C-6021, GRADE B, RADIOGRAPHIC QUALITY IDENTIFY X-RAY RECORD WITH CASTING SERIAL NUMBER
10. IN PROCESS WELD REPAIR PER FPS-1082. LIMIT WELD REPAIR TO 25% OF TOTAL PIECES IN TEST AREA. IDENTIFY WELD REPAIRS IN TEST AREA
11. VIBRO-ENGRAVE SERIAL NUMBER ON EACH PIECE AS SOON AS PRACTICABLE. USE SERIAL NUMBER TO PROVIDE RECORDS FOR TRACEABILITY OF EACH PIECE. INCLUDE IDENTIFICATION OF MELT, POUR, AND POSITION OF PIECE IN MOLD (If Multipiece Pattern is Used)

Figure 6. Cast Aluminum Coupon

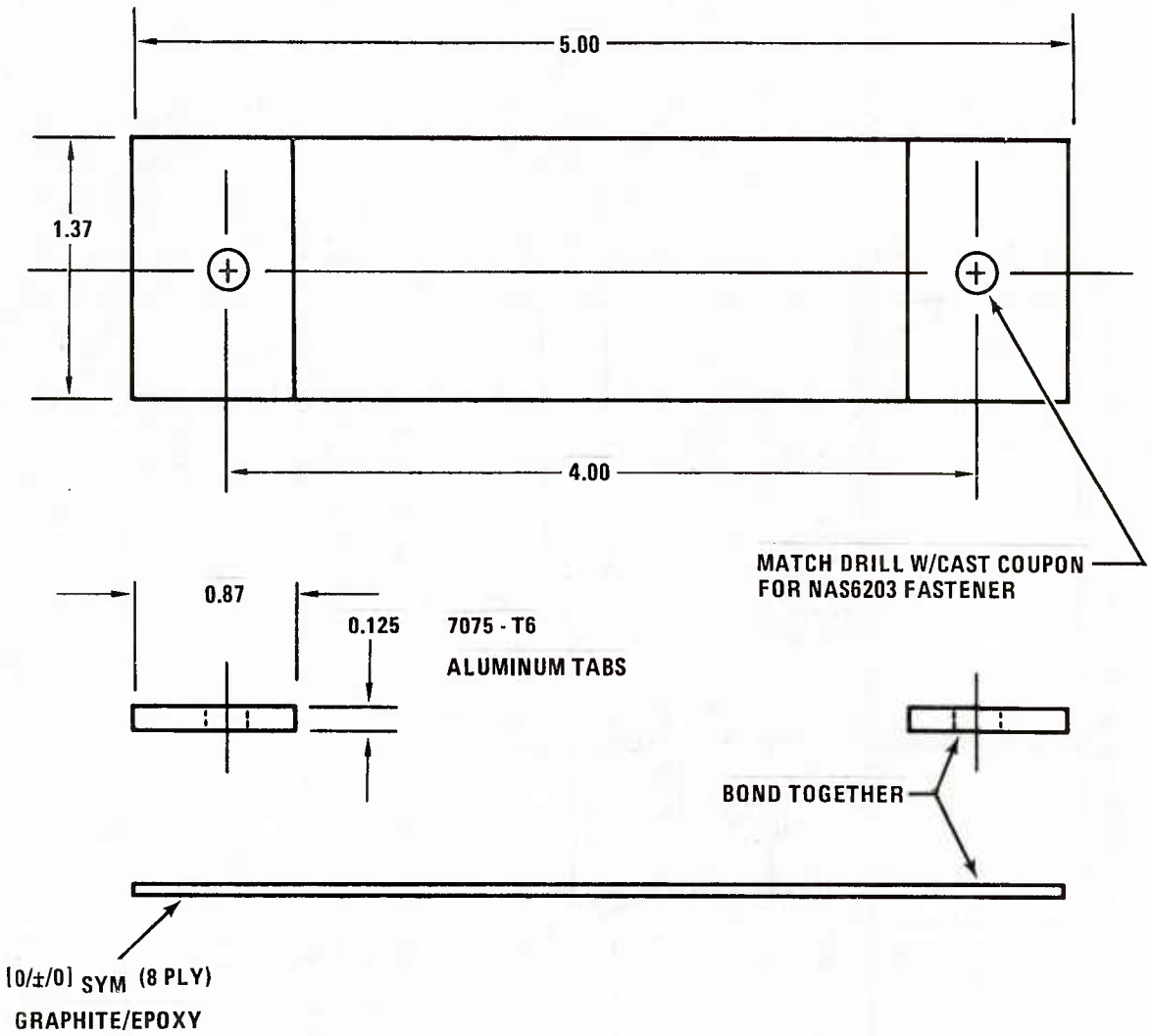

Figure 7. Strap for Cast Test Element

of the F-16 served as the model for an adhesive bonding application, as well as for the mechanically fastened baseline. The general procedures for development of cycle-by-cycle load histories for the F-16 were described in detail in the Phase I report [7].

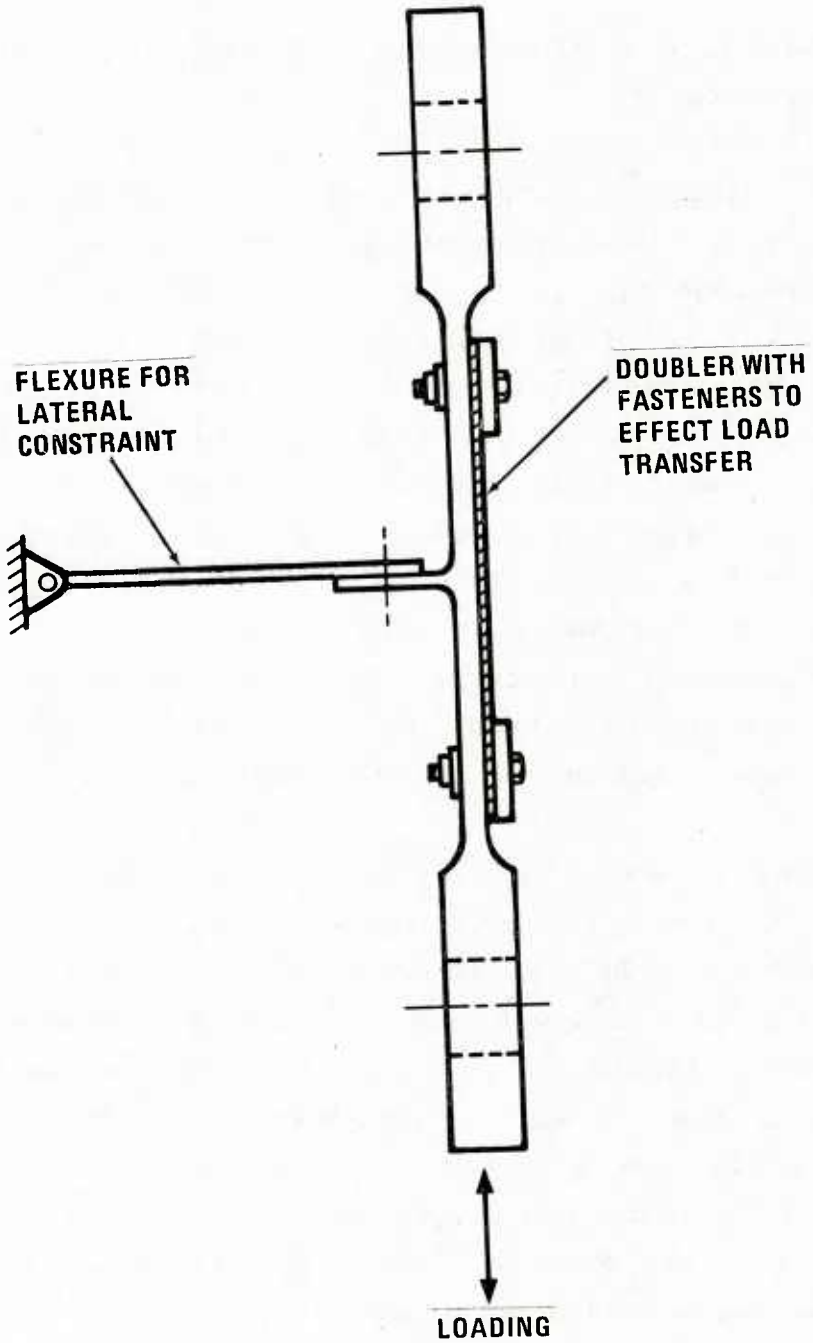

Figure 8. Assembled Cast Test Element

2.3.1 Adhesively Bonded and Mechanically Fastened Test Elements

Preliminary testing was conducted in Phase I to see if the adhesively bonded test elements could be marked with the HAL 25 fuselage splice spectrum. The HAL 25 load history contains 110,714 load points per 1000 equivalent flight hours and produces clear markings on fatigue crack surfaces in aluminum alloys. This load history, however, did not mark the scrimmed adhesive, so a different load history was tried. This spectrum, designated NOR 1 (Figure 9) is a modified test spectrum, derived from a preliminary spectrum developed by Rockwell International for the B-1 wing carry-through box structure. The spectrum contains 11,455 cycles representing each 100 flights. 1280 flights represent one lifetime, or 13,500 flight hours.

Careful searching of the fracture surface with an optical microscope revealed isolated regions of the matrix which were clearly marked by the applied spectrum load (Figure 9). The regions were small and infrequent, lying between scrim fibers. Since the scrim fibers dominated the fracture surface, it was not possible to use fractography in tracking crack growth in the scrimmed adhesive. Consequently, the crack or debond length was monitored during testing using a 1/8-inch-diameter focused ultrasonic transducer. Ultrasonic measurements of debond length were found to agree with visual measurements to within about 0.020 in. [7].

2.3.2 Cast Test Elements

The HUD 23 load history, a two-block F-16 fin root bending moment history, was originally selected as the test spectrum for the cast test elements. HUD 23 contains 80,714

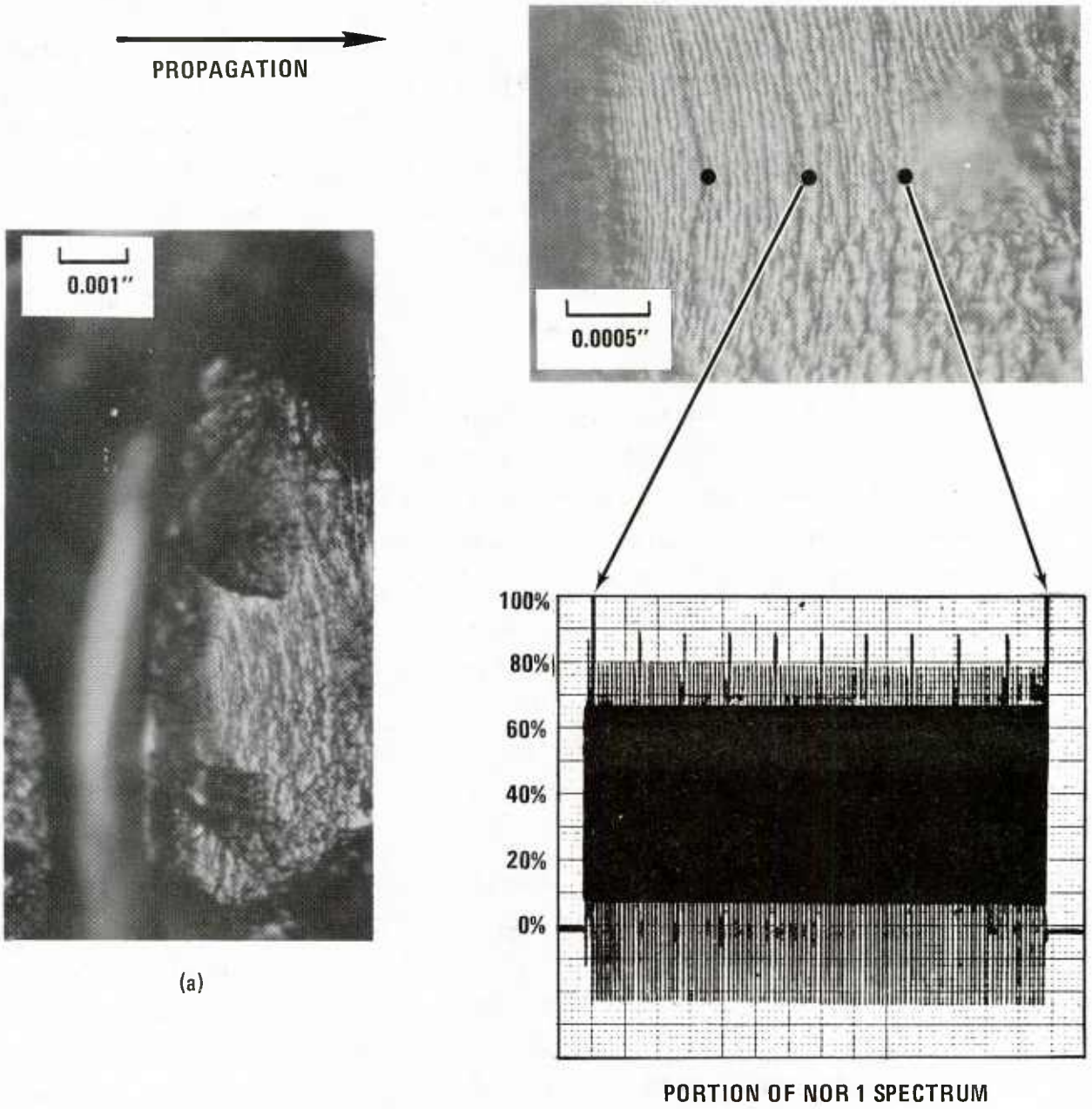

Figure 9. Optical Micrographs of FM-73M Adhesive Failure and Portion of NOR Spectrum

load points per 1000 equivalent flight hours. However, this spectrum does not contain widely varying blocks of loading which might lead to clear marks on a fatigue fracture surface. A series of modifications was made to the HUD 23 spectrum to enhance the marking ability (Figure 10). The first modification, FLA 1, was formed by appending 1660 fully-reversed 60% amplitude cycles to the end of the HUD 23 1000-hour block. The second modification, FLA 2, was formed by grouping together the loads which were greater than 50% (maximum spectrum load) and which occur during the last 150 flight hours of each 1000-hour block. The loads were arranged in ascending block sequence and added to the end of the 1000-hour block. Limited spectrum testing with the modified spectrum illustrated the difficulty in reading the crack growth history of the casting surfaces. The difficulty arises from the inherent roughness of the A357-T61 fracture surface, and the preponderance of large compressive loads in the fin root spectrum. Another modification was then made to the FLA 2 spectrum which consisted of truncating all the compressive loads and replacing them with zero load.

The resulting GAR 1 spectrum improved the markings on the fracture surface but the mark only occurred every thousand hours. Fifteen test elements were run with the GAR 1 spectrum before we decided the fractographic surface was providing too little data. The existing high loads were then re-arranged within each 100 flight hours into stepped blocks - forming the GAR 2 spectrum. This allowed reading of the fractographic surface every 100 hours. Twenty-five cast test elements were then run using the GAR 2 spectrum. Average life of the GAR 1 and GAR 2 test elements were similar. Fin root spectrum variants are shown in Figure 10.

(A) Original Spectrum

(HUD 23)

(C) Compressive Loads Truncated

(GAR 1)

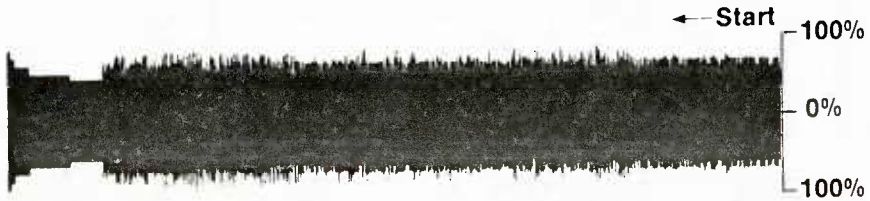

(B) Extra Marker Band

(FLA 2)

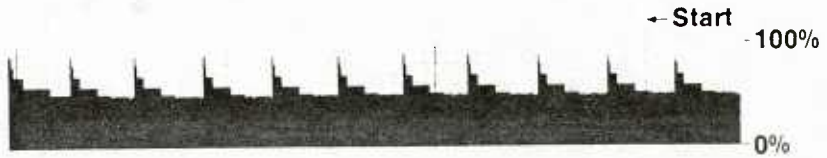

(D) High Loads Rearranged

(GAR 2)

Figure 10. F-16 Fuselage Spectrum Variants for Fractographic Markings

Since the other test element geometries were to be tested using the NOR 1 spectrum, several A357 test elements were run to see if the spectrum was suitable. The NOR 1 spectrum produces clear marks in A357 aluminum. The test plan was then changed to test 15 specimens with the GAR 1 spectrum, 25 specimens with the GAR 2 spectrum, and 50 specimens with the NOR 1 spectrum.

Further details of the spectra and modifications are given in the Phase I report [7] and Reference [16].

2.4 CRACK GROWTH ANALYSIS

Crack growth analyses were conducted using GD/FWD production crack growth computer codes. Crack growth calculations for the baseline and cast specimens were carried out using the well-established code designated R5N [17]. A completely revamped version denoted RXN [18] was used for crack growth analyses in the adhesively bonded specimens.

In this subsection the methods used to analyze crack growth will be briefly discussed for each type of specimens. The details of crack growth analyses, including stress analyses, initial flaw types and locations, and material properties used, can be found in the Phase I Report for this program [7].

2.4.1 Baseline Specimens

A stress analysis performed for the baseline specimen geometry [7] suggested that under axial loading, the largest stresses would occur at the skin/doubler interface due to induced bending. Bolt-hole cracking was predicted to be the

most prevalent failure mechanism. Therefore, four combinations of initial flaw type and location shown in Figure 11 were considered most important. These included corner and through flaws at bolt holes in the skin and doubler.

All crack growth analyses were conducted for the NOR 1 spectrum at nominal stress levels of 24 and 30 ksi. Analyses were performed for single and double (symmetric) cracks emanating from the critical fastener holes. All analyses used appropriate stress intensity factor estimates for loaded bolt holes. The starting crack size was taken as 0.001 inch. Analyses were terminated upon reaching the estimated critical crack size or upon reaching two design lifetimes.

Permuting the major parameters led to the set of crack growth analyses shown in Table 1. Maximum stress values shown in Table 1 correspond to just two levels of maximum spectrum load. Further variations in stress level are due to location within the test element.

Following a methodology developed previously at GD/FWD [19, 20] and using a modified secant method [21], crack growth rate ($\Delta a/\Delta t$) was predicted as a function of crack length, a. Examples of these transformed predictions are shown in Figure 12. Note from Figure 12 that $\Delta a/\Delta t$ vs. a pairs can be fit by a simple power law. Thus, an equation of the form

$$\frac{da}{dt} = Qa^b \qquad (1)$$

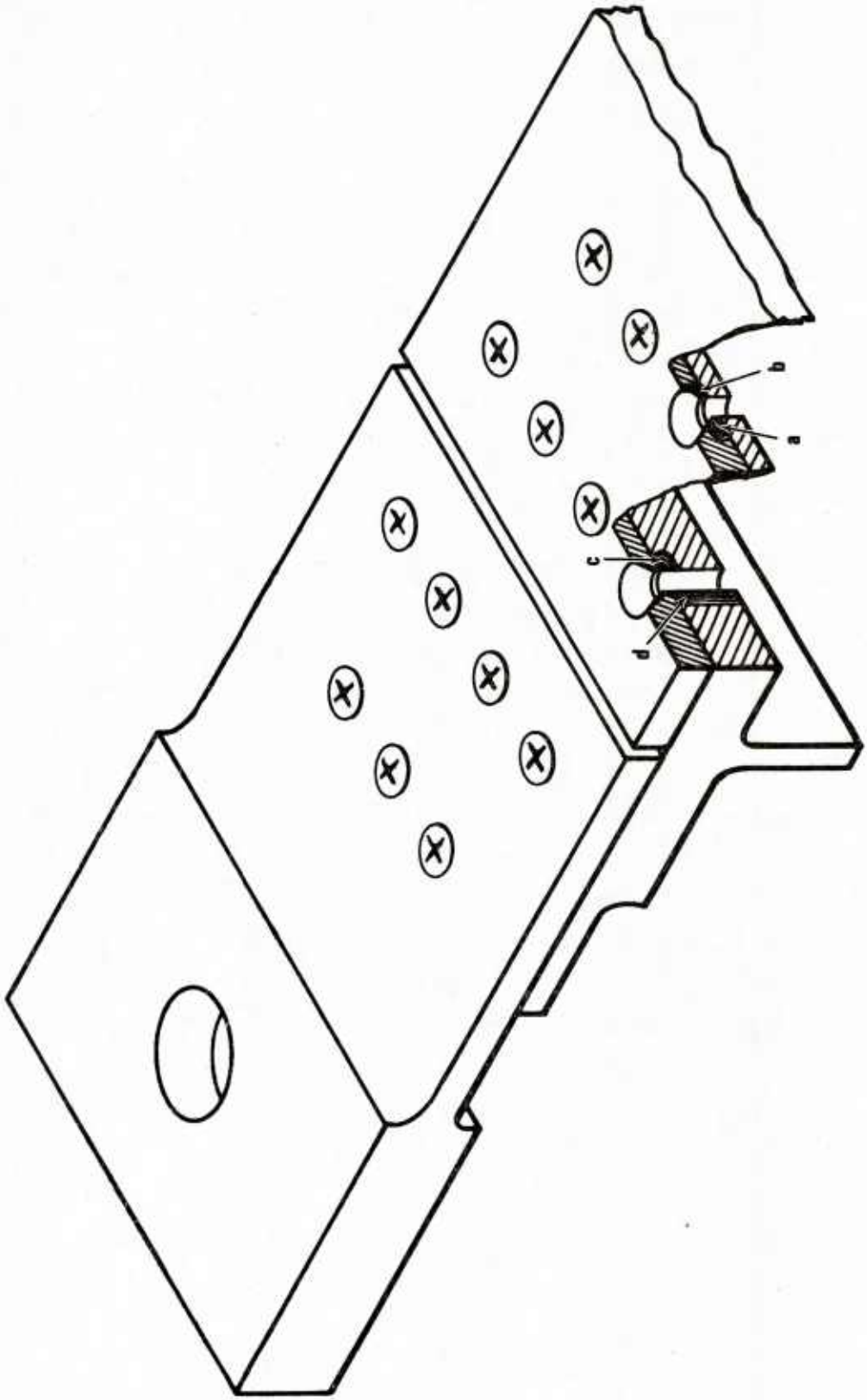

Figure 11. Initial Flaw Assumptions for Baseline Test Element

Table 1. Baseline Specimen Crack Growth Analysis Parameters

ANALYSIS NO.	FASTENER ROW	CRACK TYPE	NUMBER OF FLAWS	MAXIMUM STRESS (KSI)
B1	INNER	CORNER	SINGLE	39.21
B2	INNER	CORNER	SINGLE	31.36
B3	INNER	CORNER	DOUBLE	39.21
B4	INNER	CORNER	DOUBLE	31.36
B5	INNER	THROUGH	DOUBLE	12.64
B6	INNER	THROUGH	DOUBLE	10.11
B7	OUTER	CORNER	SINGLE	36.46
B8	OUTER	CORNER	SINGLE	29.16
B9	OUTER	CORNER	DOUBLE	36.46
B10	OUTER	CORNER	DOUBLE	29.16
B11	OUTER	THROUGH	SINGLE	28.57
B12	OUTER	THROUGH	SINGLE	22.86
B13	OUTER	THROUGH	DOUBLE	28.57
B14	OUTER	THROUGH	DOUBLE	22.86

can be used to represent predicted crack growth. Best-fit Q and b values for each of the baseline specimen crack growth predictions are given in Table 2. Figures 13 and 14 summarize the crack growth analyses of the baseline specimens.

2.4.2 Adhesively Bonded Specimens

No widely recognized method exists for analytically predicting crack growth or progressive debonding in adhesively bonded joints under cyclic loading. However,

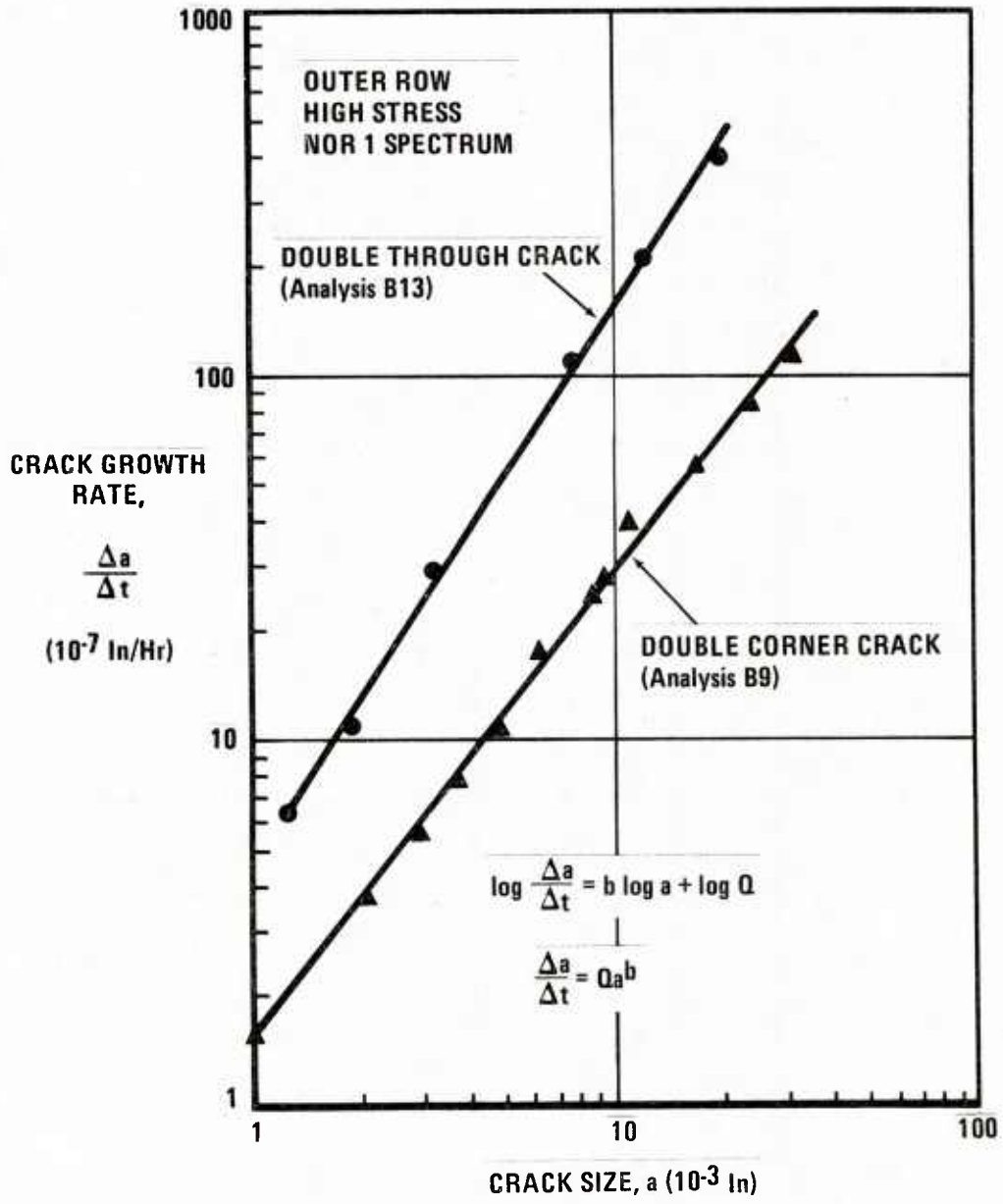

Figure 12. Sample Transformed Baseline Crack Growth Predictions

Table 2 Baseline Crack Growth Rate Parameters

ANALYSIS NO.	FASTENER ROW	CRACK TYPE	MAXIMUM STRESS (KSI)	b	Q
B1, 3	INNER	CORNER	39.21	1.52	3.2×10^{-3}
B2, 4	INNER	CORNER	31.36	3.72[1]	2.0×10^{-3}
B5	INNER	THROUGH	12.64	2.33[1]	2.4×10^{-3}
B6	INNER	THROUGH	10.11	----[2]	----
B7, 9	OUTER	CORNER	36.46	1.28	1.1×10^{-3}
B8, 10	OUTER	CORNER	29.16	1.52	2.0×10^{-3}
B11, 13	OUTER	THROUGH	28.57	1.46	1.2×10^{-2}
B12, 14	OUTER	THROUGH	22.86	1.51	7.6×10^{-3}

1 Very Slow Crack Growth
2 Roundoff Error Larger Than Crack Length Increments.

recent research efforts at GD/FWD (including the "Integrated Methodology for Adhesive-Bonded-Joint Life Predictions" [22] and "Viscoelastic Stress Analysis Including Moisture Diffusion for Adhesively Bonded Joints" [23] programs have provided an important guideline for crack growth analysis of adhesively bonded specimens in this program.

Assuming that crack growth rate can generally be expressed in terms of some linear elastic fracture mechanics (LEFM) parameters, it is recognized that calculation of such parameters requires very exacting analysis of the local stress field near the crack tip within the thin adhesive interlayer. Finite element analyses were first performed for cracked-lap-shear (CLS) specimens (Figure 15) using the MARC and GAMNAS (NASA/Langley) [24 25] computer programs

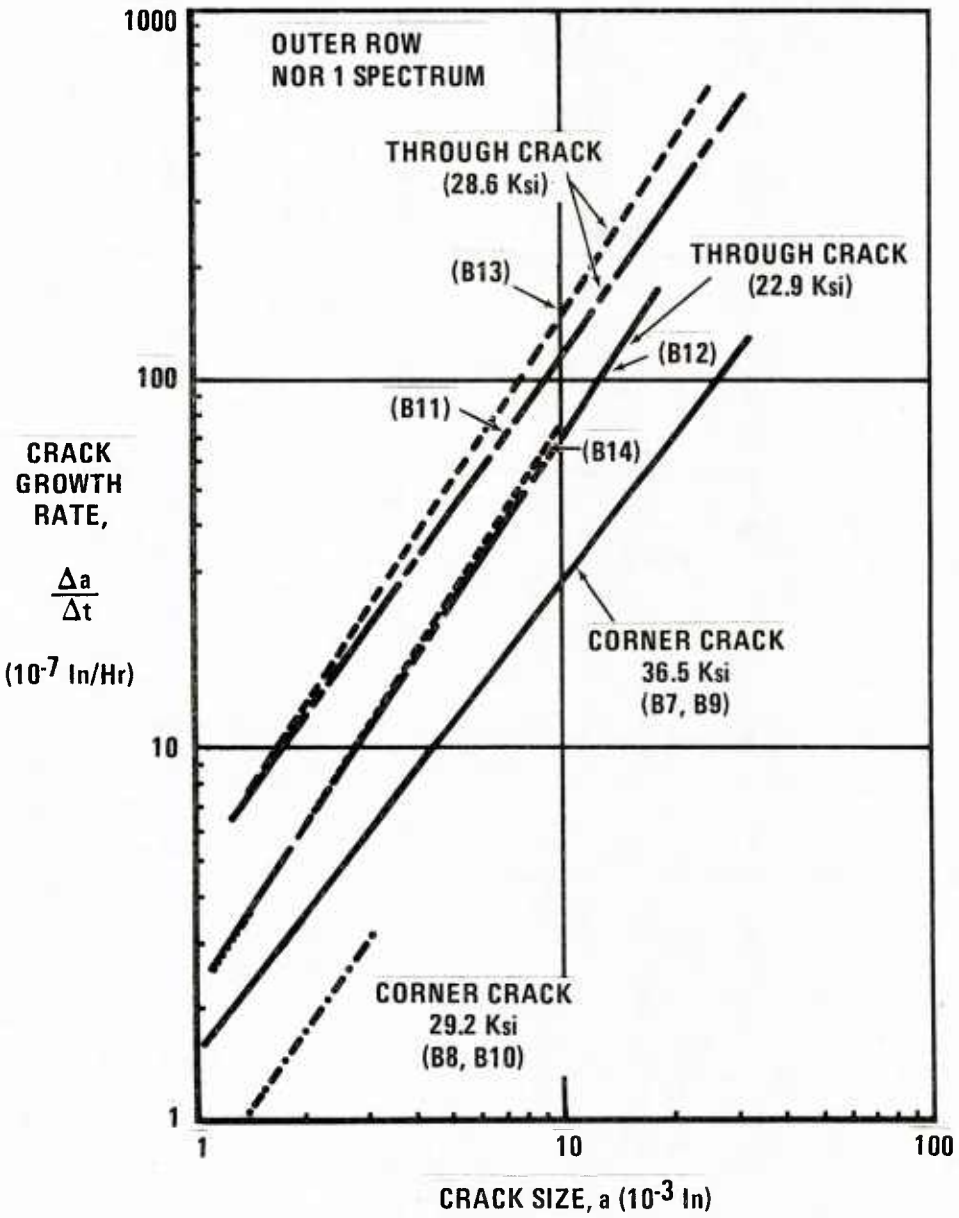

Figure 13. Summary of Baseline Crack Growth Predictions – Outer Fastener Row

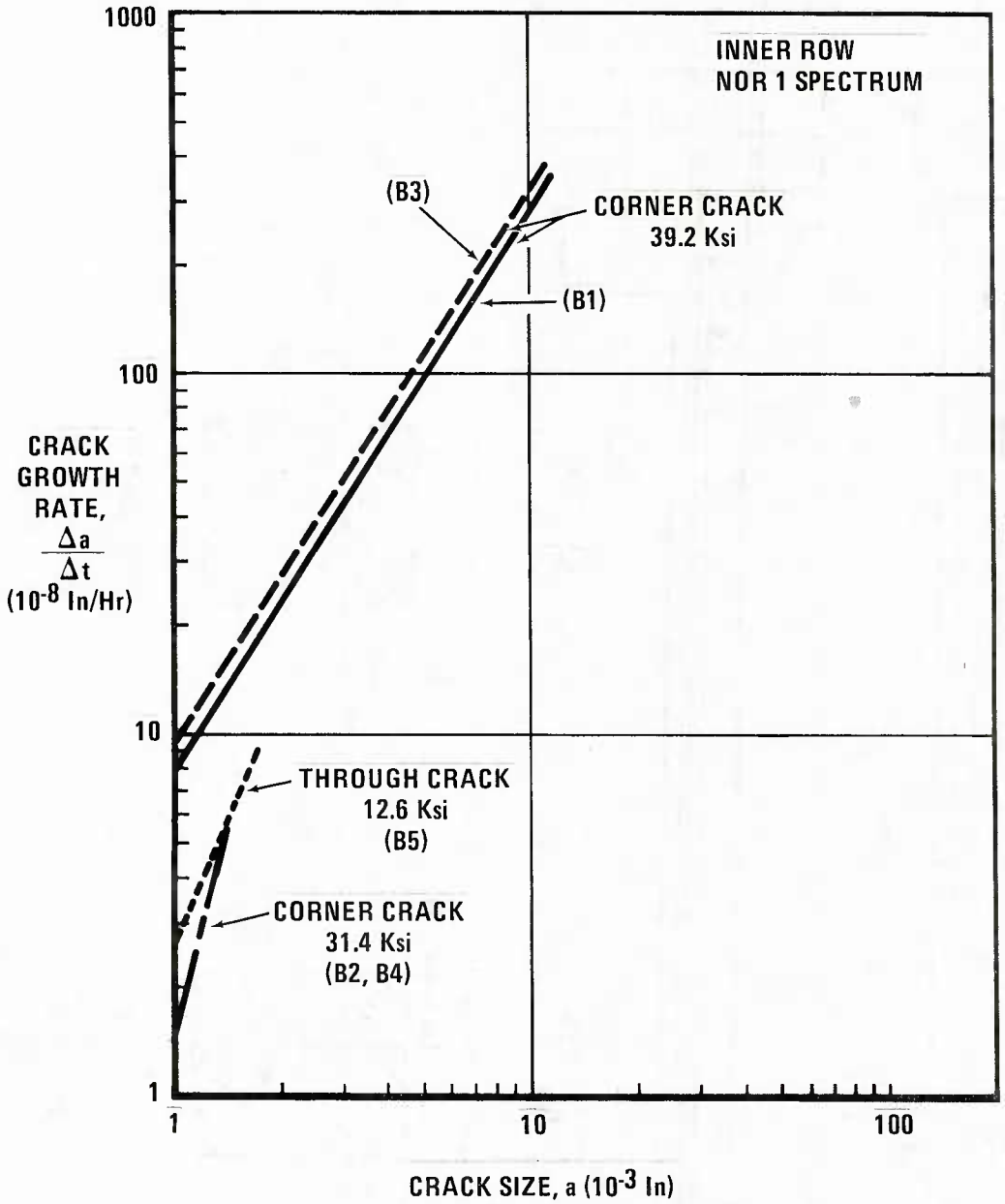

Figure 14. Summary of Baseline Crack Growth Predictions – Inner Fastener Row

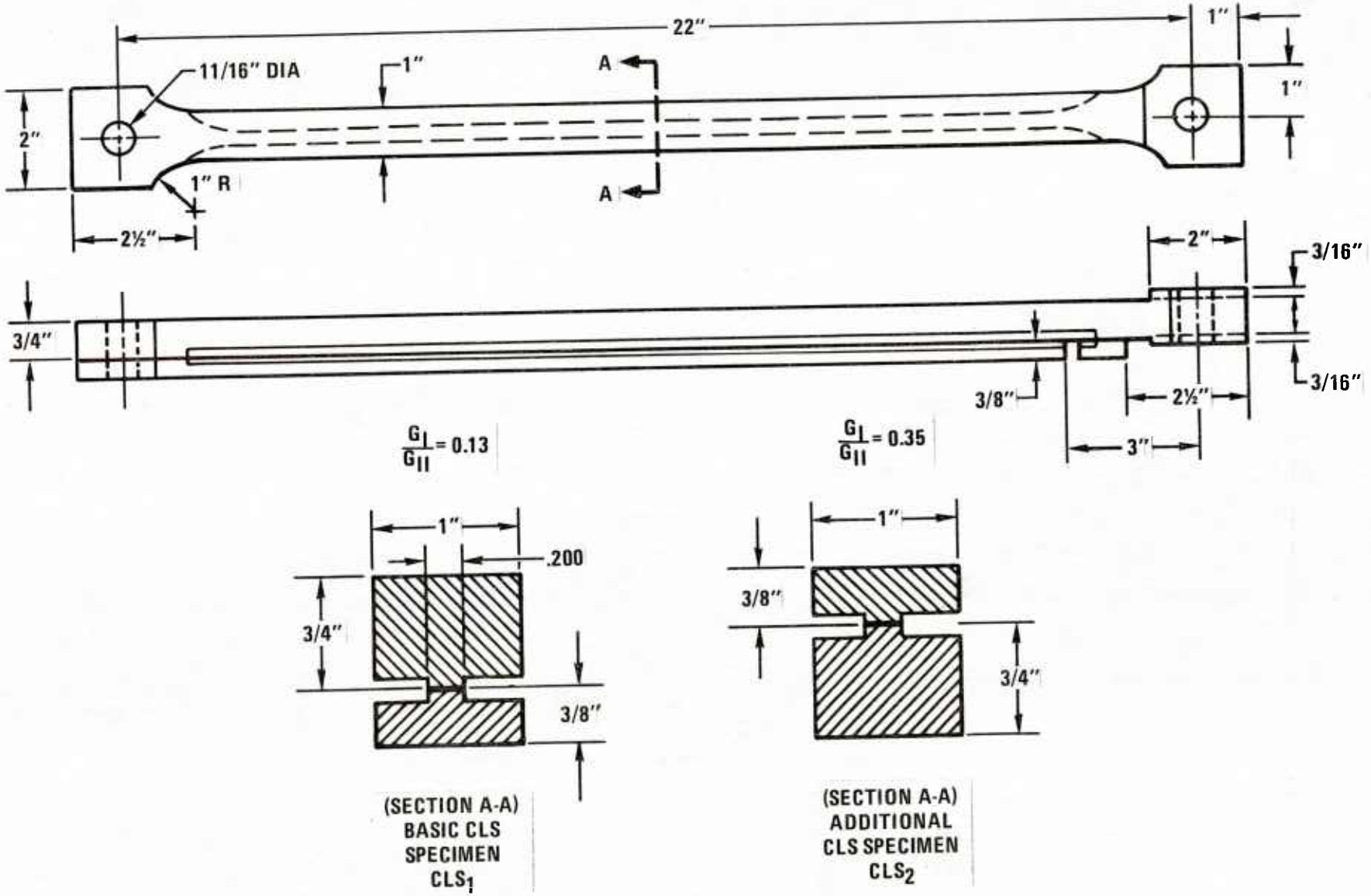

Figure 15. Cracked Lap Shear Specimen Geometry

based upon the finite element model shown in Figure 16. The results are summarized in Figures 17-19. It can be seen from Figures 17 and 18 that the predicted strain energy release rates (G) from MARC and GAMNAS analyses are consistent with each other, that there is a wide discrepancy between beam theory [9] and MARC and GAMNAS analyses, and that the dependence of G on crack length is not significant. Also, Figure 19 shows that crack growth rate (da/dN) can be related to G with a simple power law of the form:

$$\frac{da}{dN} = C\Delta G^{n} \qquad (2)$$

where C and n are constants.

Similarly, the finite element analyses were conducted for the Type A adhesively bonded specimen configuration using MARC, GAMNAS [24, 25] and NASTRAN finite element codes based upon the mesh shown in Figure 20. The calculated stress intensity factors for Mode I and II (K_I and K_{II}) from MARC analyses are given in Figures 21 and 22. Again, note that the dependence of LEFM parameters (K_I and K_{II}) on crack length is weak. (Figures 17, 18, 21 and 22).

For the crack growth prediction of our adhesively bonded specimens, the G values obtained from MARC, GAMNAS and NASTRAN analyses were evaluated. The predicted G values from MARC, GAMNAS and NASTRAN analyses are listed in Table 3. We elected to use the G value given by J. Whitcomb of NASA using GAMNAS (i.e. G = 2.0 for a stress of 12.3 ksi, Table 3). We did this because researchers at NASA/Langley

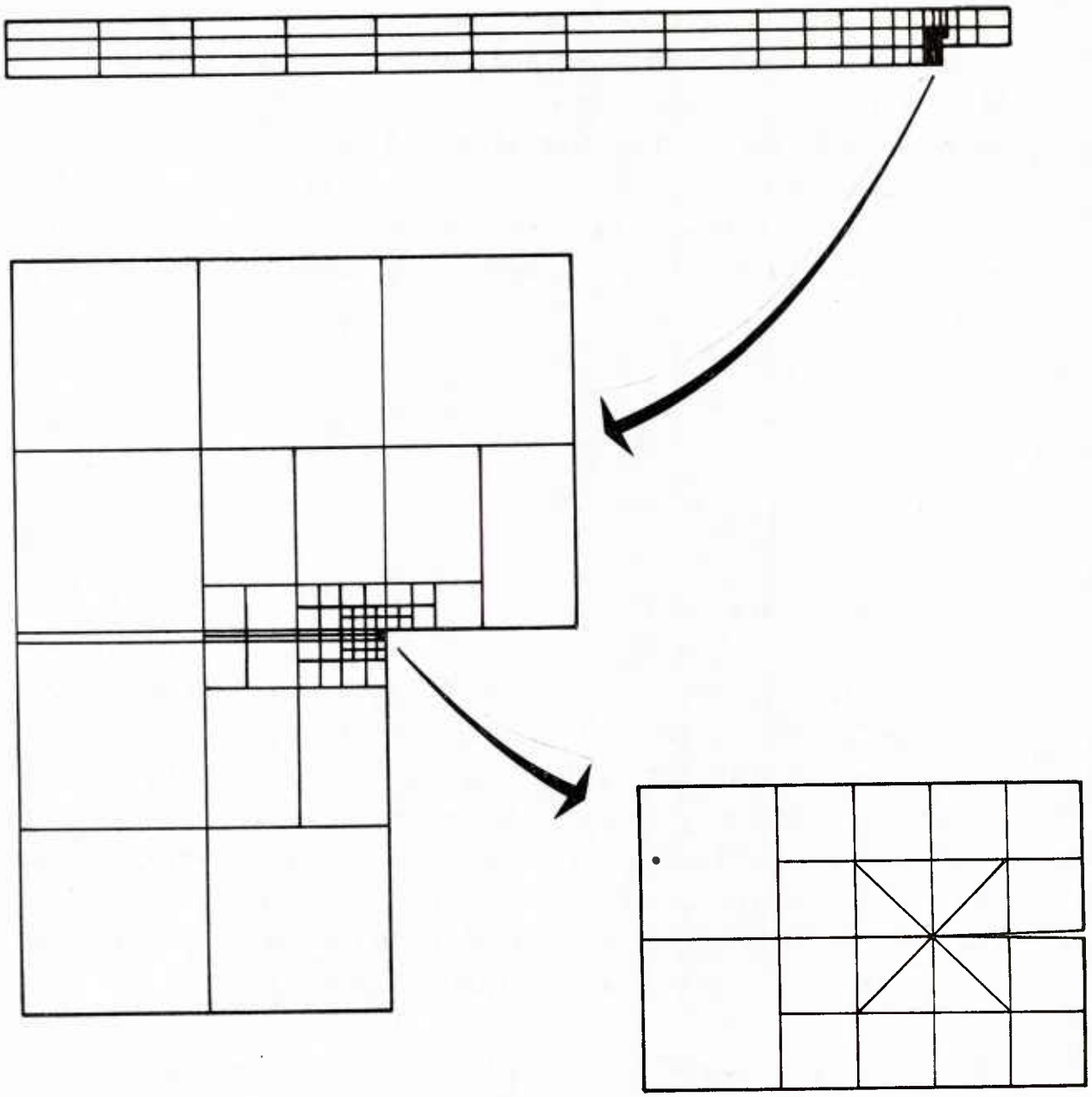

Figure 16. Finite Element Model of Cracked Lap Shear Specimen, CLS_1

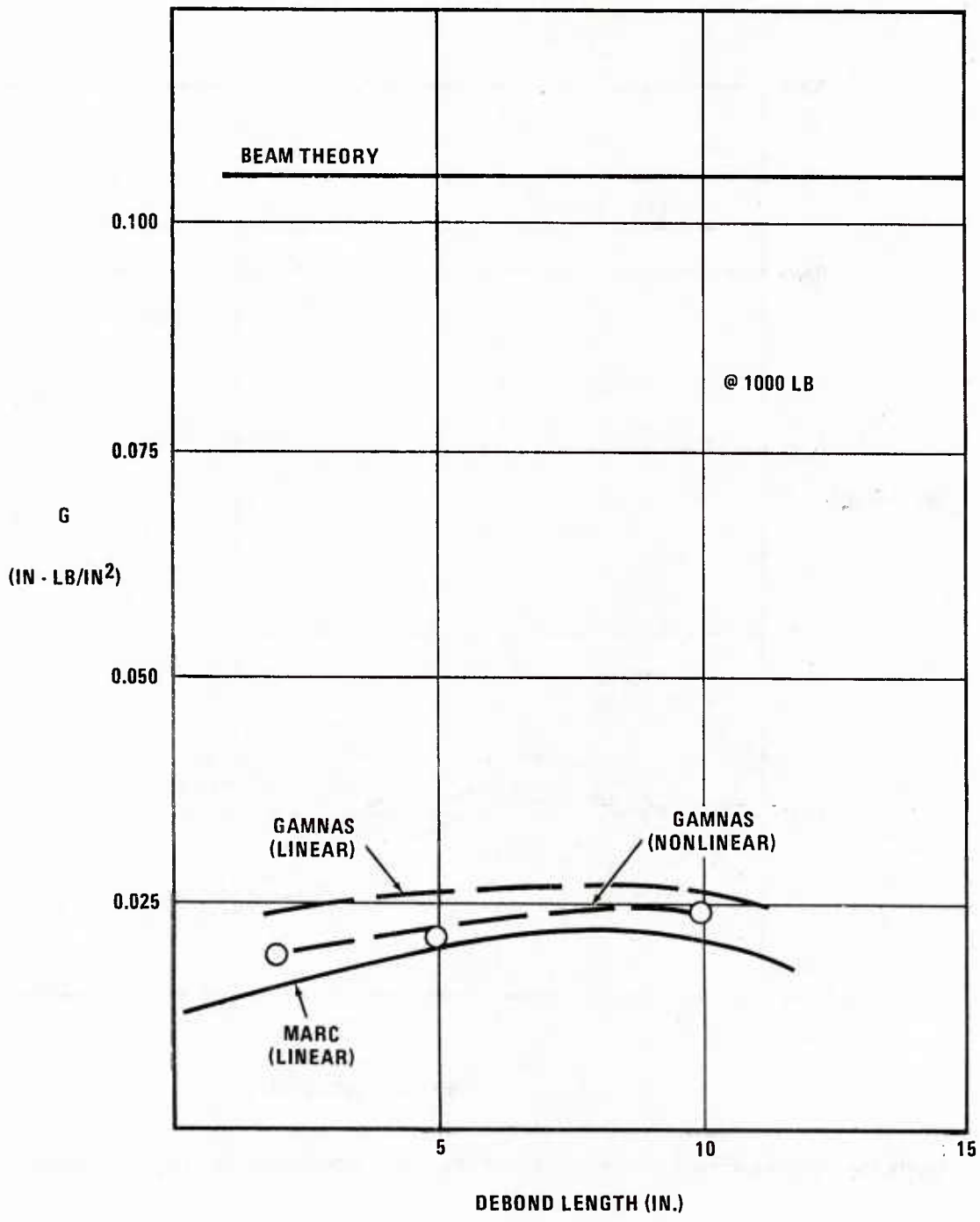

Figure 17. Predicted Crack Length Dependence of Strain Energy Release Rate for CLS_1 Specimens

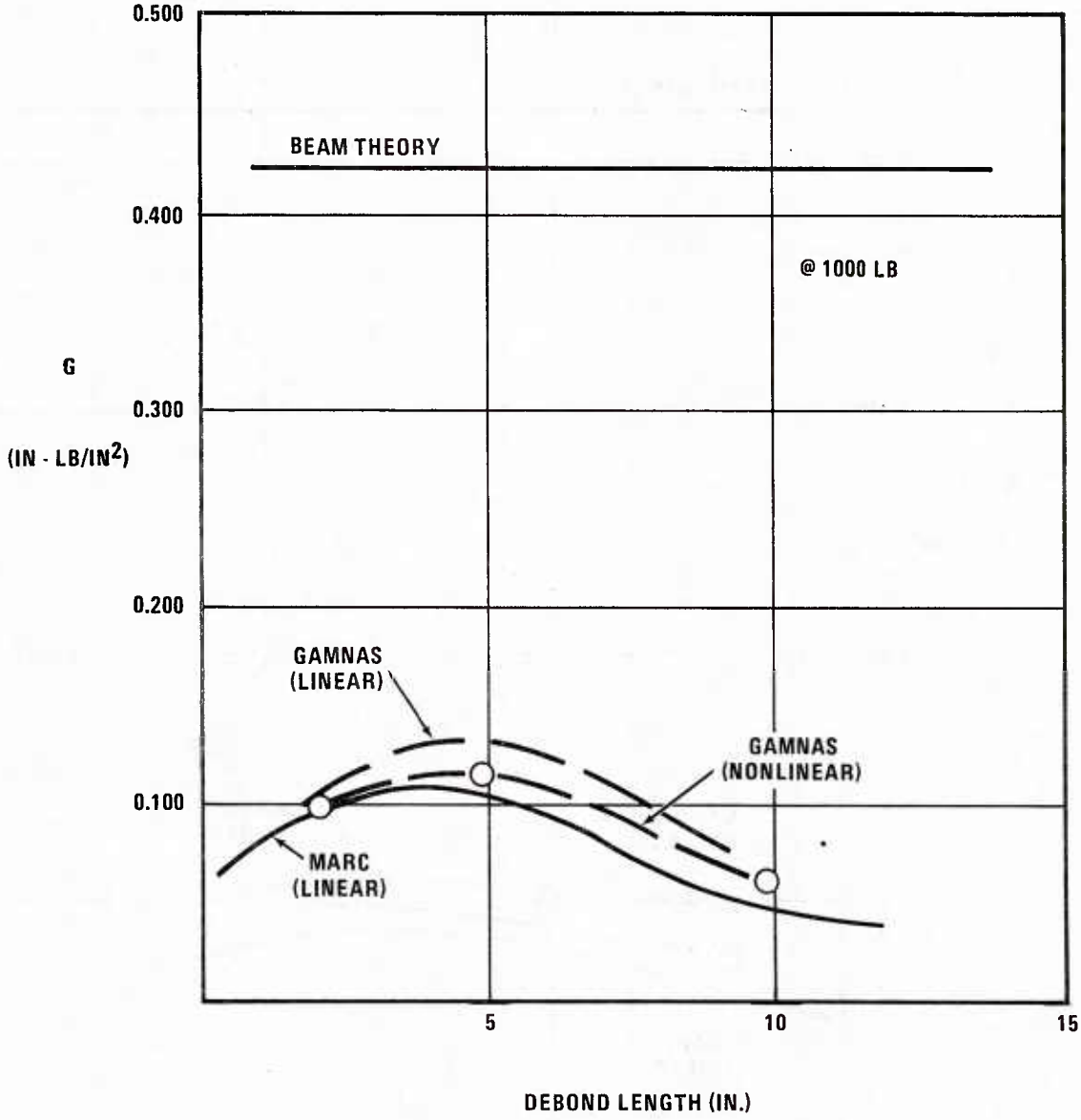

Figure 18. Predicted Crack Length Dependence of Strain Energy Release Rate for CLS_2 Specimens

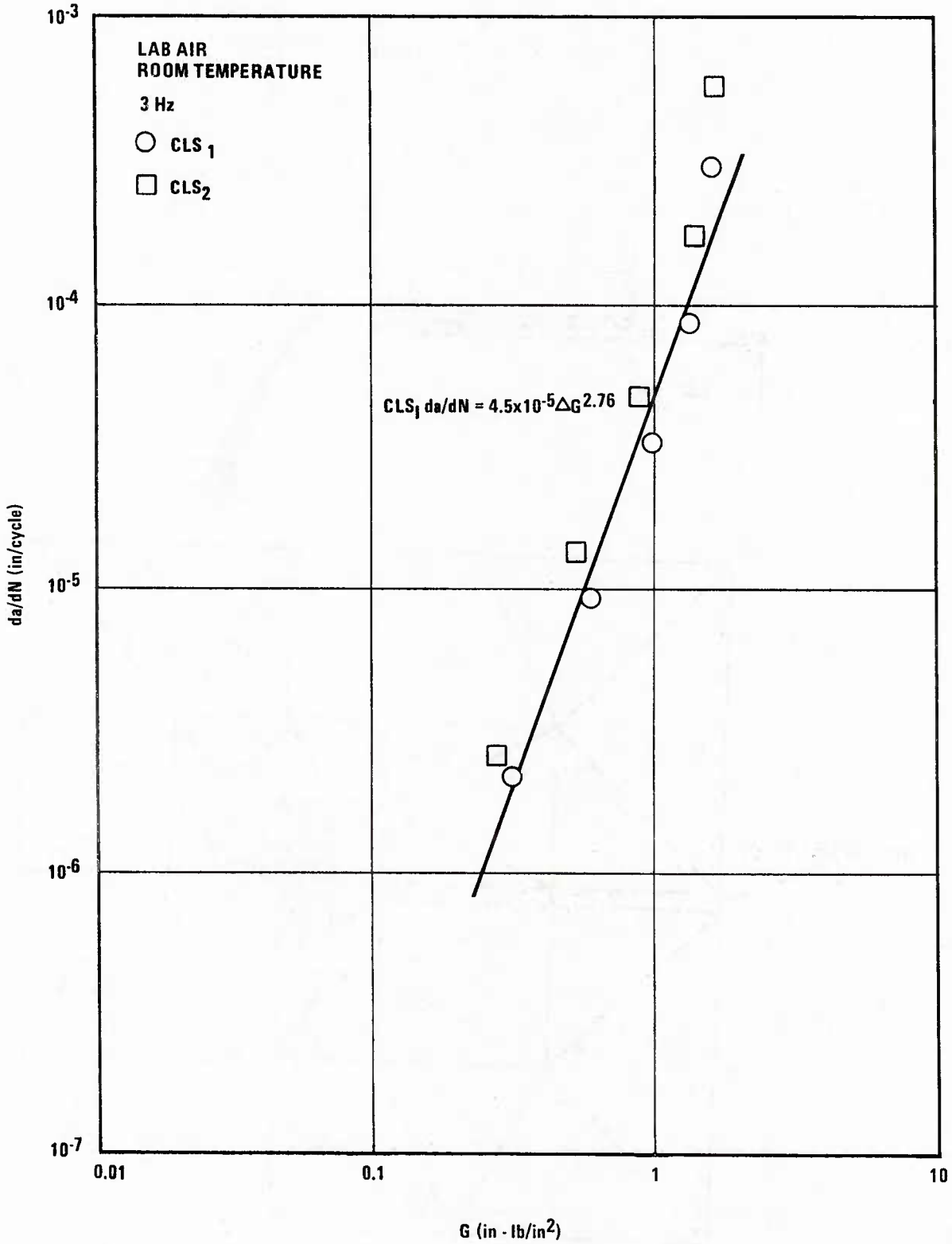

Figure 19. Comparison of CLS_1 and CLS_2 Crack Growth

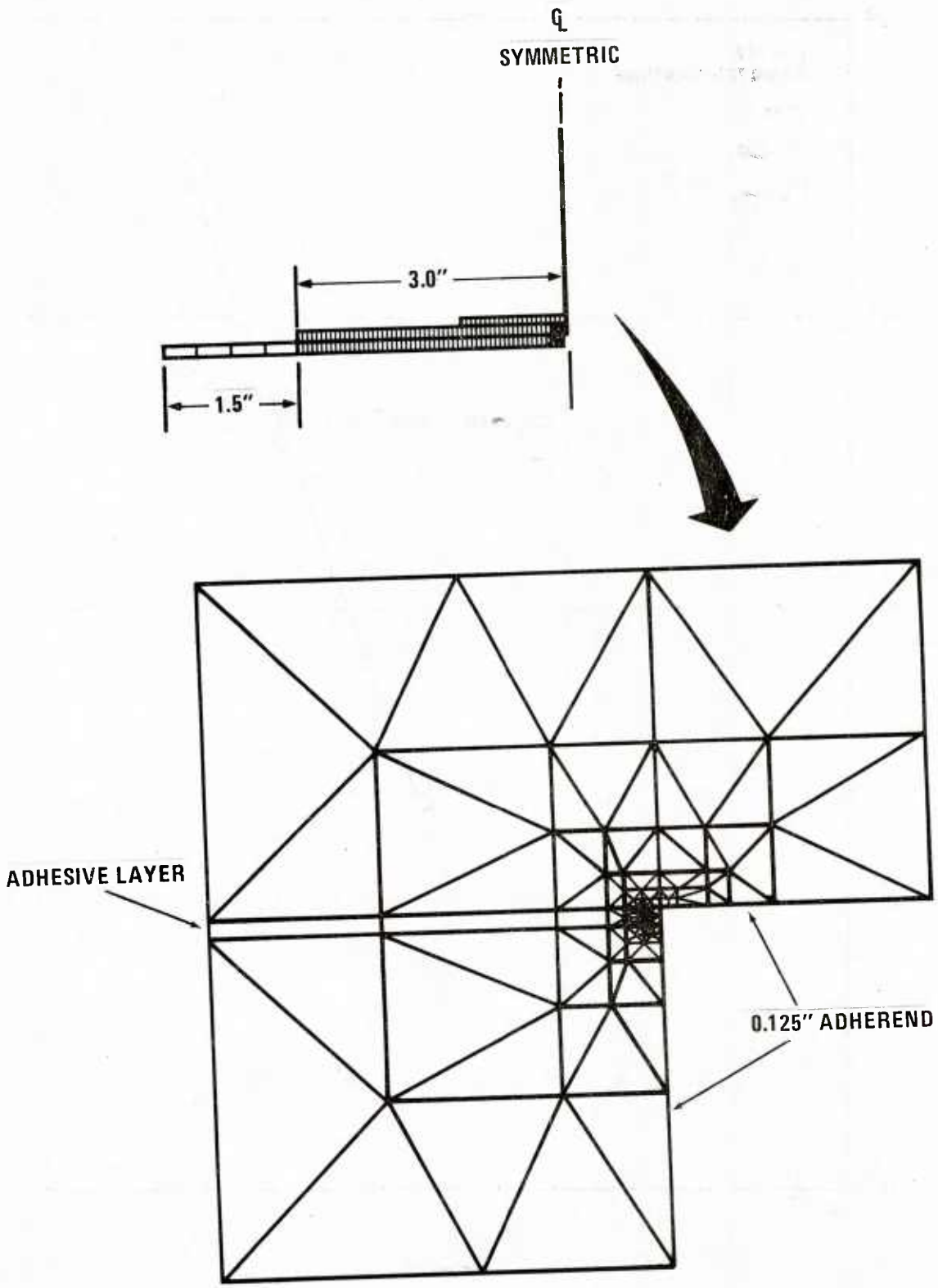

Figure 20. Finite Element Representation of the Adhesive Test Elements

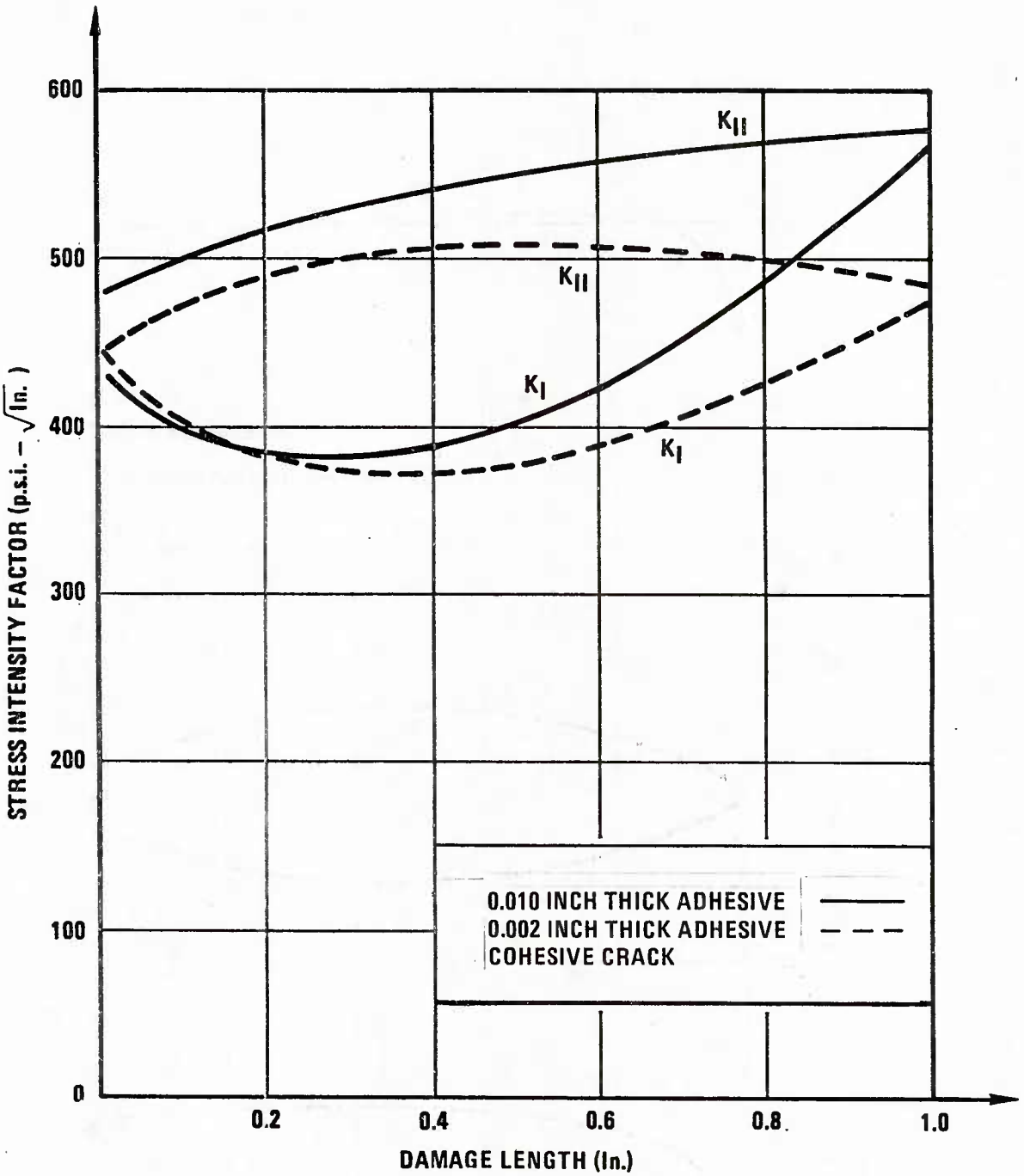

Figure 21. Variation of Stress Intensity Factors for Two Adhesive Layer Thicknesses

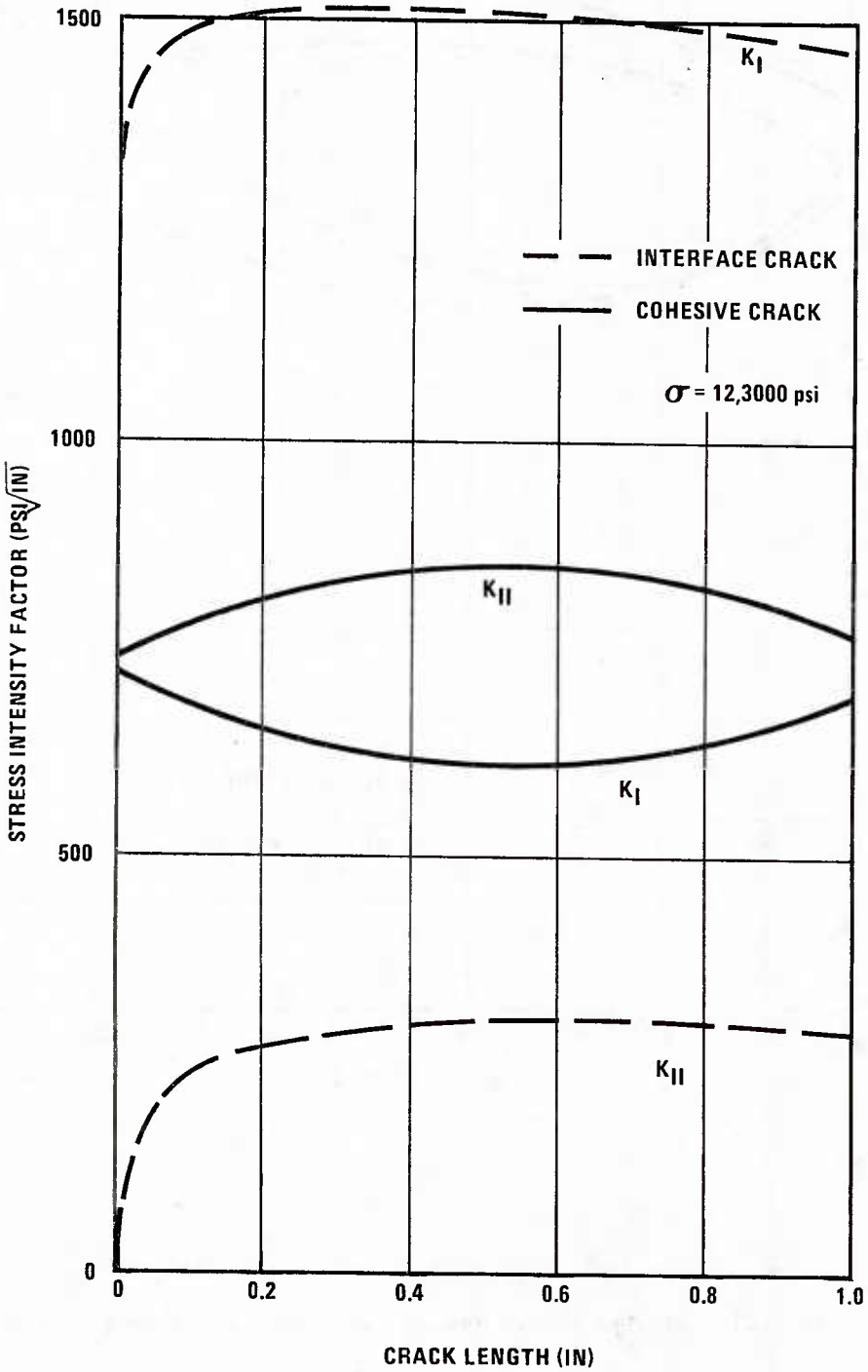

Figure 22. Variation of Stress Intensity Factors for Cohesive and Interface Cracks

Table 3. Comparison of Finite Element Analyses of Adhesive Test Elements at σ = 12.3 ksi

CODE	ANALYSIS	CRACK LENGTH (in.)	G in-lb/in^2
MARC	LINEAR	1.0	16.6
MARC	LINEAR	0.1	10.5
NASTRAN	NONLINEAR	1.0	7.8
NASTRAN	NONLINEAR	0.1	8.0
GAMNAS (Dataguru)	LINEAR	1.0	0.31
GAMNAS (Whitcomb)	NONLINEAR	1.0	2.0

felt this estimate, which accounts for geometric nonlinearity, is the most accurate of the ones they produced, and because it falls in the middle of the many disparate analyses available.

We assumed that stress intensity factor scales linearly with load. It follows that the strain energy release rate scales according to:

$$G = \left(\frac{\sigma}{12,300}\right)^2 2.0 \qquad (3)$$

Since $\Delta\sigma = (1-R)\ \sigma_{max}$, the range of strain energy release rate is related to the stress range by:

$$\Delta G = \frac{1+R}{1-R}\left(\frac{\Delta\sigma}{12,300}\right)^2 2.0 \qquad (4)$$

Material properties are taken to be those shown in Figure 19 for the CLS specimen. Thus, the crack growth rate can be expressed as:

$$\frac{da}{dN}\ (\text{in/cycle}) = 4.5\text{x}10^{-5}\left[\Delta G\left(\frac{\text{in-lb}}{\text{in}^2}\right)\right]^{2.76} \qquad (5)$$

No load interaction models were used. Cracking was assumed to be symmetric and located at the centerline, as indicated by cracks C1 and C2 in Figure 23. Cracks C3 and C4, if they occur, were assumed to affect only the critical crack length, not the growth of the central cracks. Finally, cycle-by-cycle crack growth predictions were made for the NOR 1 spectrum and maximum spectrum stresses of 24 and 30 ksi. The results are shown in Figure 24.

2.4.3 Cast Specimens

Stresses in the cast specimens were computed using simple axial and bending stress calculations. For hole/fastener combinations at the lower end of specified tolerance limits, the graphite-epoxy strap was estimated to carry one-twelfth of the total load at maximum spectrum load. This implies an average bearing stress in the fastener holes equal to 4/3 the nominal axial stress in the casting. These stress ratios were used throughout the crack growth analysis. The strap load also implies induced bending under axial load due to the non-symmetric placement of the strap. Bending stresses were calculated assuming the strap load has a line of action along the casting/strap interface.

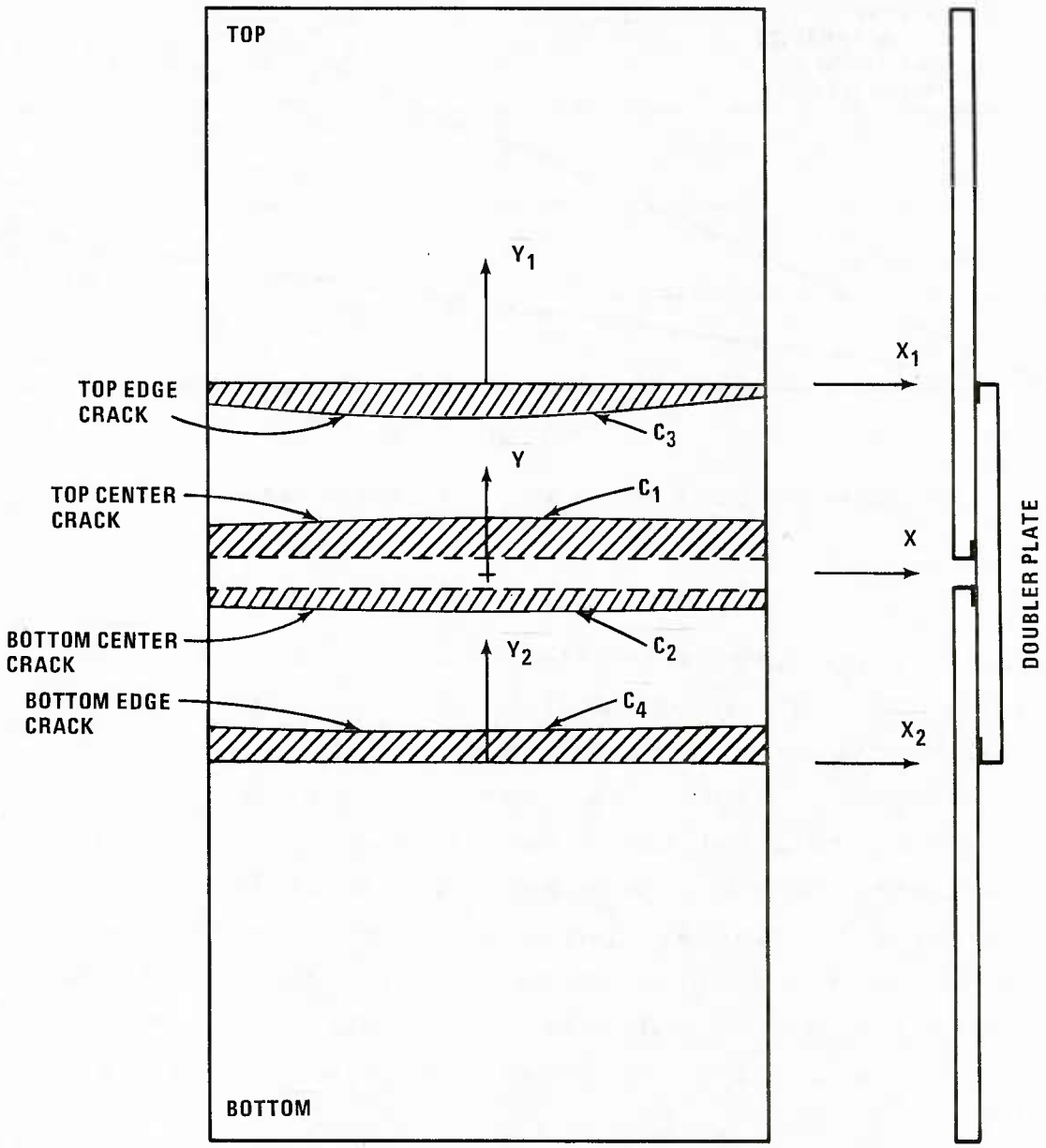

Figure 23. Strap Joint Crack Identification

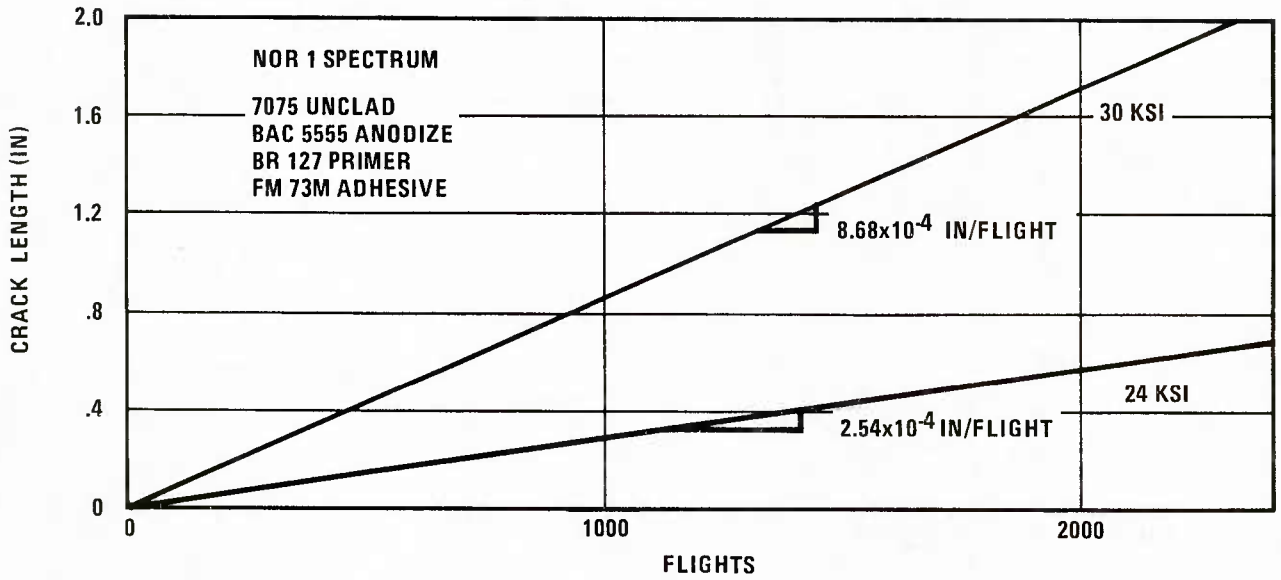

Figure 24. Crack Growth Predictions for Adhesive Test Element

Initial flaw assumptions for the cast specimen were as given in Figure 25. The loaded bolt-hole was assumed to be the critical location. Corner cracks initiating at the highest-stressed corner of the bolt-hole (i.e. away from the strap) were considered to be most likely. Both symmetric and unsymmetric cracking were modeled. A surface crack was also modeled to simulate possible casting defects. The fillet at the tee section was chosen as a possible initiation site due to the influence of the local geometry on stress during loading and metal flow and cooling during casting.

According to the spectrum fatigue test plan, crack growth analyses for the cast specimen were conducted at two load levels of the GAR 1 spectrum plus one load level of the NOR 1 spectrum. These were permuted along with critical flaw type and location to produce the analyses shown in Table 4.

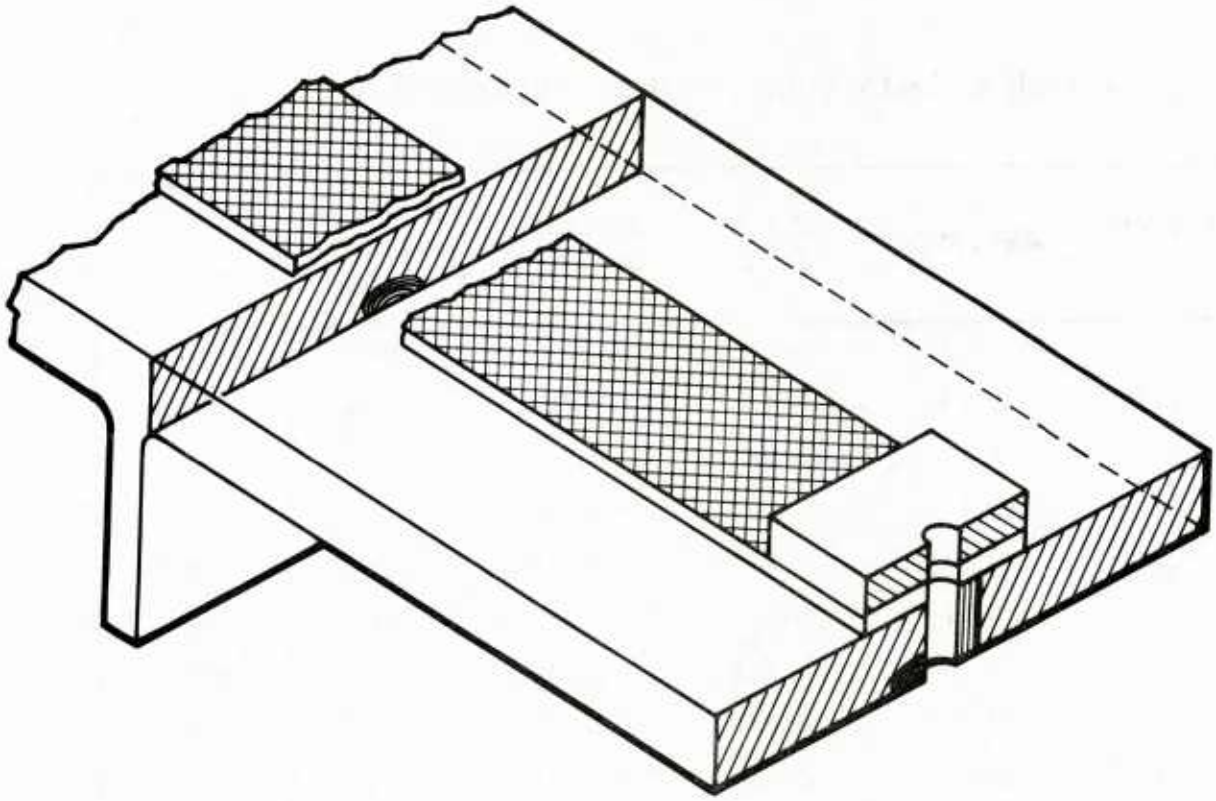

Figure 25. Initial Flaw Assumptions for Cast Test Element

Using similar procedures as for the baseline specimens, crack growth predictions for the cast specimens were conducted. The crack growth rate parameters obtained are given in Table 5. Figures 26 and 27 summarize the crack growth predictions for the cast specimens.

Table 4. Cast Specimen Crack Growth Analysis Results

ANALYSIS NO.	SPECTRUM	CRACK TYPE	NUMBER OF FLAWS	MAXIMUM SPECTRUM STRESS (KSI)	INITIAL CRACK LENGTH
C1	GAR 1	SURFACE FLAW	SINGLE	39.88	0.010
C2	GAR 1	SURFACE FLAW	SINGLE	32.85	0.010
C3	NOR 1	SURFACE FLAW	SINGLE	35.19	0.010
C4	GAR 1	CORNER	SINGLE	42.5	0.001
C5	GAR 1	CORNER	DOUBLE	42.5	0.001
C6	GAR 1	CORNER	SINGLE	35.0	0.001
C7	GAR 1	CORNER	DOUBLE	35.0	0.001
C8	NOR 1	CORNER	SINGLE	37.5	0.010
C9	NOR 1	CORNER	DOUBLE	37.5	0.010
C10	GAR 1	THROUGH	DOUBLE	34.0	0.001
C11	GAR 1	THROUGH	DOUBLE	28.0	0.001
C12	NOR 1	THROUGH	DOUBLE	30.0	0.010

2.5 INSPECTION PROCEDURES

2.5.1 Baseline Specimens

Critical initial damage was located at the fastener holes in the baseline specimens. Eddy current techniques and dial bore gauge measurements were used for measuring fastener hole quality in these holes. These inspection procedures are described below:

Eddy Current - Eddy current procedures for inspecting fastener hole quality in baseline coupons were similar to

Table 5. A357 Crack Growth Rate Parameters

ANALYSIS NO.	SPECTRUM	CRACK TYPE	MAXIMUM SPECTRUM STRESS (KSI)	b	Q
C1	GAR 1	SURFACE	32.85	1.17	1.0×10^{-4}
C2	GAR 1	SURFACE	39.88	1.26	2.3×10^{-4}
C4, 5	GAR 1	CORNER	42.5	1.12	1.1×10^{-3}
C6,7	GAR 1	CORNER	35.0	1.09	6.1×10^{-4}
C10	GAR 1	THROUGH	34.0	0.62	1.4×10^{-4}
C11	GAR 1	THROUGH	28.0	0.64[1]	9.0×10^{-5}
C3	NOR 1	SURFACE	35.19	1.57[1]	4.6×10^{-5}
C8, 9	NOR 1	CORNER	37.5	0.82	6.3×10^{-5}
C12	NOR 1	THROUGH	30.0	0.42	1.9×10^{-5}

1 VERY SLOW CRACK GROWTH

those described in the "Fastener Hole Quality" program [4]. An automated eddy current inspection unit was used for inspecting fastener holes. The unit consists of an Automation Industries EM 3300 eddy current unit, a mini-scanner head and a dual channel recorder. The eddy current signal, after being filtered and amplified, is sent to a dual channel recorder.

Considerable insight was gained during the Fastener Hole Quality program into the types of initial defects that most seriously affect the fatigue behavior of fastener holes. The axial or vertical scratch in a fastener hole has been identified as an initial defect that significantly affects the fatigue behavior of fastener holes under no-load

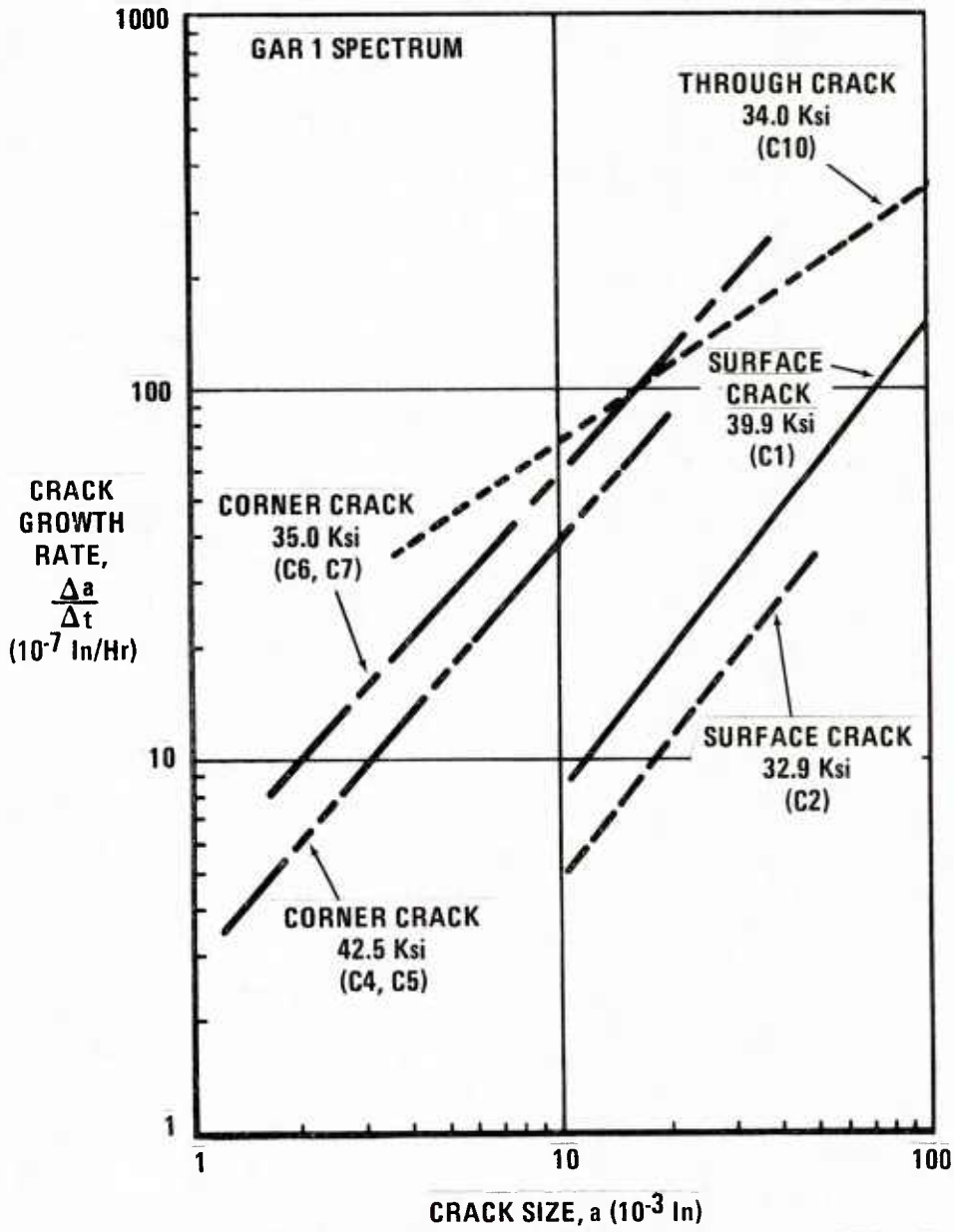

Figure 26. Summary of Cast Crack Growth Predictions – GAR 1 Spectrum

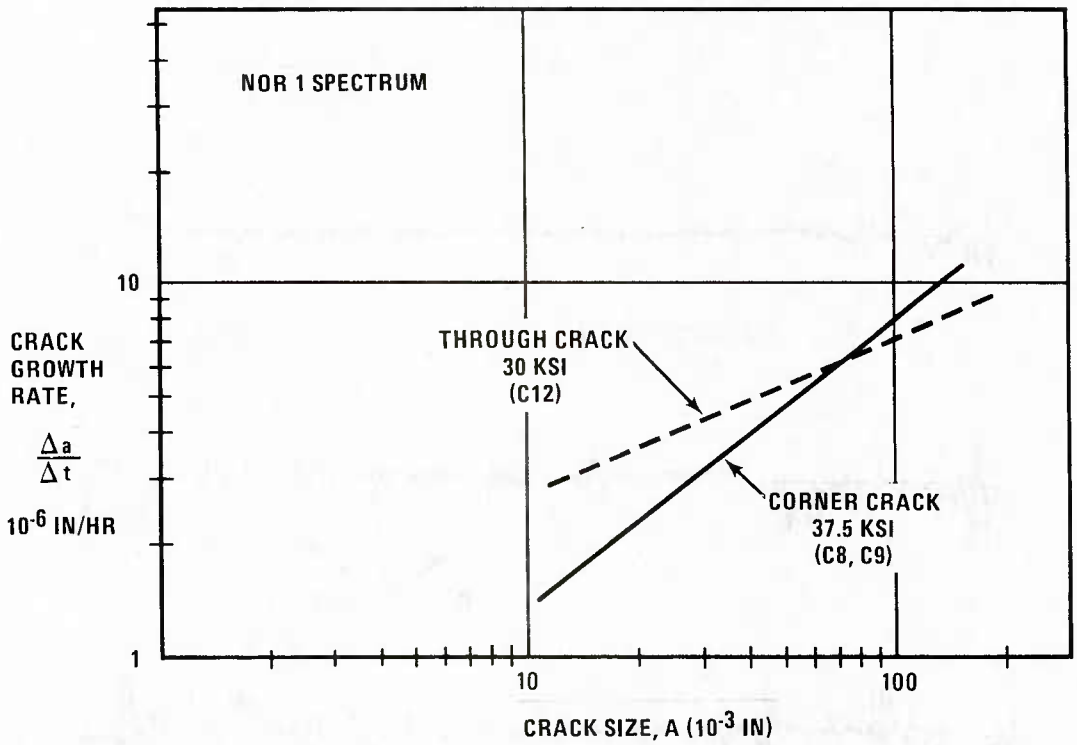

Figure 27. Summary of Cast Crack Growth Predictions – NOR 1 Spectrum

transfer conditions. Consequently, the eddy current technique has been optimized to detect axial scratches. Shown in Figure 28 are eddy current signatures of typical manufacturing induced axial scratches. A signal-to-noise ratio of about 7 has been achieved in the detection of this type of initial defect.

Despite the sensitivity of eddy current inspection, it is difficult to detect some of the smallest axial scratches or voids which can adversely affect fatigue performance. It is possible, however, to monitor variations in hole dimensions, such as hole out-of-roundness, with eddy current inspection. Also, surface roughness can easily be detected.

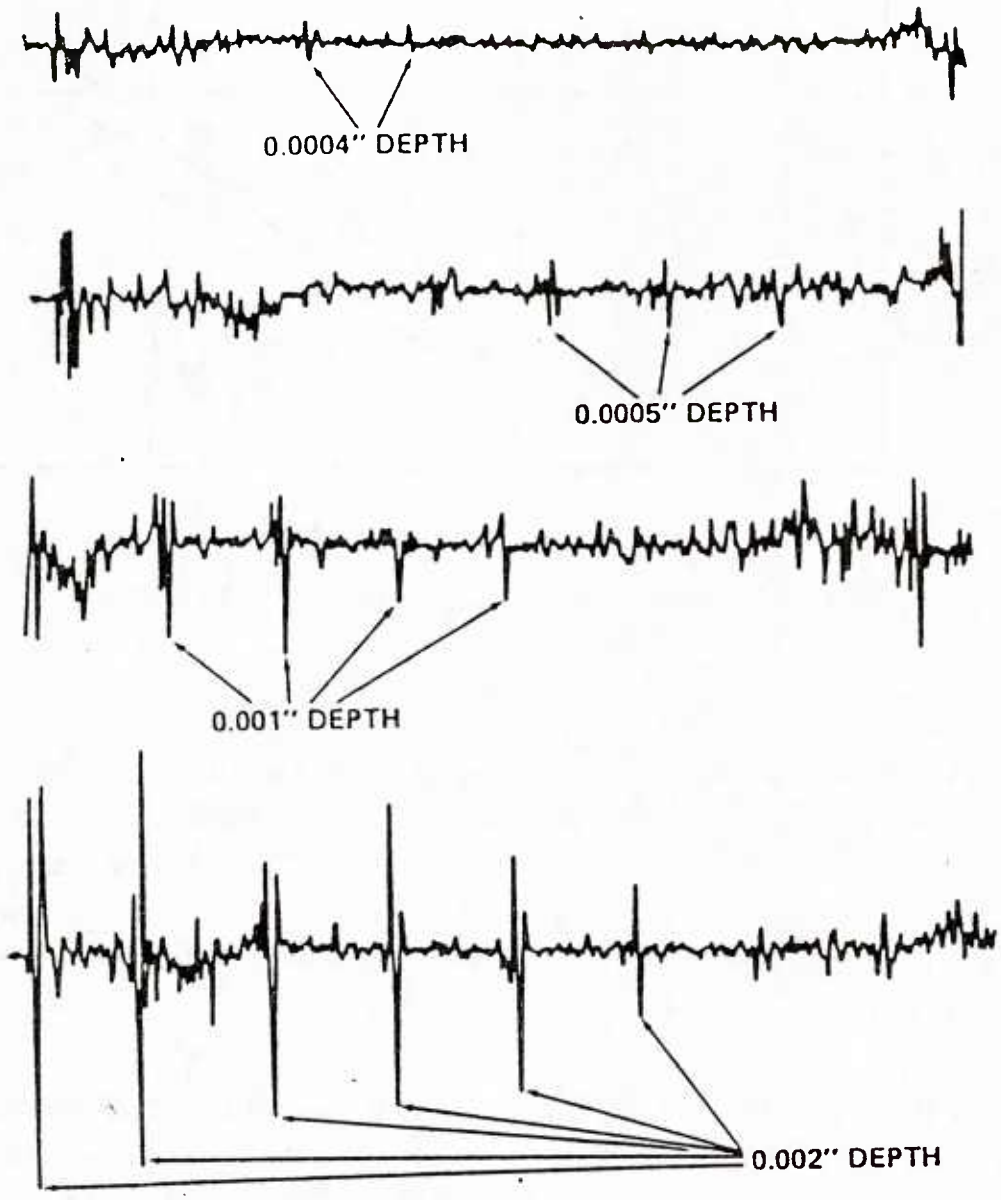

Figure 28. Sensitivity of Eddy Current to Surface Defects

Dial Bore Gauge - A dial bore gauge (Brice Model No. 1) was used to measure the diameter of the fastener holes at different orientations (Figure 29), and thus, give a relative measure of out-of-roundness (OOR). Measurements were taken at different depths in the hole, also, to determine if hole tapering was present. Numbering of the holes for dial bore gauge and eddy current measurements were in accordance with Figure 30.

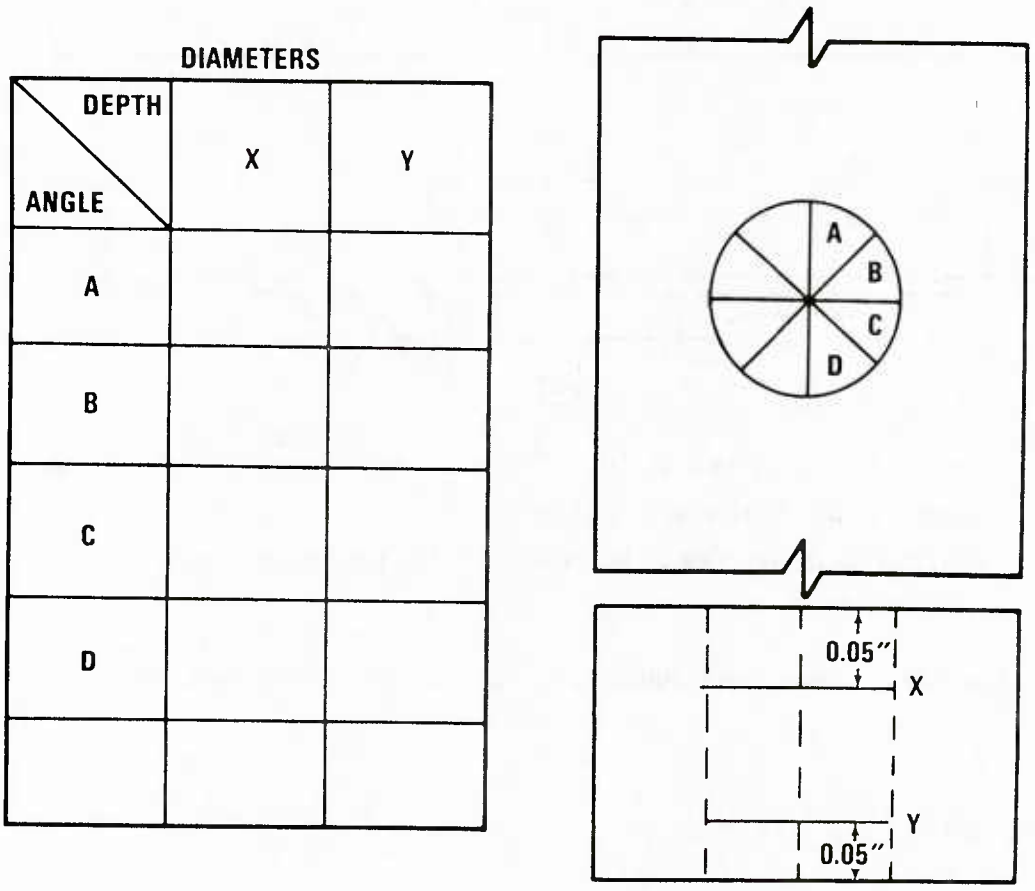

Figure 29. Dial Bore Gauge Inspection Scheme

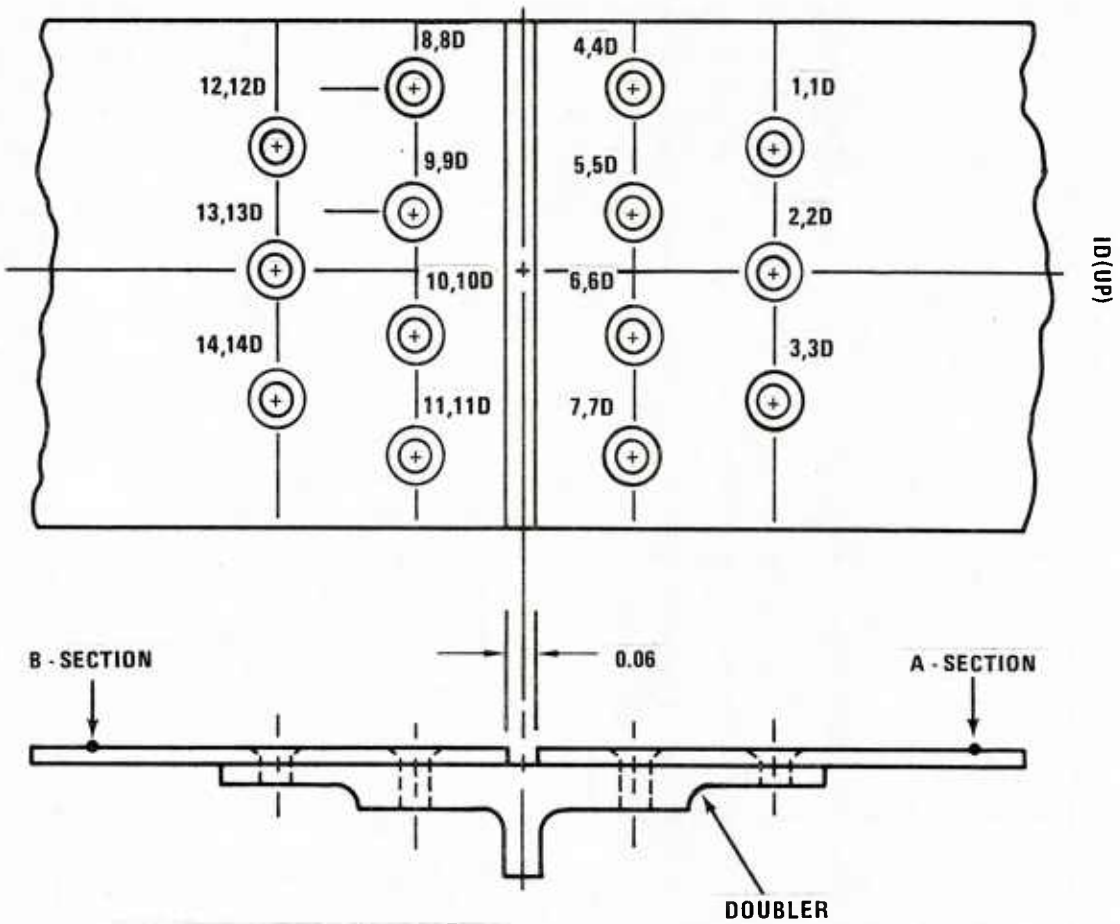

Figure 30. Fastener Hole Identification for Conventionally-Fastened Test Element

2.5.2 Adhesive Specimens

For the adhesively bonded specimens, ultrasonic inspections were performed on every specimen in the transmission mode. Porosity, disbonds and voids (absence of adhesive) can be detected by this method.

Ultrasonic C-scans were taken with the samples immersed in an Automation Industries research tank. Measurements were made with 5MHz transducers with a separation of 5.0 inches. A flaw level of 20% was used for these scans. Radiographic inspection was used as a second method of inspection. Although not as sensitive as ultrasonic inspection, gross porosity and voids could be detected using x-rays. Adhesive-thickness measurements were also made on selected unscrimmed coupons. A sheet micrometer was used for these measurements.

2.5.3 Castings

The two primary inspection techniques for inspecting the cast coupons were x-ray and eddy current. For castings, radiography is the most useful method for detecting the types of defects which might be expected, including porosity, inclusions, and some planar defects such as shrinkage cracks. The test section of each casting was inspected using three exposures: one normal to the test section, and one for each fillet at the base of the tee. Specimens were x-rayed according to MIL-C-6021, Grade B, radiographic quality. This inspection technique is not especially sensitive, however, to small defects in the bore of fastener holes.

Eddy current inspection of the fastener holes was performed in order to try to find small defects in the bore of the hole. Eddy current techniques used for the castings were identical to those described previously for the baseline coupons. In addition, dial bore gauge readings were taken on selected specimens. Numbering of the holes and angle orientation for eddy current and dial bore gauge measurements are shown in Figure 31.

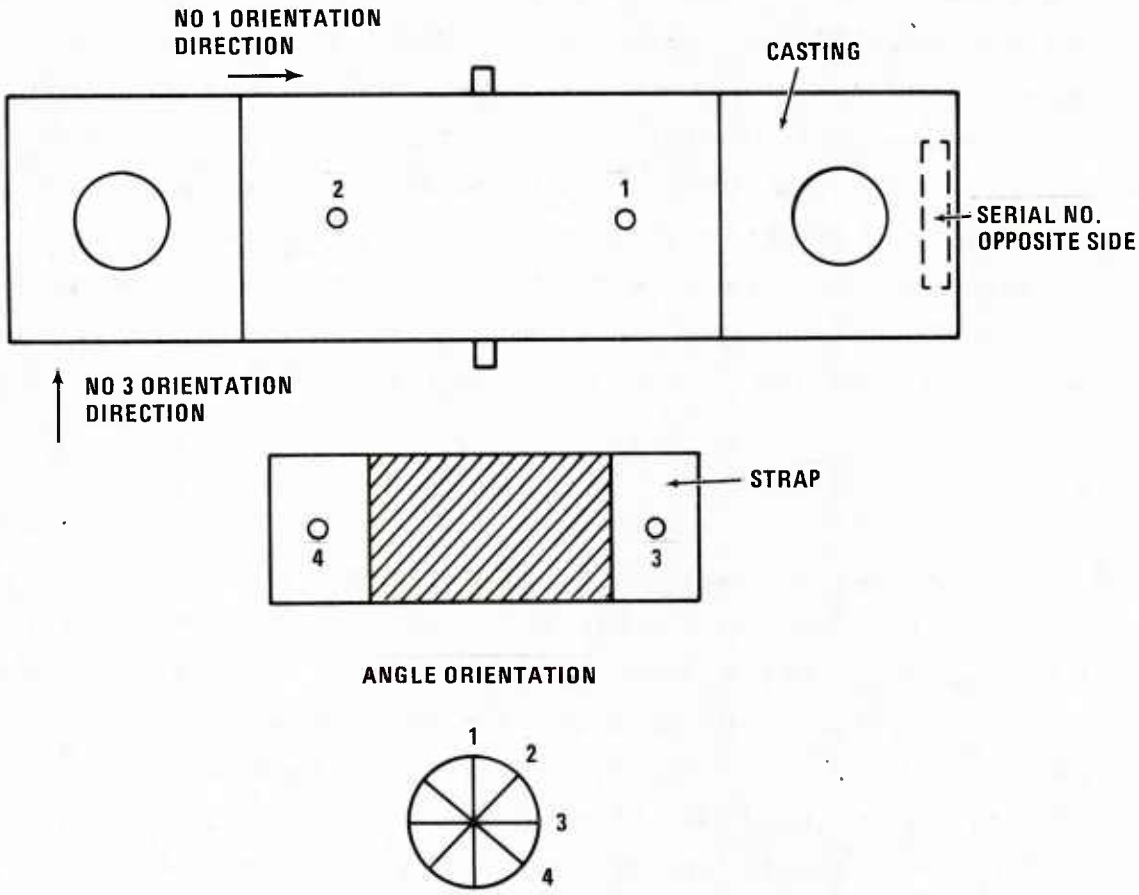

Figure 31. Cast Coupon Eddy Current and Dial Bore Gage Orientation

2.6 SPECTRUM FATIGUE TESTING

All specimens were spectrum fatigue tested for the equivalent of two lives or until failure, whichever occurred first. Two equivalent lives for all F-16 spectra represent 16,000 flight hours. For the NOR 1 spectrum, two lives represent 27,000 flight hours, or 2560 flights. Following testing, unfailed specimens were reinspected (except Type B, specimens) and then monotonically tested to failure.

Testing was in computer-controlled test frames within the Metallurgical and Materials Research Laboratories. Load cells in these facilities are periodically calibrated under Air Force supervision. Test rates were set so that program and feedback loads agree to within two percent at all load levels.

Each specimen configuration includes a tee. Specimens which undergo compressive loads were laterally constrained through a mechanical connection to the tee. Connection was through a flexure bar to avoid introducing unwanted axial loads into the specimen.

The baseline and cast specimens were tested without instrumentation other than test frame load cells. Crack length measurements were made fractographically after specimen failure. Adhesively bonded specimens were periodically examined ultrasonically to determine crack length, as explained previously.

Table 6 summarizes the spectrum fatigue test plan. The experimental results obtained from the spectrum fatigue testing are presented in Sections 3.2 through 3.6.

2.7 FRACTOGRAPHY

2.7.1 Mechanically-Fastened Specimens

The NOR 1 spectrum produced easily distinguishable markings on the fracture surfaces of the 2124-T851 and 2024-T81 aluminum baseline specimens. Fractographic data were obtained using a Bausch and Lomb stereomicroscope and digital X-Y stage micrometers. The data were read continuously from the final crack length back to the origin.

Table 6. Spectrum Fatigue Test Matrix

					TOTAL
ADHESIVE SPECIMENS (TYPE A + A')	TYPE: SPECTRUM: STRESS: QUANTITY:	SCRIMMED NOR 1 30 KSI 19	SCRIMMED NOR 1 24 KSI 19	UNSCRIMMED NOR 1 30 KSI 20	58
BASELINE SPECIMENS (TYPE B + B')	TYPE: SPECTRUM: STRESS: QUANTITY:	SEALANT NOR 1 30 KSI 16	SEALANT NOR 1 24 KSI 19	NO SEALANT NOR 1 24 KSI 10	45
CAST SPECIMENS (TYPE C)	SPECTRUM: STRESS: QUANTITY:	NOR 1 30 KSI 50	GAR 1 34 KSI 20	GAR 1 28 KSI 20	90
					193

If faying surface sealant was present on the fracture surface, then the specimens were soaked overnight in Toluene. The softened sealant was then easily removed with a synthetic brush.

2.7.2 Cast Test Elements

Even after rearrangement of the GAR 2 spectrum, the fractographic surface was still too rough to read continuously from the final crack length back to the origin.

The point of origin of the crack was generally poorly detailed. The data were collected using a Zeiss universal microscope with digital X-Y stage micrometers and readout. The cast surfaces were best examined using brightfield imaging, with Nomarski differential interference contrast. Data was collected in a discontinuous manner as follows: (1) the edge of the hole bore of the side with the most fractographic markings was designated to be the zero point; (2) the specimen surface was then systematically scanned until spectrum markings were observed; (3) definable crack growth increments (Δa) were then measured; (4) The distance between the center of the marked area and the bore hole was taken to be the crack length, a, at the time the marks were produced. This procedure, illustrated in Figure 32, was used in reading test elements tested with the GAR 2 and NOR 1 spectra. The final crack length was generally the only data which could be unambiguously obtained for the GAR 1 spectrum specimens.

2.7.3 Adhesive Specimens

Adhesively bonded specimens could not be adequately examined by fractography, due to scrim fibers throughout the fracture surface.

Adhesively bonded specimens were periodically examined during testing to determine crack length. One method used was ultrasonic scanning to detect progressive adhesive disbonding or cohesive fatigue failure. The ultrasonic pulse echo technique was used to monitor fatigue damage in these spectrum loaded specimens. A Mark IV Ultrasonic Tester (Sonic Instruments, Inc.) was used in conjunction with a 10MHz contact transducer. Reflected signals from the

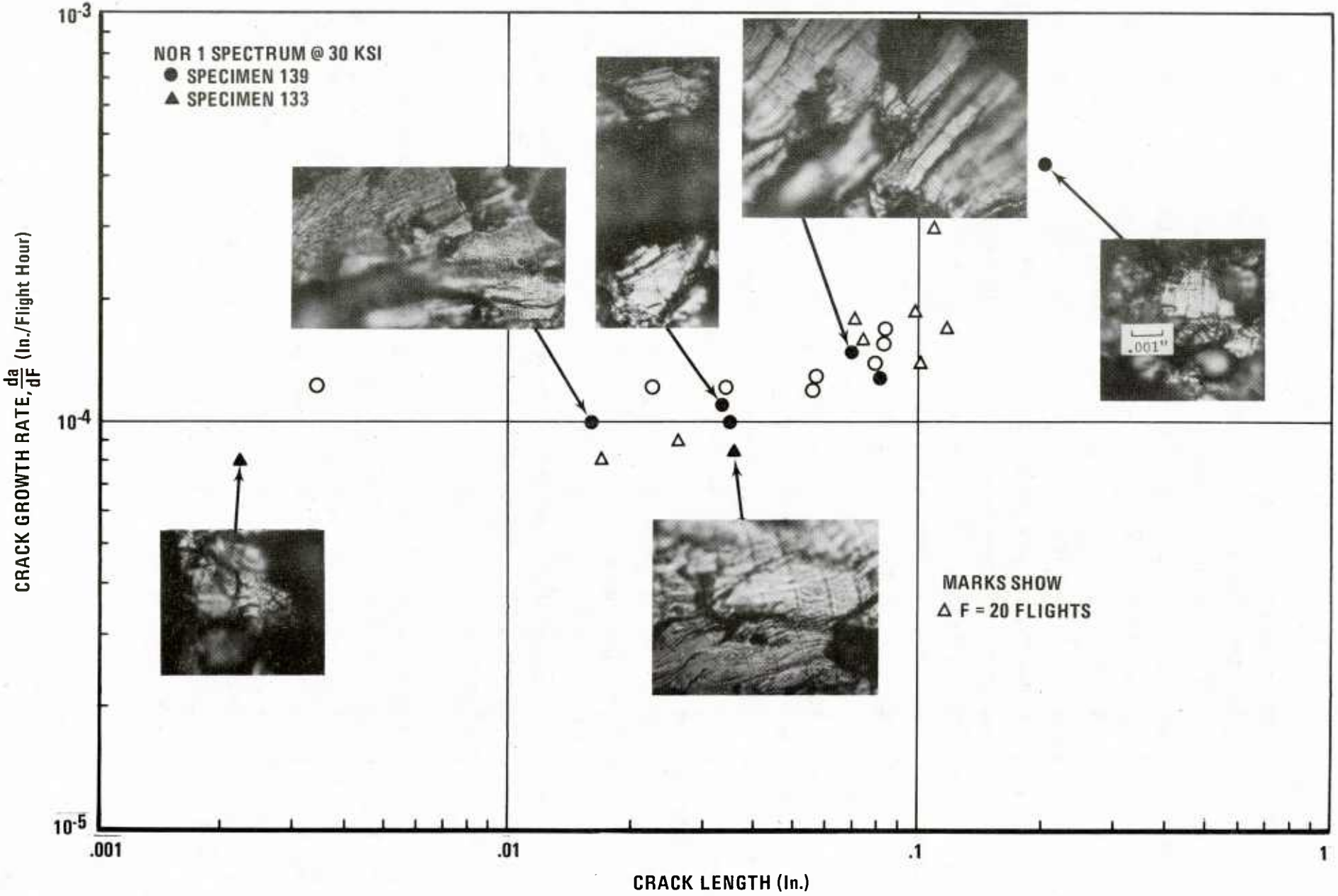

Figure 32. Scheme for Obtaining Crack Growth Rate Data in Castings

adhesive bondline were used to monitor debonding as a function of cycling.

Debond lengths were measured from the edge of the original bonded surfaces. Readings were taken at eight separate locations as shown in Figure 33. Each pair of readings measure the debond at one edge of an overlap. The locations were placed to correspond to the Gauss integration points for the 5-inch-wide specimen. This enabled the debond area (and average effective length) to be determined exactly for any shape of crack front, as long as the crack front profile could be represented by a cubic, or lesser order, function.

Compliance measurements were also made each time the debond was measured ultrasonically. These also showed relative debond lengths quite well. However, absolute crack length varied from specimen to specimen for a given compliance. This variation could be as much as 0.20 inch. Since this is larger than the error found from ultrasonic measurements, the crack lengths determined from the compliance measurements were not used for analysis.

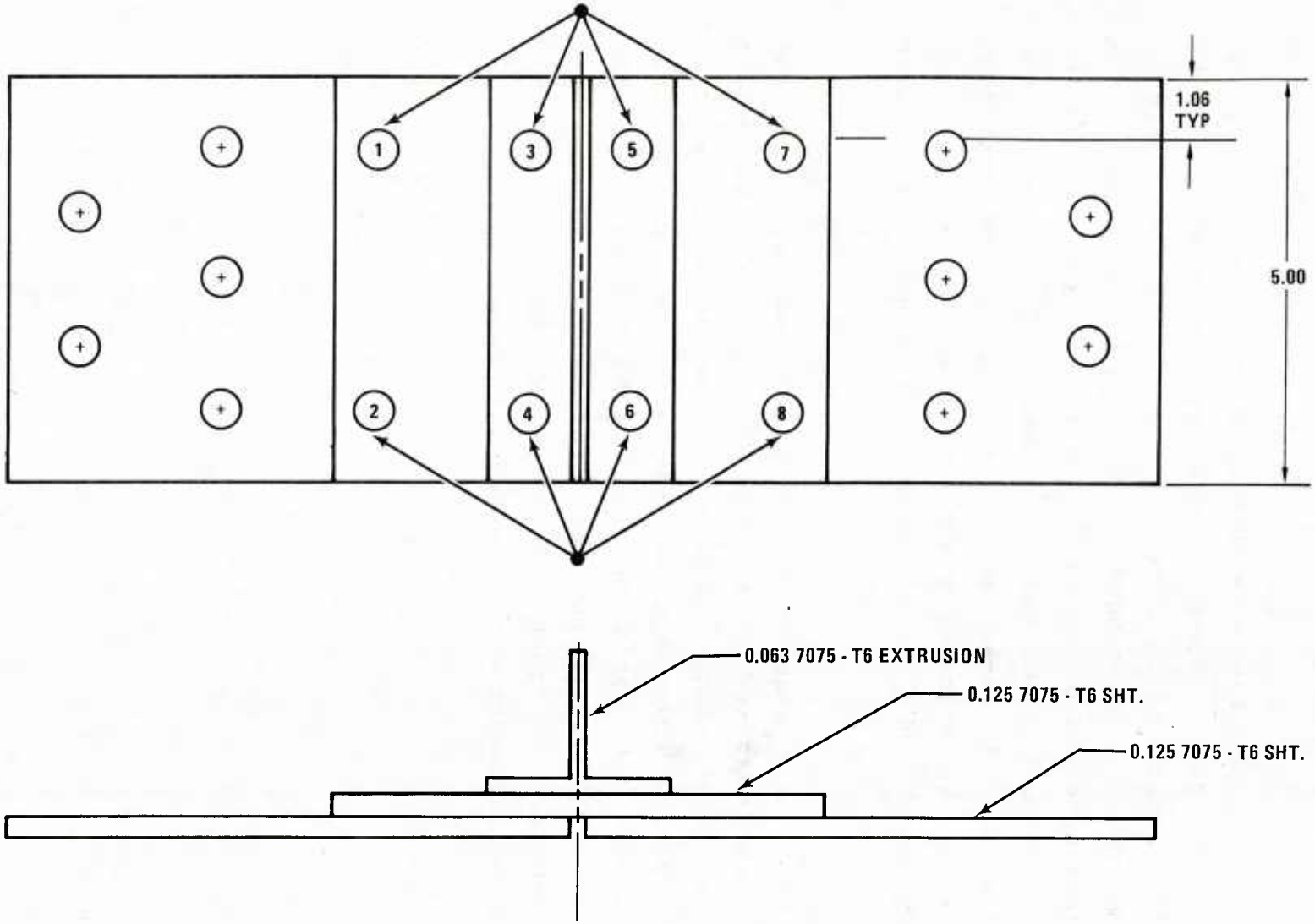

Figure 33. Locations for Ultrasonic Crack Length Readings

SECTION III

RESULTS

3.1 NONDESTRUCTIVE INSPECTION AND TEST RESULTS

3.1.1 Baseline Specimens

Inspection results for baseline coupons are shown in Tables 7, 8, and 9. Specimens are ordered from lowest to highest with respect to failure time. Columns headed TTCI, EIFS, and q indicate structural performance and are discussed in Sections 3.3 through 3.5. Also shown in Tables 7-9 are the locations of the failure origins. For the set of specimens containing no sealant, all failures occurred away from the fastener holes as in Figure 34. These coupons had fatigue crack origins at the mating surfaces between the doubler and the A- or B- sections. We did not anticipate this mode of failure, expecting the crack to initiate at the nearby hole. Since all NDI data was taken in regard to the fastener holes, no correlation could be made between inspection results and EIFS data for specimens with no sealant.

Typical eddy current scans are shown in Figure 35. In general, no correlation was observed between eddy current amplitude and EIFS. For specimens containing sealant, fatigue failure occured either in the highest stressed rows containing holes numbered 1, 2, or 3 or holes numbered 12, 13, 14 (see Figure 30). Eddy current results indicated that the hole quality was about the same in all of the holes.

Table 7 Test Results for Baseline Specimens Tested With NOR 1 Spectrum at 24 KSI (B24B)

Spec Number	Order of Failure	Failure Time (Flts)	Failure Location	TTCI @ a_o = .2 (Flt Hrs)	EIFS x 10^{-1} (In.)	Q_i x 10^{-4}	Inspection Results Out-of-Roundness (In.)
50	1	878.9	(a)	7068	.5228	1.268	.0014
45	2	888.7	(a)	7281	.4946	1.241	.0008
33	3	1028.9	(a)	8732	.3256	1.241	.0015
41	4	1053.1	(a)	8692	.3297	1.376	.0015
20	5	1068.8	(a)	9233	.2858	1.137	.0006
26	6	1078.8	(a)	8288	.3730	.9931	.0006
55	7	1098.8	(a)	9237	.2760	.8639	.0014
53	8	1098.8	(a)	9106	.2884	.7981	.0009
18	9	1198.8	(a)	10852	.1477	.9499	.0013
25	10	1438.7	(a)	10810	.1505	.6878	.0020
52	11	1452.5	(a)	11824	.09152	.7826	.0002
10	12	1538.7	(a)	12563	.05870	.7125	--------
35	13	1648.9	(a)	12441	.06355	.6249	.0014
51	14	1678.9	(a)	13961	.01796	.7599	.0015
6	15	1744	(a)	9925	.2158	.5504	.0012
5	16	1758.7	(a)	15641	.0004151	.7285	--------
38	17	1798	(a)	14629	.007377	.5955	.0015
16	18	2070.6	(a)	10256	.1898	.5650	.0003
36	19	2278.8	(b)	19609	-.06146	.7179	.0022

(a) Outer row of fastener holes in skin splice.
(b) Inner row of fastener holes in doubler.

Table 8 Test Results for Baseline Specimens Tested With NOR 1 Spectrum at 30 KSI (B30B)

Spec Number	Order of Failure	Failure Time (Flts)	Failure Location	TTCI @ a_o = .2 (Flt Hrs)	EIFS x 10^{-1} (In.)	Q_i x 10^{-3}	Inspection Results Hole Diameter (In.)
31	1	298.7	(a)	2965	.5595	.2101	<.254
44	2	368.9	(a)	3011	.5449	.2554	<.254
2	3	378.9	(a)	3303	.4569	.2443	<.254
14	4	398.7	(a)	3231	.4779	.3299	<.254
9	5	418.8	(a)	3849	.3157	.2877	<.254
17	6	436.9	(a)	2900	.5804	.2399	<.254
23	7	458.7	(a)	4361	.2096	.2116	<.254
42	8	498	(a)	4253	.2299	.1673	<.254
13	9	498.7	(a)	4255	.2295	.1529	One Hole > .254" Dia.
19	10	498.9	(a)	4819	.1348	.1666	<.254
11	11	519	(a)	4854	.1299	.2607	<.254
21	12	598.7	(a)	5099	.09803	.1476	<.254
27	13	598.7	(a)	4812	.1358	.1414	<.254
22	14	668.8	(a)	5121	.09551	.1463	<.254
7	15	898.8	(a)	8715	-.07775	.1789	One Hole > .254" Dia.
46	16	1283	(a)	9643	-.2111	.6378	<.254

(a) Outer row of fastener holes in skin splice

Table 9 Test Results for Baseline Specimens Tested With NOR 1 Spectrum at 24 KSI No Sealant (BNS 24B)

Spec Number	Order of Failure	Failure Time (Flts)	Failure Location	TTCI @ a_o = .2 (Flt Hrs)	EIFS x 10^{-5} (In.)	Q_i	Inspection Results Hole Diameter (In.)
3	1	1801.7	Edge of Hole	19004	.8648	.09668	Two Holes > .254" Dia.
24	2	2128.8	Doubler	22431	.6481	.05909	<.254
39	3	2658.7	Doubler	28039	.4396	.06993	<.254
21	4	2658.6	Doubler	28037	.4396	.06678	<.254
8	5	2670.3	Doubler	28150	.4365	.110	One Hole > .256" Dia.
54	6	3039	Doubler	32046	.3483	.04560	>.254
30	7	3308.8	Doubler	34892	.3004	.08579	Several Holes > .256" Dia.
49	8	3558.8	Doubler	37528	.2646	.04434	<.254
48	9	3708.8	Doubler	39114	.2462	.1158	<.254
40	10	3819	Doubler	40276	.2339	.07696	<.254

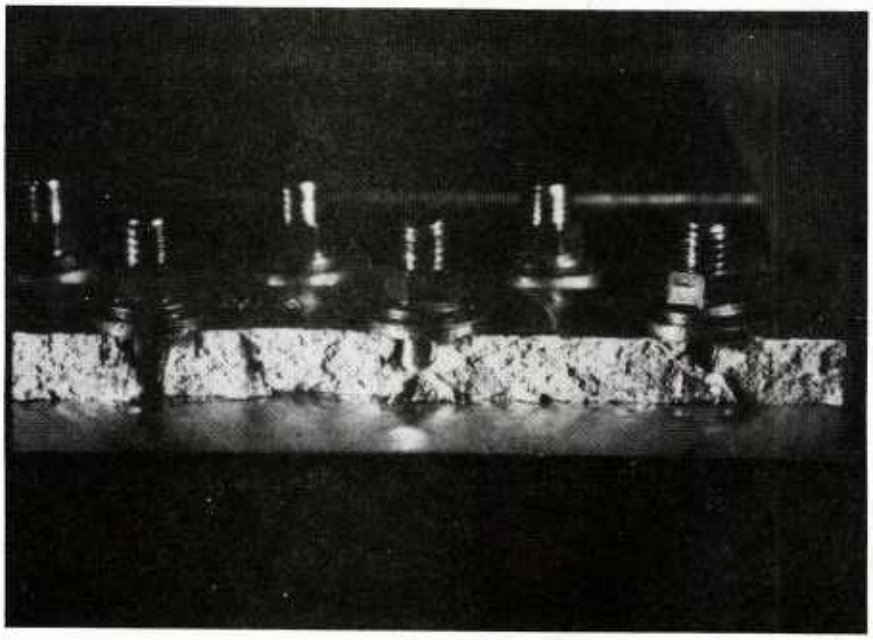

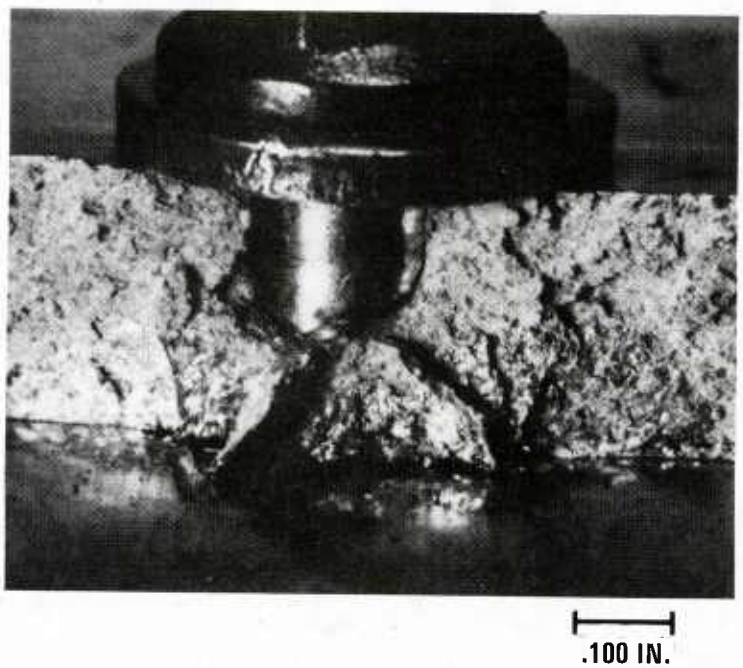

Figure 34. Fretting Fatigue Initiation in Short Transverse Orientation in 2124-T851 Plate. Baseline Specimens with no Sealant

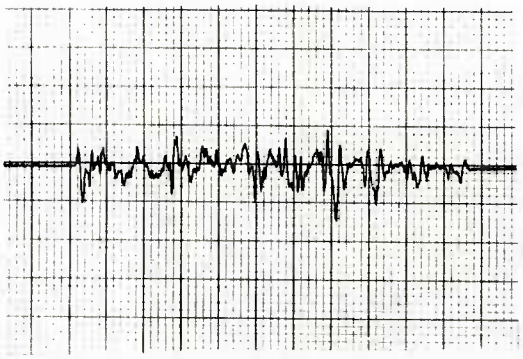

(a) Hole No. 1

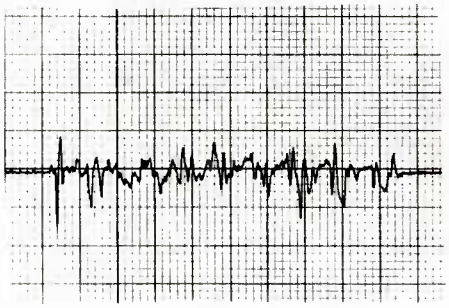

(b) Hole No. 2

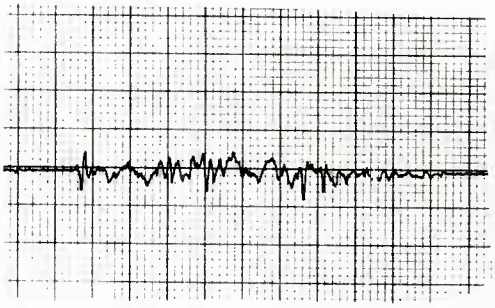

(c) Hole No. 3

Figure 35. Typical Eddy Current Scans of Holes in Baseline Specimens. Specimen No. 42, EIFS = .0183; (a) Hole No. 1, (b) Hole No. 2 and (c) Hole No. 3

Dial bore gauge results also indicated little correlation between hole quality parameters such as out-of-roundness or oversized holes with EIFS and TTCI. Results are shown in Figures 36 and 37 for complex splice coupons tested under the NOR 1 spectrum at a maximum spectrum stress of 24 ksi.

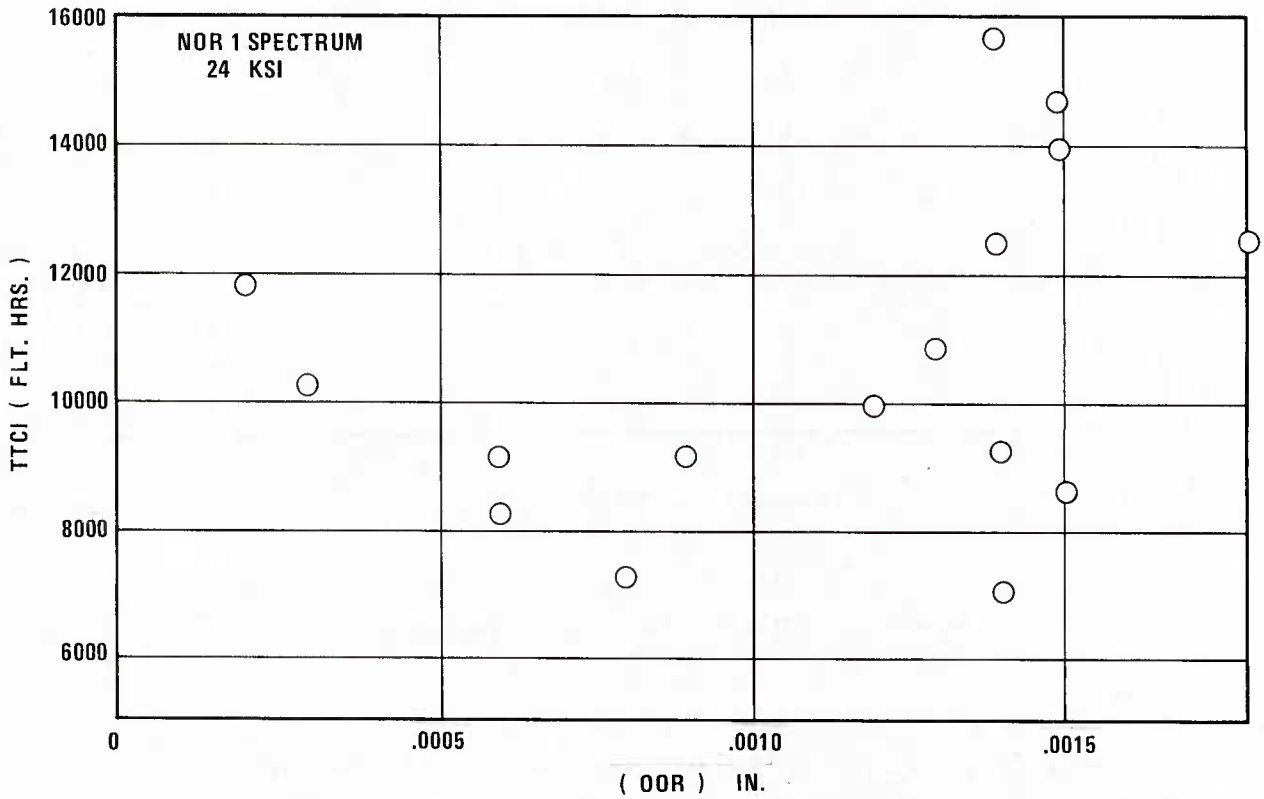

Figure 36. TTCI vs Hole Out-of-Roundness in Baseline Specimens

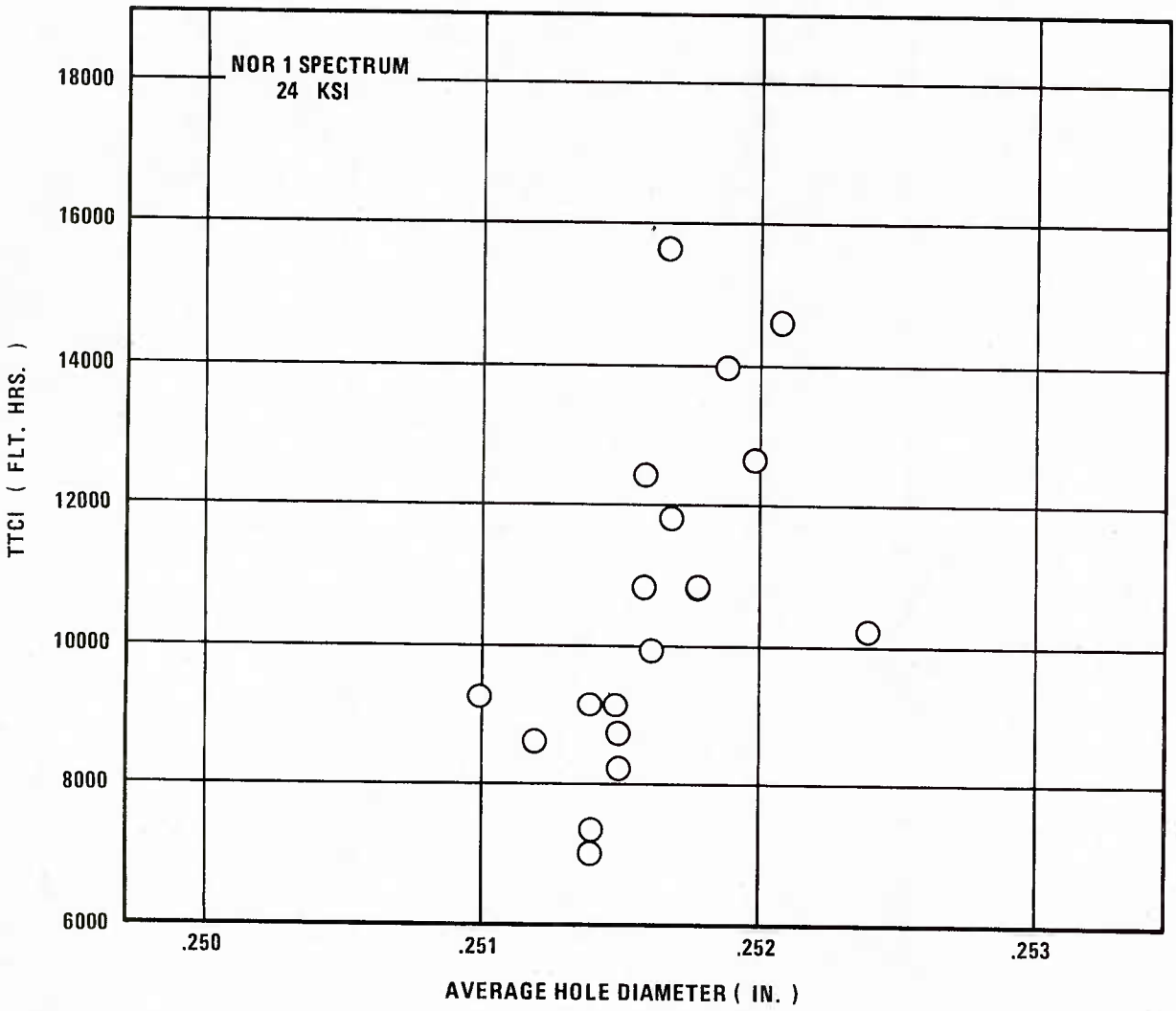

Figure 37. TTCI vs Hole Diameter in Baseline Specimens

The results of little or no correlation between fatigue behavior and hole quality as measured by the different NDE techniques are consistent with results obtained from the "Fastener Hole Quality" program [Ref. 4]. In that program it was found that flaws which degraded the cosmetic hole quality, such as rifling marks, gouges, drill tool chatter marks, etc., did not necessarily affect structural fatigue performance.

3.1.2 Adhesive Specimens

Inspection and test results for adhesive coupons are shown in Tables 10, 11, and 12. Also shown in Tables 10-12 are the locations of the failure origins.

In general, no correlation could be made between fatigue properties and ultrasonic C-scan records prior to testing (see Tables 10-12). A typical ultrasonic C-scan of an unscrimmed adhesive coupon is shown in Figure 38. Similarly, very little distinction in quality of adhesive coupons were revealed from X-ray radiographs.

It is interesting to compare the scrimmed adhesive and the unscrimmed adhesive specimens which were tested identically. The characteristic time to form a 0.5-inch debond (i.e. β) in the unscrimmed specimens was 278 percent of the time in the scrimmed adhesive specimens. Median failure time in the unscrimmed specimens was 180 percent larger than in the scrimmed adhesive specimens. The lesser benefit in failure time for unscrimmed specimens was because most of the scrimmed adhesive specimens failed due to failure of the adhesive; whereas fourteen of the unscrimmed adhesive specimens failed due to fracture of the aluminum adherends before complete disbonding could occur. This finding suggests that fatigue and fracture performance of adhesively bonded joints can be significantly improved by using an adhesive with little or no scrim content. The large areal fraction of the fracture surface taken up by Dacron fibers in the scrimmed adhesive specimens suggests that the fiber/adhesive interface is a preferential location for crack growth under spectrum loading conditions.

Table 10 Test Results for Adhesive Specimens Tested With NOR 1 Spectrum at 24 KSI (AB124)

Spec Number	Order of Failure	Failure Time (Flts)	Failure Location	TTCI @ a_o = .5 (Flt Hrs)	EIFS (In.)	Q x 10 $^{-4}$	Ultrasonic C-Scan Rating	Radiography Rating
34	1	429	Al alloy	10917	.1732	.3166	Good	Good
19	2	626.8	Al alloy	12601	.1247	.3166	Good	Good
25	3	1249	Adhesive	5103	.3452	.9219	Fair	Good
24	4	1355	Al alloy	12033	.1410	.3089	Good	Good
17	5	1857.8	Al alloy	12512	.1273	.3638	Good	Good
40	6	2380	Adhesive	7820	.2641	.4310	Good	Good
32	7	2539	Adhesive	9979	.2006	.3425	Good	Good
36	8	2560	(a)	18546	-.03434	.2108	Good	Good
31	9	2560	(b)	8926	.2315	.4223	Fair	Good
29	10	2560	(b)	8997	.2294	.3975	Fair	Good
27	11	2560	(b)	6910	.2912	.3082	Good	Good
22	12	2560	(b)	12941	.1150	.3143	Fair	Good
14	13	2560	Al alloy (a)	11205	.1649	.1872	Good	Good
12	14	2560	Al alloy (a)	18402	-.03050	.3204	Good	Good
9	15	2560	Al alloy (a)	19987	-.07378	.3212	Good	Good
5	16	2560	Al alloy (a)	10090	.1973	.2062	Good	Good
39	17	2596	(b)	9500	.2146	.4999	Poor	Good
7	18	3160	Adhesive	8090	.2561	.1475	Good	Good
3	19	3329	(b)	4992	.3486	.2846	Fair	Good

(a) Test stopped. Pulled. Failed in Al Alloy.
(b) Test stopped. Pulled. Failed in Adhesive.

Table 11 Test Results for Adhesive Specimens Tested With NOR 1 Spectrum at 30 KSI (AB130)

Spec Number	Order of Failure	Failure Time (Flts)	Failure Location	TTCI @ a_o = .05 (Flt Hrs)	EIFS (In.)	Q x 10 $^{-3}$	Ultrasonic C-Scan Rating	Radiography Rating
18	1	398.9	Adhesive	2497	.2738	.1454	Fair	Good
21	2	473.2	Adhesive	1865	.3281	.1838	Fair	Good
23	3	531	Adhesive	2320	.2888	.1644	Fair	Good
20	4	568.7	Al alloy	2668	.2594	.1687	Good	Good
26	5	659	Adhesive	3620	.1828	.1020	Fair	Good
10	6	661.2	Adhesive	2232	.2693	.1120	Good	Good
8	7	690	Al alloy	2977	.2339	.1120	Good	Good
16	8	749	Al alloy	3426	.1980	.1237	Good	Good
15	9	799	Al alloy	3801	.1690	.1029	Good	Good
11	10	805	Al alloy	5395	.05913	.1309	Good	Good
13	11	808.9	Adhesive	4530	.1157	.1442	Good	Good
4	12	919.2	Al alloy	2013	.3152	.09622	Good	Good
37	13	929	Adhesive	3745	.1732	.1210	Fair	Good
38	14	1036	Adhesive	4447	.1216	.1013	Good	Good
33	15	1044	Adhesive	3528	.1900	.09529	Good	Good
35	16	968	Adhesive	4047	.1505	.1222	Good	Good
28	17	1067	Adhesive	4114	.1456	.07853	Fair	Good
30	18	1089	Adhesive	6758	-.002591	.09507	Good	Good
6	19	1456.8	Al alloy	3759	.1722	.06788	Fair	Good

Table 12 Test Results for Unscrimmed Adhesive Specimens Tested With NOR 1 Spectrum at 30 KSI (UB130)

Spec Number	Order of Failure	Failure Time (Flts)	Failure Location	TTCI @ a_o = .5 (Flt Hrs)	EIFS (In.)	$Q_i \times 10^{-4}$	Inspection Results Ultrasonic C-Scan Rating
6	1	188.8	Al alloy	*	*	*	Poor
8	2	199	Al alloy	*	*	*	Fair
11	3	589	Al alloy	13706	-.1076	.4939	Good
16	4	749	Al alloy	12998	-.1040	.4509	Fair
14	5	688.7	Al alloy	9489	.04721	.5124	Fair
19	6	538.8	Al alloy	8427	.09496	.5124	Good
20	7	654.8	Al alloy	6923	.1647	.5124	Good
12	8	929	Al alloy	9992	.02531	.5124	Good
1	9	978.8	Al alloy	9615	.04169	.5124	Fair
5	10	1428.7	Al alloy	11245	-.02570	.5124	Poor
4	11	1478.7	Al alloy	10840	-.00874	.4726	Poor
18	12	1678.7	Adhesive	6597	.1800	.4714	Good
17	13	1304.9	Al alloy	13087	-.1081	.7107	Good
15	14	1589	Al alloy	7715	.1277	.9328	Good
7	15	1866.7	Adhesive	8640	.08526	.5635	Good
10	16	1908	Adhesive	13122	-.1097	.3406	Good
9	17	1870	Al alloy	11166	.02233	.5038	Fair
3	18	2039	Adhesive	10499	.00429	.5227	Fair
13	19	2378.8	Adhesive	8899	.07357	.5050	Good
2	20	2539	Adhesive	9625	.04122	.5120	Fair

* Not used in calculations.

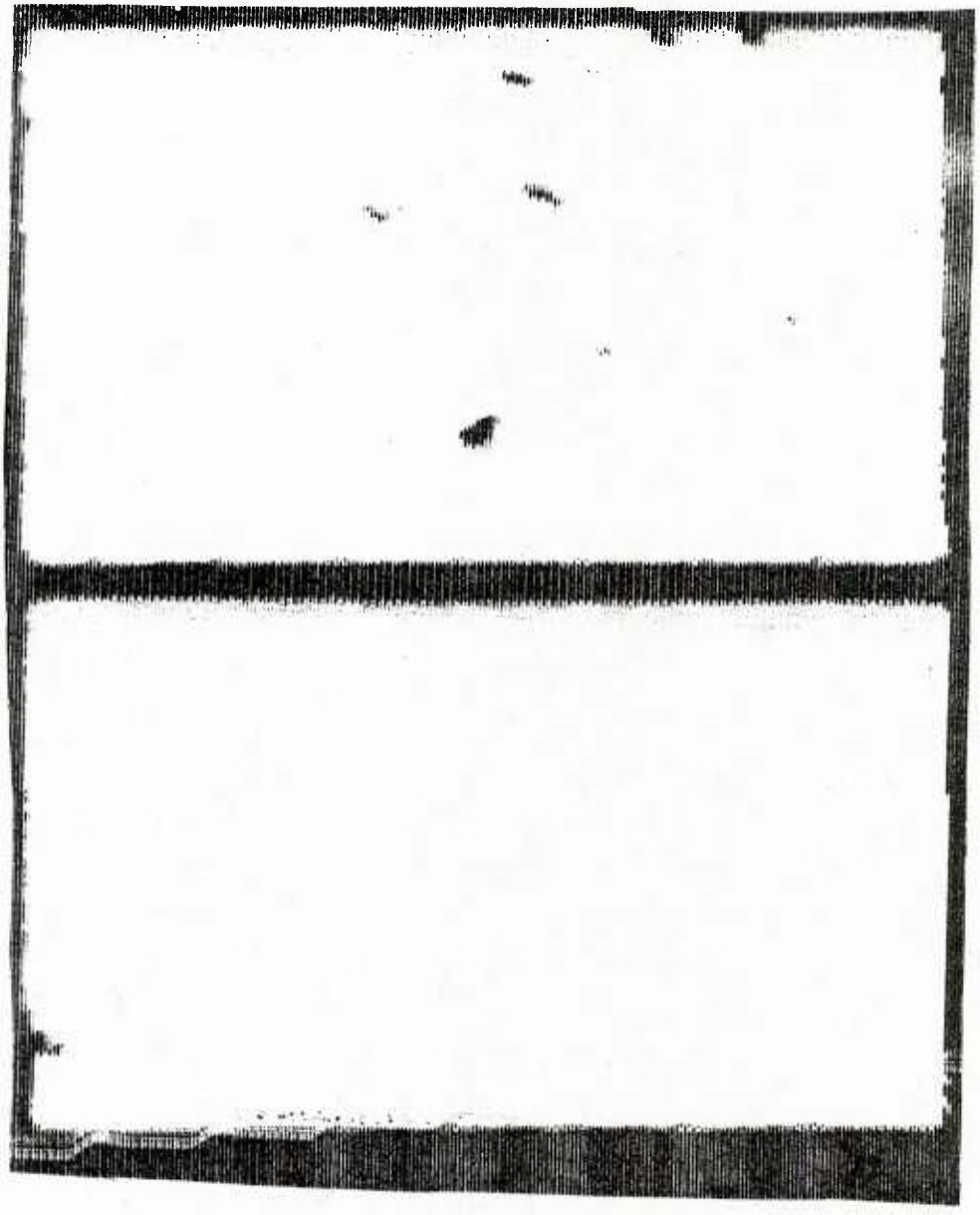

Figure 38. Typical C-Scan of an Adhesive Specimen

3.1.3 Cast Specimens

Inspection and test results for three test conditions are given in Tables 13-15. No significant porosity, inclusions, or planar defects were observed in any of the x-ray radiographs. Typical eddy current scans are shown in Figure 39. In general, there was little correlation between eddy current amplitudes and fatigue properties of the castings. A plot of amplitude as a function of time-to-crack initiation is shown in Figure 40. The two specimens with the worst fatigue properties also were the noisiest in terms of eddy current amplitude (Specimens No. 110 and 134). Otherwise, no trend could be established between the two.

Several defects which had not been found during inspection were readily found on some of the cast fracture surfaces. These included porosity in the two shortest-lived specimens, Nos. 110 and 134 (Figure 41). These defects were close enough to the hole surface to surmise that the "noise" in the eddy current traces for these specimens was due to their presence. These defects, lying so close to the edge of the hole where the local stress is highest, did initiate fatigue cracks. A particularly obvious example of this phenomenon is shown in Figure 41 for a large defect in specimen 16. Striations in the left photograph clearly center on the defect, rather than on the edge of the hole. However, it cannot be said that defects at critical locations in the castings necessarily led to premature failure. Several defects were found in castings with intermediate or long lives. In fact, the specimen with the defects judged to be most severe was specimen number 16, which had two large cracks on the fracture plane arising from separate defects (Figure 41). This specimen had the

Table 13 Test Results for Castings Tested With NOR 1 Spectrum at 30 KSI (CB130)

Spec Number	Order of Failure	Failure Time (Flts)	Failure Location	TTCI @ a_o = .2 (Flt Hrs)	EIFS x 10^{-3} (In.)	Q	Inspection Results	
							Radiography Ratings Class II	Eddy Current Amplitude of Largest Defect (Rel. Units)
110	1	198.6	Fastener Hole	2095	2.634	.2600	Good	5
134	2	298.7	Fastener Hole	3151	1.566	.9783	Good	7
151	3	358.8	Fastener Hole	3784	1.238	1.398	Good	2
106	4	398.7	Fastener Hole	4204	1.081	.9472	Good	4
99	5	398.7	Fastener Hole	4209	1.079	1.570	Good	2
94	6	398.7	Fastener Hole	4208	1.080	.9109	Good	-
81	7	398.7	Fastener Hole	4210	1.079	1.834	Good	-
50	8	488.9	Fastener Hole	5158	.8301	1.687	Good	2
147	9	498.98	Fastener Hole	5253	.8106	.6636	Good	4
144	10	498.7	Fastener Hole	5265	.8083	.5701	Good	4
140	11	498.7	Fastener Hole	5252	.8108	.2255	Good	3
122	12	498.7	Fastener Hole	5254	.8104	.5218	Good	4
111	13	498.7	Fastener Hole	5261	.8090	.6385	Good	4
105	14	498.7	Fastener Hole	5262	.8088	.7123	Good	4
100	15	598.7	Fastener Hole	6319	.6379	.7574	Good	3
51	16	598.7	Fastener Hole	6319	.6380	.9555	Good	-
148	17	599	Fastener Hole	6320	.6379	.6159	Good	-
102	18	599	Fastener Hole	6319	.6380	1.791	Good	3
133	19	698.7	Fastener Hole	7382	.5213	.3486	Good	3
30	20	698.7	Fastener Hole	7366	.5228	.1525	Good	4
36	21	743	Fastener Hole	7837	.4823	.2270	Good	3
139	22	798.7	Fastener Hole	8423	.4391	.3031	Good	4
125	23	798.8	Fastener Hole	8426	.4389	.2108	Good	-
146	24	798.7	Fastener Hole	8415	.4396	.4779	Good	2
45	25	798.8	Fastener Hole	8427	.4388	.7267	Good	4

Table 13 Test Results for Castings Tested With NOR 1 Spectrum at 30 KSI (CB130) (Cont'd)

Spec Number	Order of Failure	Failure Time (Flts)	Failure Location	TTCI @ a_o = .2 (Flt Hrs)	EIFS x 10^{-3} (In.)	Q	Inspection Results	
							Radiography Ratings Class II	Eddy Current Amplitude of Largest Defect (Rel. Units)
107	26	898.8	Fastener Hole				Good	-
98	27	898.8	Fastener Hole				Good	-
49	28	898.8	Fastener Hole	9481	.3763	.3675	Good	2
34	29	898.8	Fastener Hole	9485	.3761	.4625	Good	3
24	30	897.8	Fastener Hole	9474	.3767	.2846	Good	3
112	31	898.8	Fastener Hole	9482	.3763	.4099	Good	2
9	32	898.8	Fastener Hole	9480	.3764	.4272	Good	3
129	33	998.8	Fastener Hole	10539	.3278	.2268	Good	-
41	34	998.8	Fastener Hole	10527	.3284	.6298	Good	2
138	35	1098.8	Fastener Hole	11588	.2897	.9705	Good	3
80	36	1098.8	Fastener Hole	11593	.2895	.3396	Good	3
128	37	1098.8	Fastener Hole	11588	.2897	.3428	Good	2
15	38	1468.9	Fastener Hole	15491	.1982	.3050	Good	3
119	39	1678.7	Fastener Hole	17687	.1667	.1943	Good	2
54	40	1778.7	Fastener Hole	18762	.1543	.1372	Good	2
2	41	1868.7	Fastener Hole	19712	.1446	.1240	Good	-
6	42	1978.7	Fastener Hole	20858	.1343	.1773	Good	3
64	43	1978.7	Fastener Hole	20874	.1342	.1064	Good	2
109	44	1978.7	Fastener Hole	20883	.1341	.2105	Good	-
10	45	2148	Fastener Hole	22645	.1206	.1003	Good	4
5	46	2478.8	Fastener Hole	26120	.1000	.09836	Good	2
52	47	2478.8	Fastener Hole	26145	.0999	.1807	Good	2
16	48	2938.9	Fastener Hole	31000	.0799	.4379	Good	-
117	49	3058.7	Fastener Hole	32263	.0758	.1167	Good	-
68	50	3840	Fastener Hole	40502	.0563	1.069	Good	-

Table 14 Test Results for Castings Tested With GAR 1 Spectrum at 28 KSI (CGAR 28)

Spec Number	Order of Failure	Failure Time (Flt Hrs)	Failure Location	TTCI @ a_o = .2 (Flt Hrs)	EIFS x 10^{-3} (In.)	Q_i x 10^{-1}	Inspection Results	
							Radiography Ratings	Comments
17	1	6350.2	Fastener Hole	6348	.8422	.4448	Good	
120	2	7025	Fastener Hole	7016	.7399	.4448	Good	
124	3	7723.2	Fastener Hole	7709	.6549	.4448	Good	
20	4	8723.4	Fastener Hole	8735	.5568	.4448	Good	
23	5	9779.8	Fastener Hole	9771	.4813	.4448	Good	
19	6	10039.2	Fastener Hole	10004	.4667	.02541	Good	
115	7	10779.8	Fastener Hole	10767	.4241	.4448	Good	
150	8	10846.7	Fastener Hole	10847	.4200	.4448	Good	
92	9	11471.1	Fastener Hole	11465	.3908	.04179	Good	(b)
37	10	12779.8	Fastener Hole	12773	.3395	.4448	Good	(a), (b)
38	11	13282	Fastener Hole	13239	.3240	.09056	Good	
18	12	13775.2	Fastener Hole	13766	.3079	.09275	Good	
39	13	13999.2	Fastener Hole	13998	.3012	.05180	Good	(a)
35	14	16236.3	Fastener Hole	16183	.2492	.04066	Good	
127	15	17092.9	Fastener Hole	17089	.2321	.03951	Good	(a)
25	16	17999.3	Fastener Hole	17992	.2170	.05420	Good	
1	17	17999.9	Fastener Hole	18000	.2169	.06005	Good	(a)
3	18	19092.9	Fastener Hole	19062	.2012	.03065	Good	
4	19	22562.7	Fastener Hole	22560	.1614	.03176	Good	
29	20	16000 hr	Fastener Hole	16012	.2527	.04448	Good	No Failure

(a) Surface crack away from bolt hole
(b) Porosity on fracture surface

Table 15 Test Results for Castings Tested With GAR 1 Spectrum at 34 KSI (CGAR 34)

Spec Number	Order of Failure	Failure Time (Flt Hrs)	Failure Location	TTCI @ a_o = .2 (Flt Hrs)	EIFS x 10^{-3} (In.)	Q_i	Inspection Results	
							Radiography Ratings	Comments
121	1	1063.1	Fastener Hole	1061	1.370	.1825	Good	
88	2	1281.8	Fastener Hole	1282	1.074	.03844	Good	
118	3	1352.6	Fastener Hole	1353	1.002	.1825	Good	
97	4	1749.6	Fastener Hole	1757	.7143	.1825	Good	
99	5	1934.3	Fastener Hole	1936	.6301	.02751	Good	
53	6	1934.4	Fastener Hole	1935	.6304	.01712	Good	
149	7	2063.1	Fastener Hole	2062	.5803	.1825	Good	
87	8	2471	Fastener Hole	2471	.4586	.08452	Good	
101	9	2654.9	Fastener Hole	2655	.4177	.01919	Good	
021	10	2736.3	Fastener Hole	2744	.4002	.1825	Good	
42	11	2749.5	Fastener Hole	2749	.3991	.01755	Good	
114	12	2999.2	Fastener Hole	3000	.3563	.04918	Good	
116	13	3063.1	Fastener Hole	3058	.3475	.1825	Good	
132	14	3999.7	Fastener Hole	4002	.2445	.07060	Good	
33	15	3999.9	Fastener Hole	4001	.2446	.01145	Good	
8	16	4471	Fastener Hole	4472	.2115	.01342	Good	
22	17	4779.8	Fastener Hole	4785	.1936	.1825	Good	
43	18	5185	Fastener Hole	5184	.1743	.01280	Good	(a)
47	19	5934.3	Fastener Hole	5934	.1461	.01705	Good	
108	20	6749.5	Fastener Hole	6740	.1236	.006010	Good	(a), (b)

(a) Surface crack away from fastener hole
(b) Porosity on fracture surface

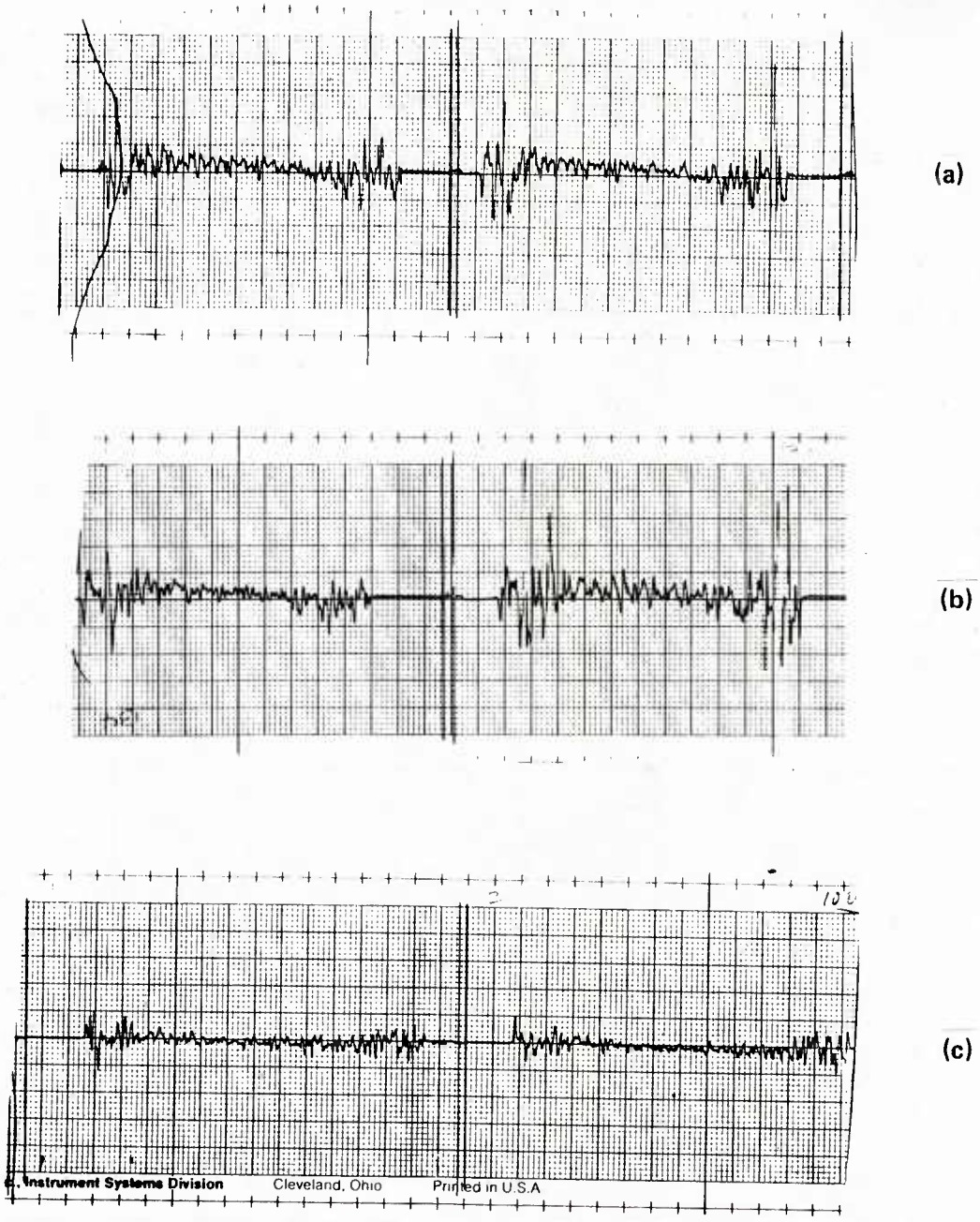

Figure 39. Eddy Current Bolt Hole Scans in the Cast Specimens; (a) Specimen No. 110, (b) Specimen No. 134, and (c) Specimen No. 100

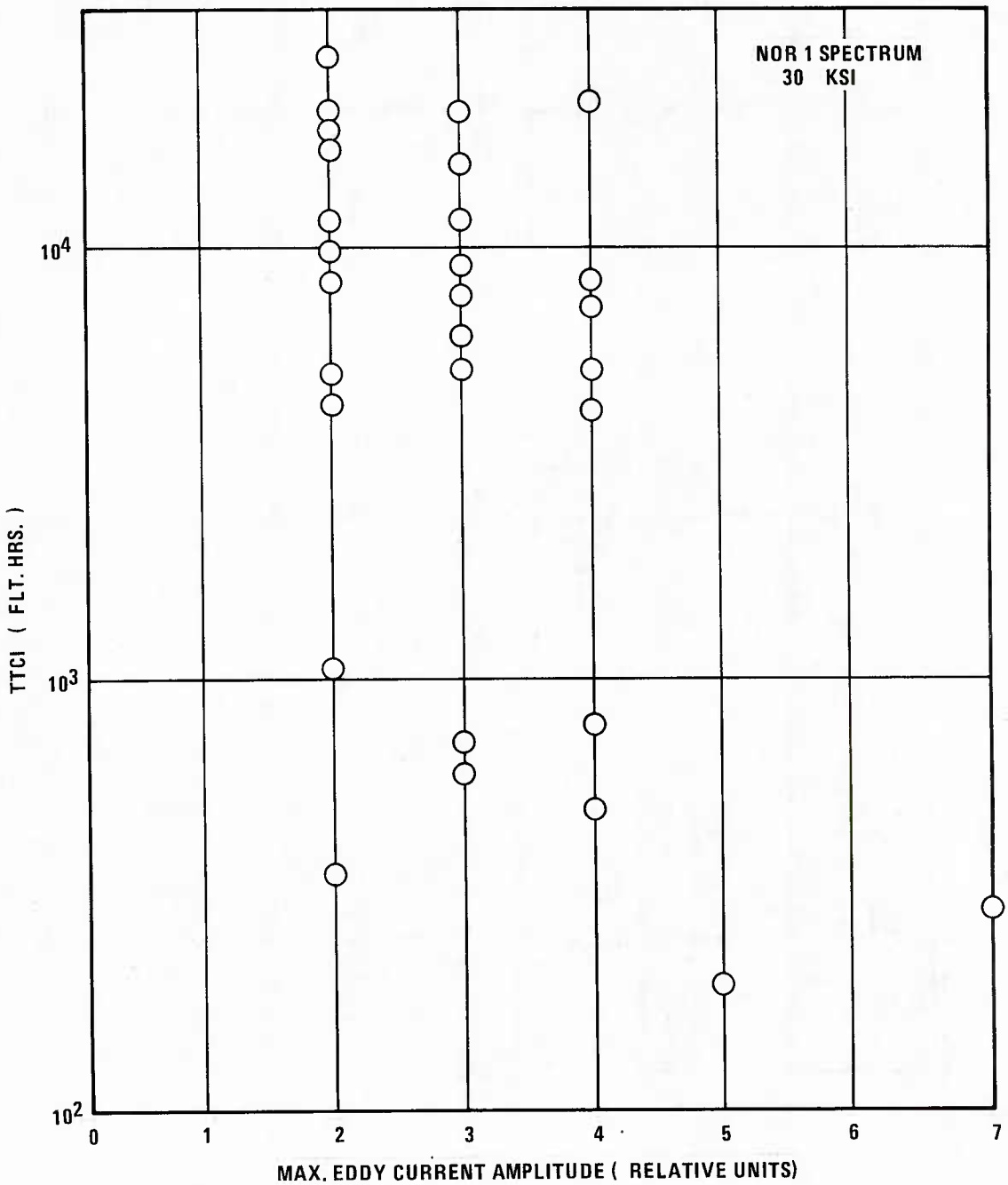

Figure 40. Maximum Eddy Current Amplitude as a Function of TTCI in Castings

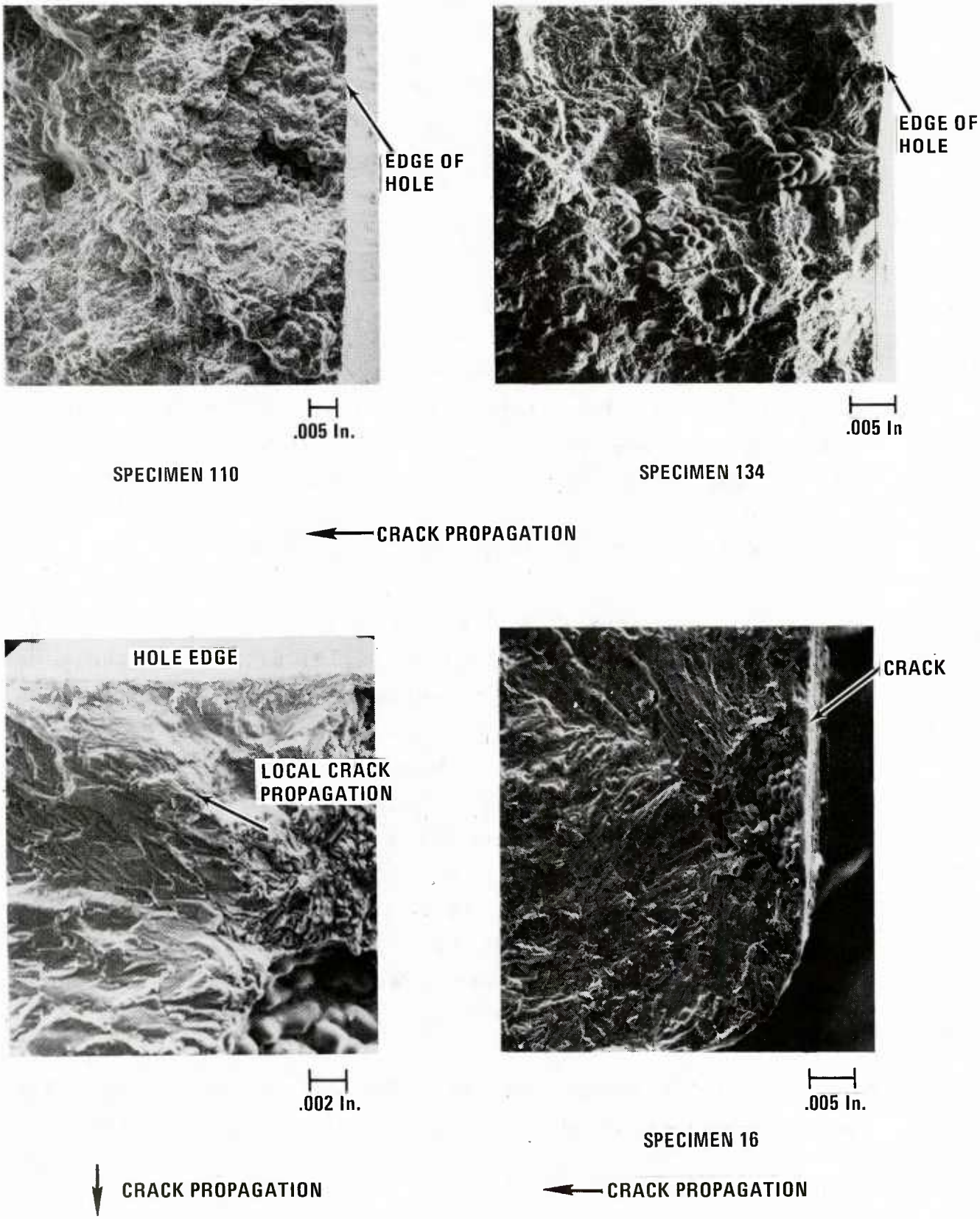

Figure 41. Defects in Cast Fracture Surfaces

third longest life of fifty specimens in the sample. Therefore, we concluded:

a) Although some casting defects did appear to cause early failures, the defects were generally too small to be reliably detected,

b) We could not show a good correlation between defects and overall structural performance.

We performed a small amount of work to try to determine if early failures were related to rapid crack growth, or if this might be related in some way to the A357 microstructure. Some evidence of a possible cause of early failure was found. Details are provided in Appendix C.

3.2 INITIAL FATIGUE QUALITY MODEL PARAMETERS

The "Fastener Hole Quality" program [4] and "Durability Methods Development" programs [5,19,20], along with this program [7], have helped to establish a model for initial fatigue quality based on the equivalent initial flaw size (EIFS) concept. The basic elements of the initial fatigue quality (IFQ) model include a power law crack growth description containing parameters Q and b and a Weibull distribution describing the time for a fatigue crack to grow to any arbitrary size, a_o. The Weibull distribution is described by parameters α, β, and ϵ. The concepts of the IFQ model and the procedures for determining IFQ model parameters are described in detail in Appendix A.

Table 16 summarizes the IFQ model parameters for this program. Table 16 shows that the values of b, α, and $Q\beta$ do

not vary with the test condition. These invariance conditions must be satisfied in order for the equivalent initial flaw size (EIFS) distribution to be generic, that is, independent of spectrum or stress level. This property is desirable since we expect the initial fatigue quality to depend on structural concept, material, and manufactured quality rather than on subsequent service conditions.

The information in Table 16 is a complete description of the results of approximately two hundred spectrum tests. It contains all the information necessary for determining the crack growth performance of each structural concept. It is the information needed for predicting crack growth behavior, as shown in Sections 4.2 through 4.4. Q and b in Table 16 describe the average crack growth for each test condition, according to equation 1. The parameters α, β, and ϵ describe the time to initiate a crack of arbitrary size a_o. The upper bound of the EIFS distribution, x_u, is determined by the other parameters. These parameters and their use will be described in more detail in the following sections.

3.3 TIME-TO-CRACK-INITIATION DISTRIBUTION

An arbitrary crack size a_o can be selected such that it can be unambiguously observed from fractography. The time required for an initial defect to become a fatigue crack of size a_o is defined as the time-to-crack-initiation (TTCI). As presented in Appendix A, observed TTCI value are known to be fit very well by a three-parameter Weibull distribution. Therefore, a fractographically observed TTCI distribution can be expressed as:

Table 16. IFQ Model Parameters

SPECIMEN	SPECTRUM	STRESS (KSI)	a_o (IN.)	Xu (IN.)	Q	b	α	β	Qβ	AVG a_{crit} (IN.)
ADHESIVELY BONDED (SCRIMMED)	NOR 1	24	.5	.5	3.3793×10^{-5}	.1259	3.1591	12282	.41504	.829
		30	.5	.5	1.0531×10^{-4}	.1259	3.1591	3941	.41504	1.1061
ADHESIVELY BONDED (UNSCRIMMED)	NOR 1	30	.5	.5	5.1239×10^{-5}	.0489	5.0095	10983	.56277	---
BASELINE SEALANT	NOR 1	24	.2	.2	7.1785×10^{-5}	.5674	3.4808	12068	.86630	.375
		30	.2	.2	1.6465×10^{-4}	.5674	3.4808	5261	.86630	.297
BASELINE NO SEALANT	NOR 1	24	.2	.2	7.3075×10^{-2}	1.5732	4.0235	34115	2492.96	.263
CAST	NOR 1	30	.2	.2	5.5364×10^{-2}	1.7607	2.0015	13097	725.1	.194
	GAR 1	28	.2	.2	4.8446×10^{-2}	1.7607	2.0015	14967	725.1	.109
	GAR 1	34	.2	.2	1.9877×10^{-1}	1.7607	2.0015	3648	725.1	.076

Note: $\varepsilon = 0$ For All Data Sets.

$$F_T(t) = P[T \leq t] = 1 - \exp\left\{-\left[\frac{t-\epsilon}{\beta}\right]^{\alpha}\right\} \quad ; \; t > \epsilon \qquad (6)$$

where T is a random variable indicating TTCI, α is the shape parameter, β is the scale parameter, and ϵ is the lower bound of TTCI.

Eq. 6 may be transformed into:

$$\log\left\{-\ln\left|1-F_T(t)\right|\right\} = \alpha \log (t-\epsilon) - \alpha \log \beta \qquad (7)$$

Eq. 7 shows that $-\ln[1-F_T(t)]$ vs. $(t-\epsilon)$ is plotted as a straight line on log-log scale paper.

Figures 42-47 show the TTCI distributions obtained from this program. Each data point represents the $-\ln [1-i/(n+1)]$ vs. $(TTCI-\epsilon)$ pair for each specimen, where $i/(n+1)$ is the TTCI rank of the specimen within the individual data set. The straight line in Figures 42-47 is the $F_T(t)$ distribution giving the best least squares fit to the plotted $-\ln[1-F_T(t)]$ vs.$(TTCI-\epsilon)$. $F_T(t)$ can be calculated from Eq. 6 using the parameters α, β, and ϵ presented in Table 16. The slopes of the straight lines in Figures 42-47 are directly related to the parameter α. As mentioned earlier, the parameter α is not expected to be a function of the spectrum type and stress level. Therefore, a set of identical test specimens is expected to have the same slope even though tested under various spectrum types and stress levels.

From Figures 42-45 note that the observed TTCI values are fit quite well by a three-parameter Weibull distribution for adhesively bonded, baseline-with-sealant, and baseline-with-no-sealant specimens. The higher stress level shifts

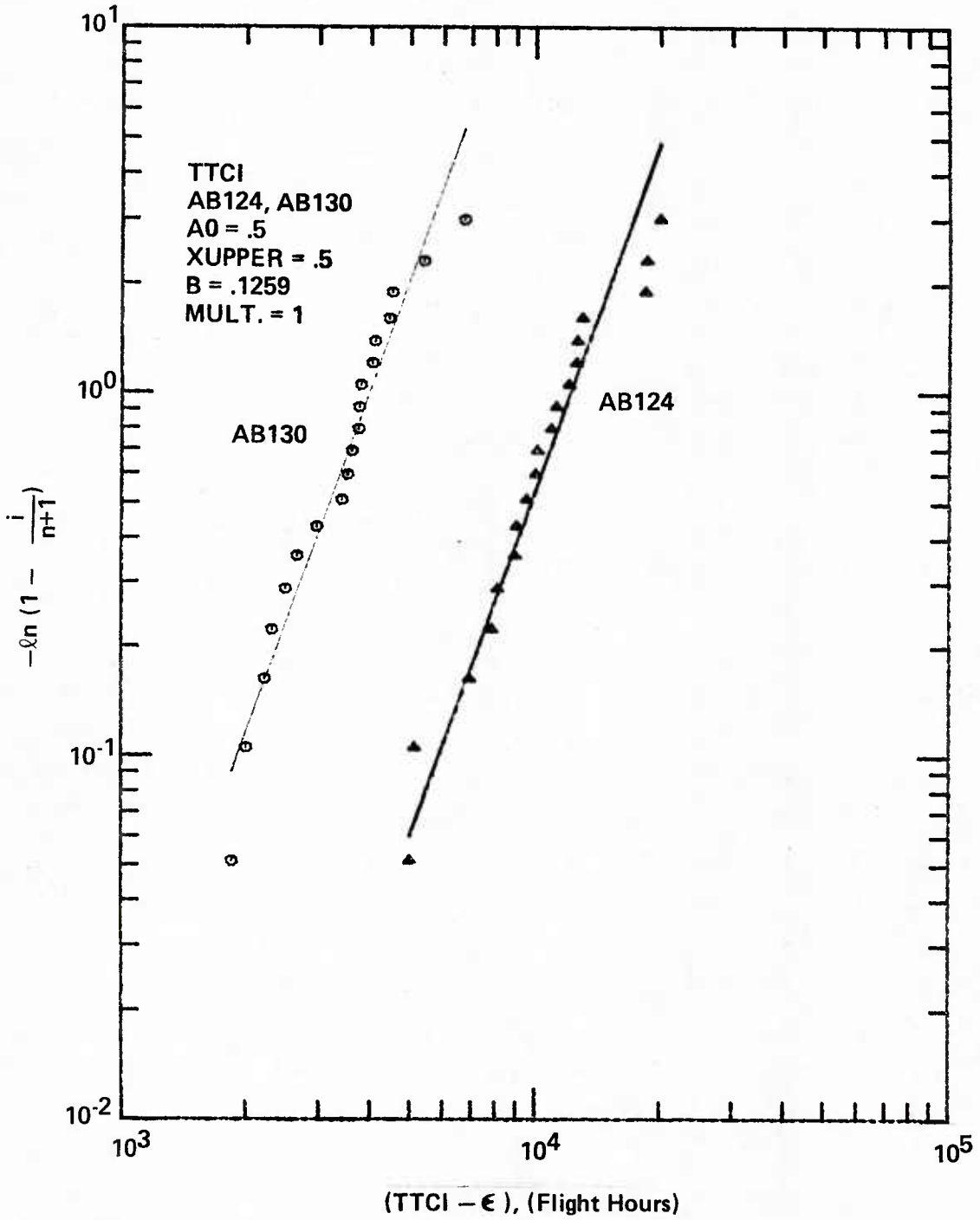

Figure 42. TTCI Distributions for Adhesively Bonded Specimens

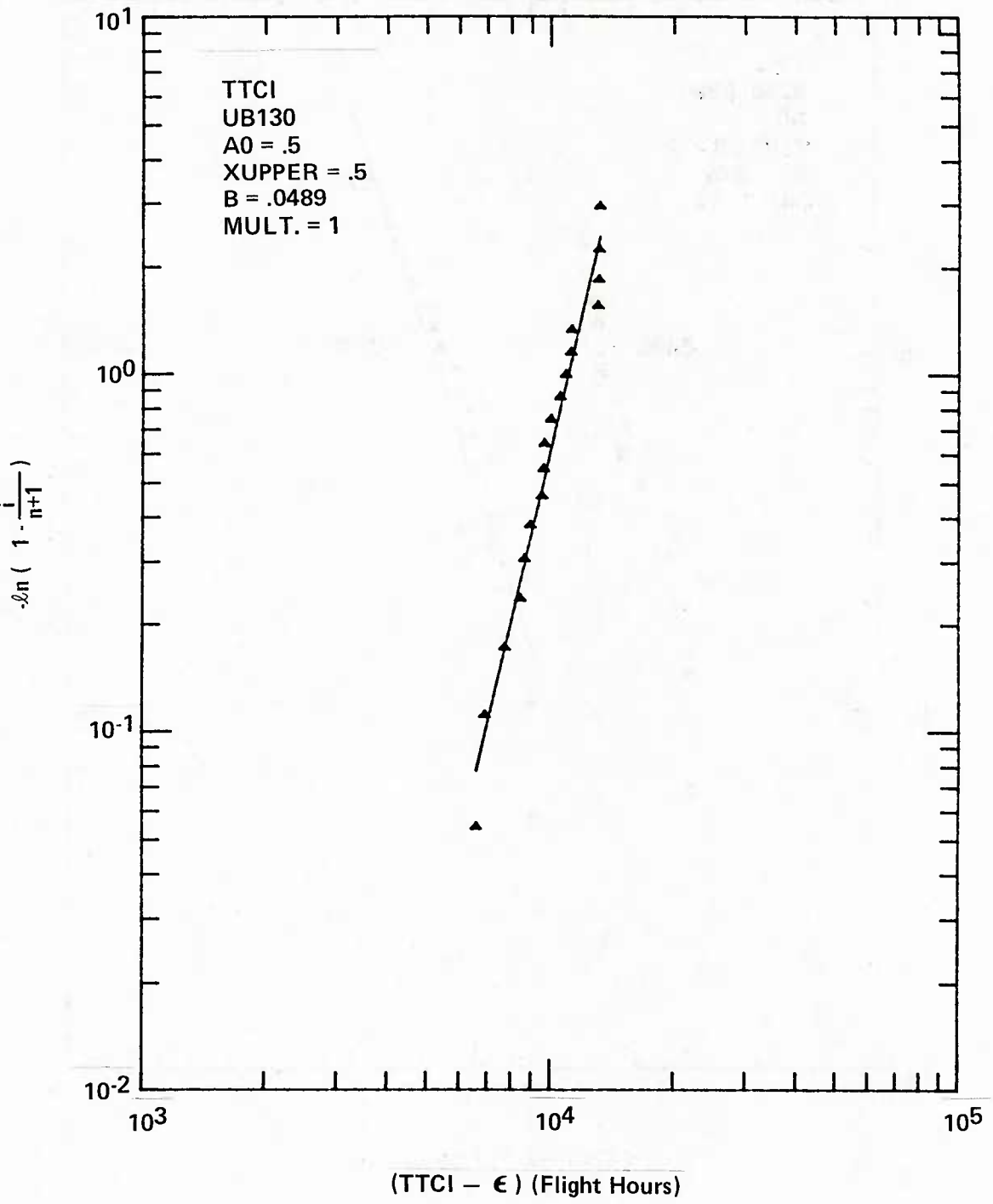

Figure 43. TTCI Distribution for Unscrimmed Adhesively Bonded Specimens

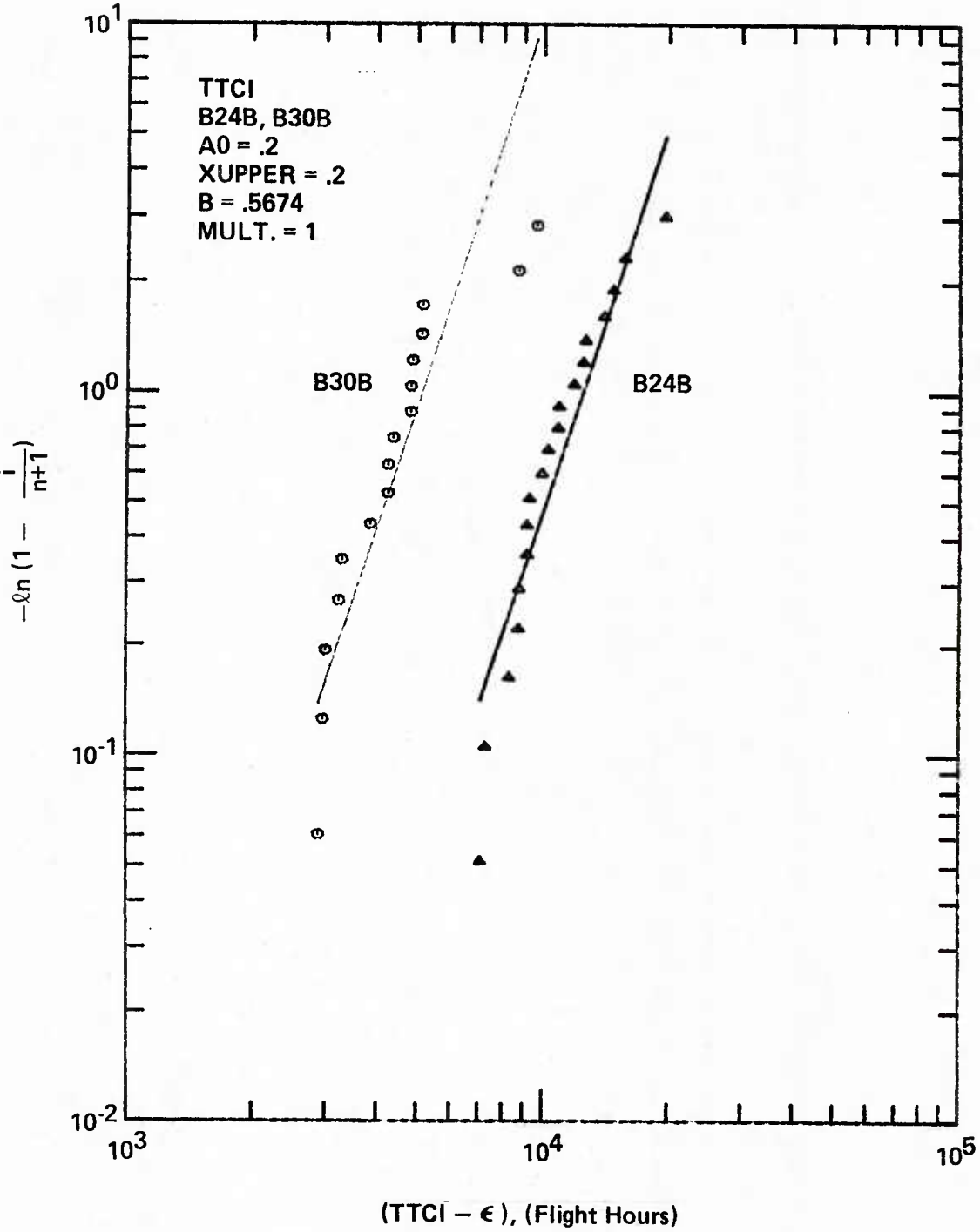

Figure 44. TTCI Distributions for Baseline Specimens

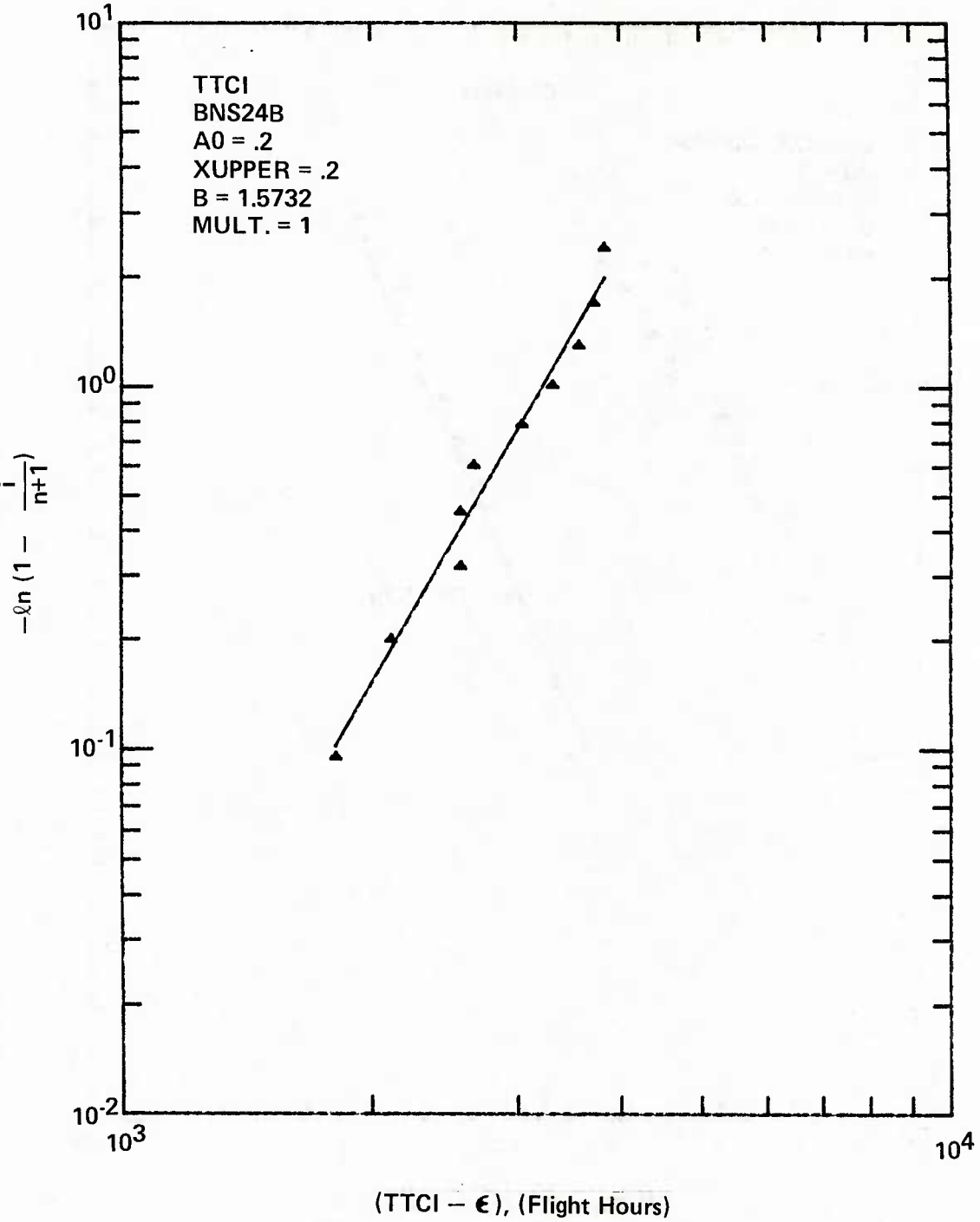

Figure 45. TTCI Distributions for No Sealant Baseline Specimens

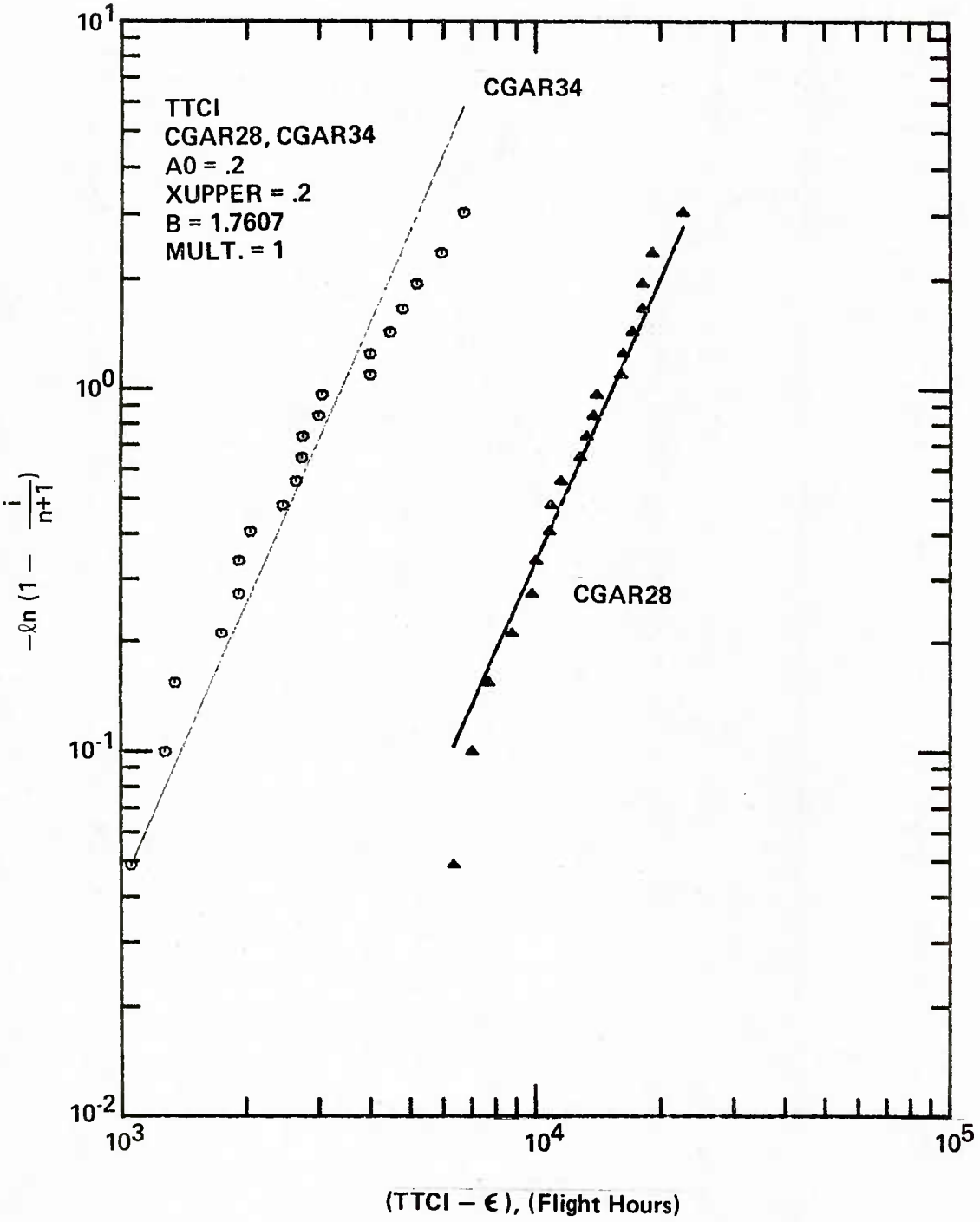

Figure 46. TTCI Distributions for Cast Specimens — GAR 2 Spectrum

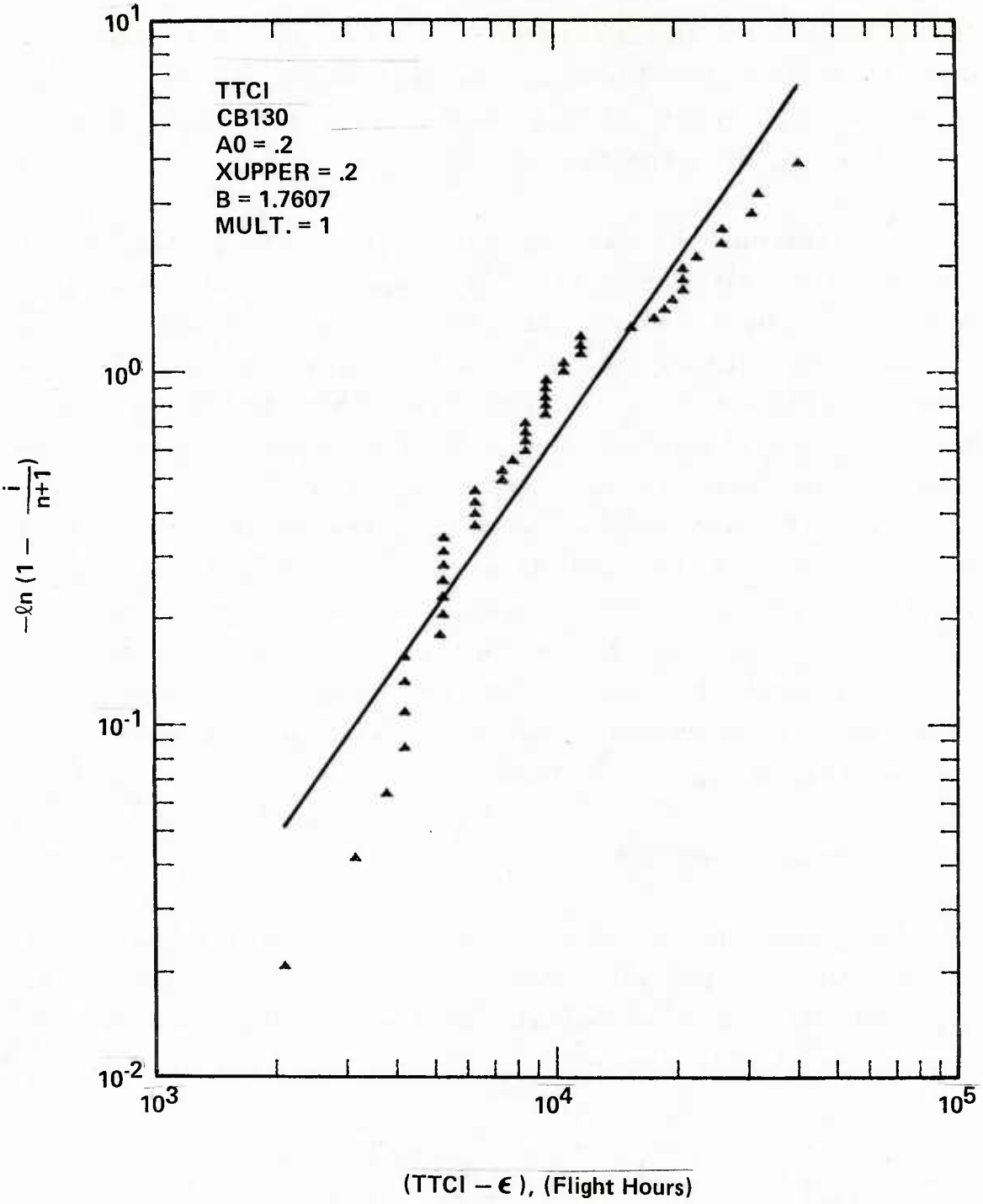

Figure 47. TTCI Distributions for Cast Specimens – NOR 1 Spectrum

the data points to the left (i.e. shorter TTCI) compared with those from the lower stress level, but the data points from two different stress levels are fit well by TTCI distributions with the same slope.

In the case of cast specimens, the data points do not seem to fit quite as well. Cast specimen test conditions were varied by changing the spectrum type as well as the stress level. If we look at two data sets obtained from GAR spectra (Figure 46), we can find that those two TTCI distributions appear to have the same slope. However, the data set observed for the NOR 1 spectrum seems to have a somewhat different slope, indicating that α is not constant for the best fit to each data set. To keep the analysis tractable for preliminary design, we have treated the data as if all conditions for a generic EIFS distribution must hold. Consequently, we used the best common fit to all cast data for all subsequent analyses. Generic IFQ parameters for castings are given in Table 16.

3.4 EIFS DISTRIBUTION

As described in Appendix A, the EIFS distribution can be derived from the TTCI distribution by extrapolating TTCI backward using a crack growth analysis. The EIFS distribution can be written as:

$$F_{a(o)}(x) = \exp\left\{ - \left[\frac{x^{-c} - x_u^{-c}}{cQ\,\beta} \right]^{\alpha} \right\} ; \quad o < x \leq x_u \qquad (8)$$

where x is a random variable indicating a(o), the crack size at time zero (or EIFS), c is b-1, and x_u is the upper bound of

the EIFS distribution which is defined as:

$$x_u = [a_0^{-c} + CQ\varepsilon]^{-1/c} \tag{9}$$

Eq. 8 can be used to find the probability that the EIFS is less than a given size, x, using parameters for any structural concept found in Table 16.

In some instances the EIFS for a specimen may be given as a negative number. This, in effect, causes the analysis to predict that some time is required to reach a crack length of zero. We interpret this physically to mean that some time was required to initiate fatigue cracks in our unflawed specimens. In these cases the backward extrapolation of the crack growth curve can intersect the abcissa at positive time, or intersect the ordinate at negative crack size. For such cases, x in Eq. 8 is negative so that Eq. 8 is undefined. This can be remedied by using Eq. 8' whenever x is negative.

$$F_{a(o)}(x) = \exp\left\{-\left[\frac{-(-x)^{-c} - x_u^{-c}}{cQ\beta}\right]^{\alpha}\right\} \tag{8'}$$

Eq. 8 may be transformed into:

$$\log\left[-\ln F_{a(o)}(x)\right] = \alpha \log (x^{-c} - x_u^{-c}) - \alpha \log CQ\beta; \quad o<x<x_u \tag{10}$$

Eq. 10 shows that $-\ln F_{a(o)}(x)$ vs. $(x^{-c} - x_u^{-c})$ is plotted as a straight line on log-log paper. The slope of the straight line is directly related to the parameter α.

Figures 48-52 show the EIFS distributions obtained from this program. Each data point in Figures 48-52 represents the $-\ln(i/n+1)$ vs. $(EIFS^{-c} - x_u^{-c})$ pair for each specimen, where $i/(n+1)$ is the EIFS rank of the specimen among the set of identical test specimens. The straight lines in Figures 48-52 are plotted from $-\ln F_{a(o)}(x)$ vs. $(x^{-c} - x_u^{-c})$. $F_{a(o)}(x)$ can be calculated from Eq. 8 using the parameters Q, b, α, β, and x_u presented in Table 16.

As shown in Figures 48-52 the experimental EIFS distributions (data points) are reasonably fit by the best fit EIFS function (straight lines) given by Eq. 8. What should be noted here is that for a given set of identical test specimens all the data points obtained from different test conditions merge more or less into a single EIFS distribution. This tends to confirm the assumption that the EIFS distribution is generic, as described in Section 3.2.

3.5 CRACK GROWTH RATE DISTRIBUTION

The crack growth rate of an individual specimen can be represented by Eq. 11:

$$\frac{da(t)}{dt} = \hat{Q}_i \, a^{b^*}(t) \qquad (11)$$

where b^* is a constant for all specimens of a given type. At a specific crack size, such as a_o, the crack growth rate variation is uniquely determined by Q_i. That is, for all constant a ,

$$\frac{da}{dt} \propto \hat{Q}_i$$

Therefore, the variation in Q_i describes the variation in crack growth rate among a set of specimens for all crack sizes.

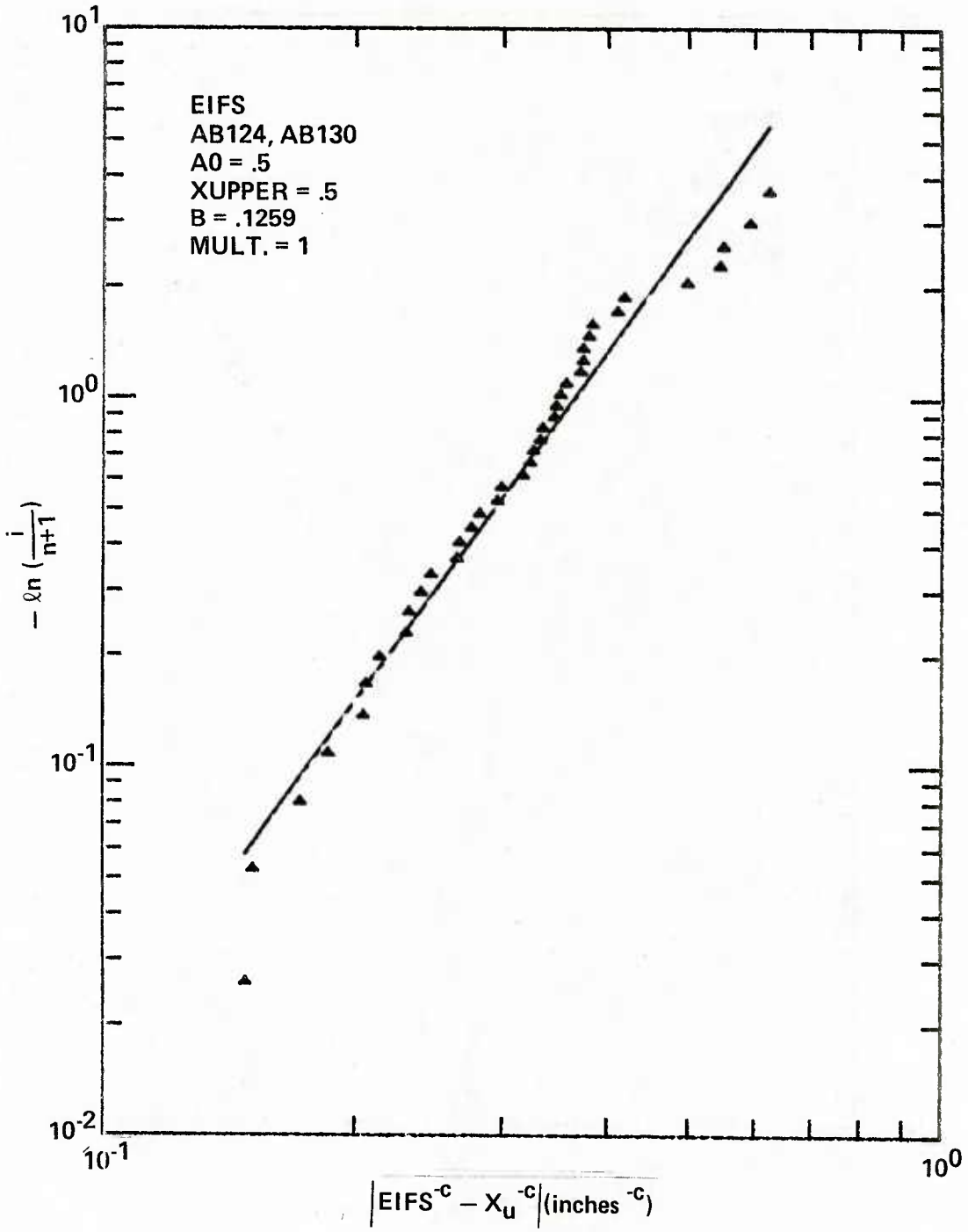

Figure 48. EIFS Distributions for Adhesively Bonded Specimens

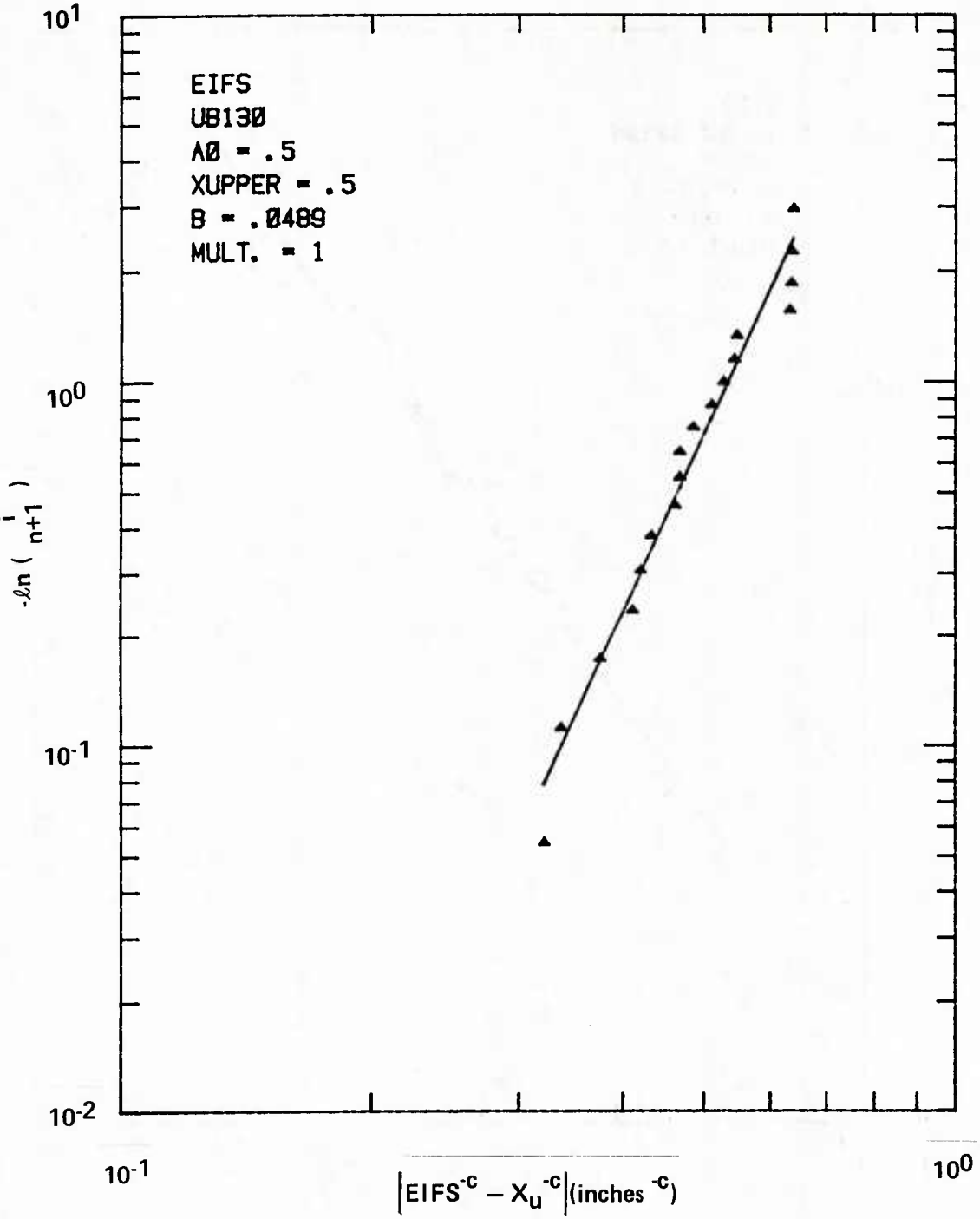

Figure 49. EIFS Distribution for Unscrimmed Adhesively Bonded Specimens

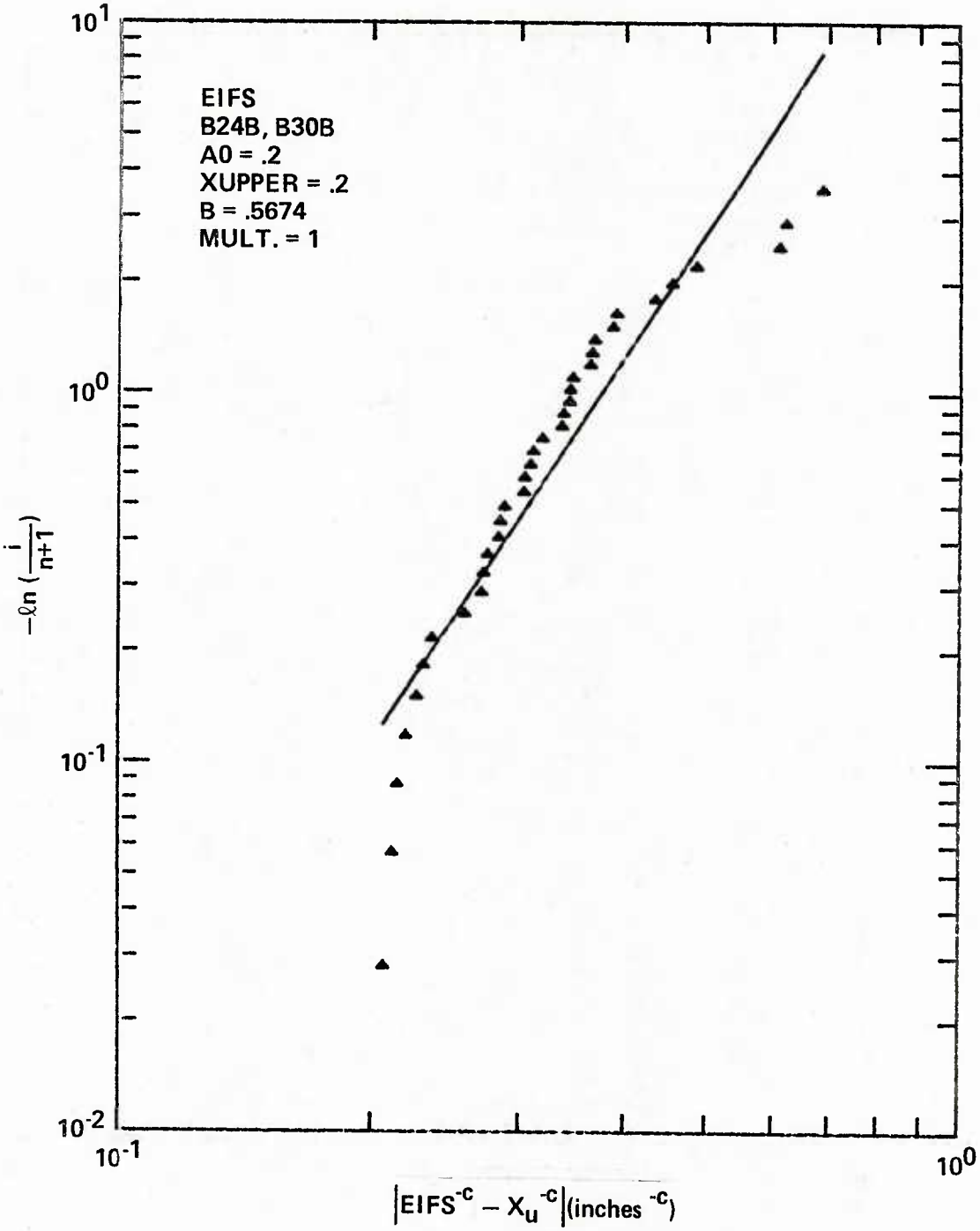

Figure 50. EIFS Distributions for Baseline Specimens

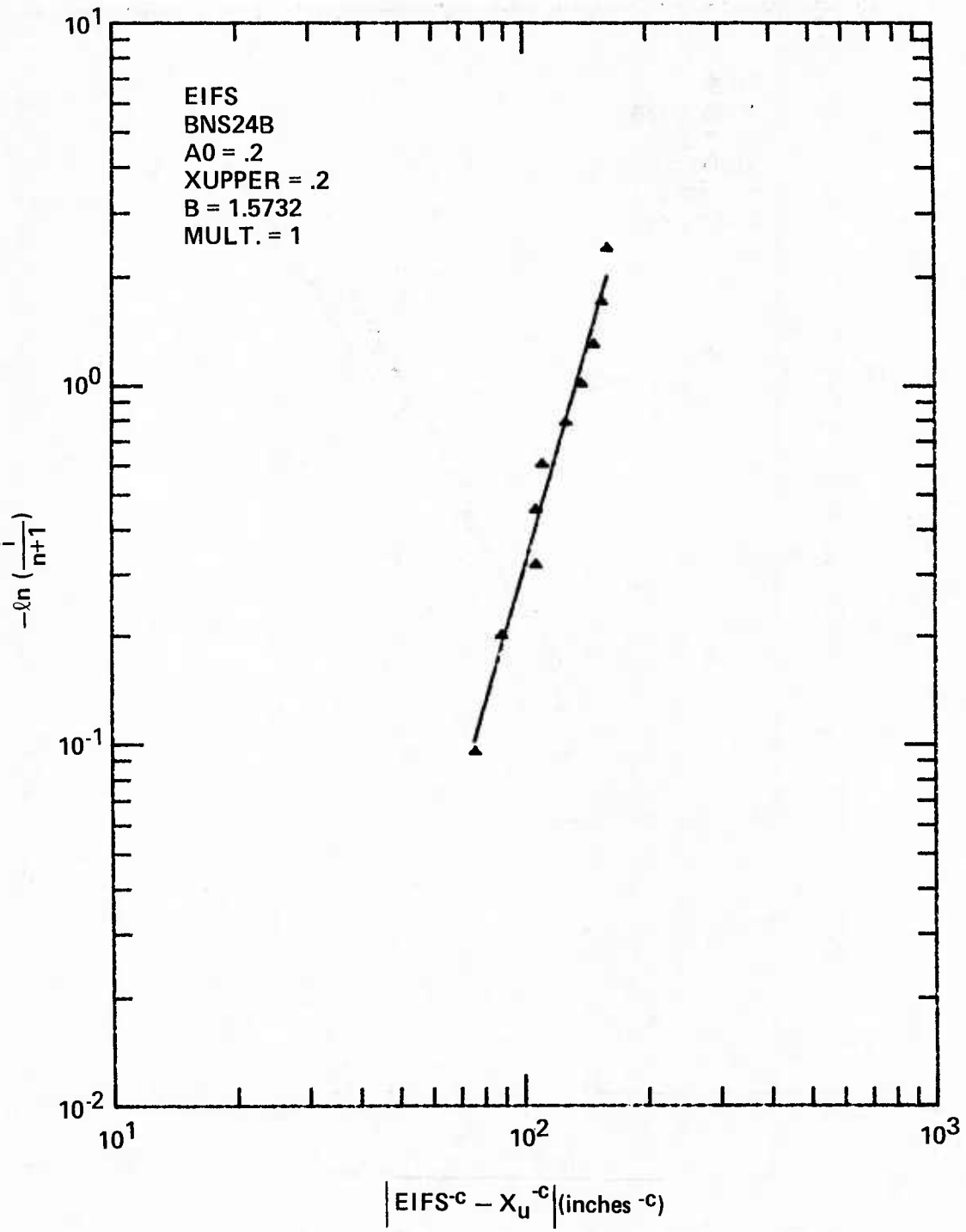

Figure 51. EIFS Distributions for No Sealant Baseline Specimens

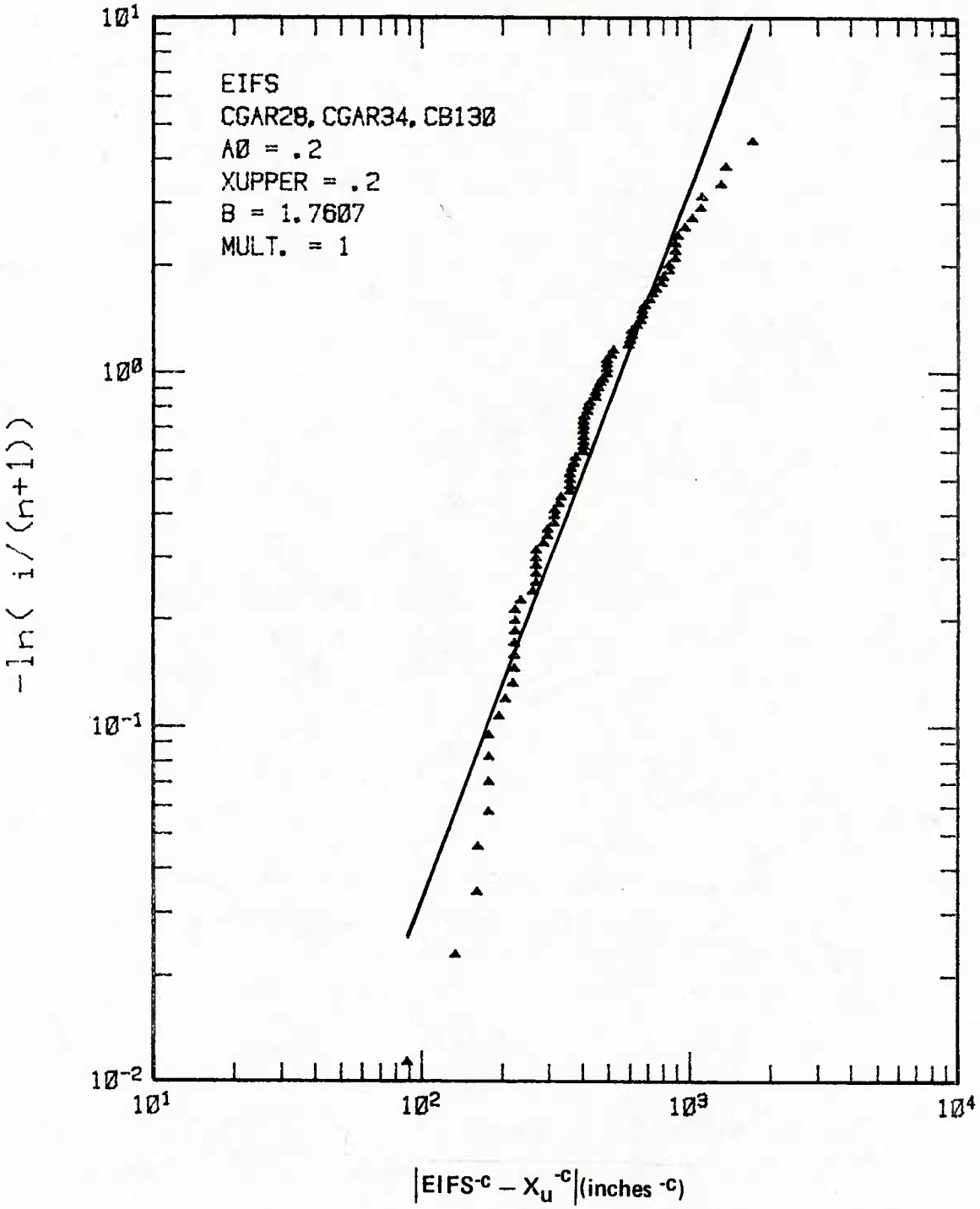

Figure 52. EIFS Distributions for Cast Specimens

Figures 53-55 show the distribution of the crack growth parameter $\hat{Q}_i$ for each joining concept tested with the NOR 1 spectrum at 30 ksi. Each data point in Figures 53-55 represents the log $\hat{Q}_i$ vs. i/(n+1) pair. The straight lines in Figures 53-55 were determined from the two-parameter log-normal distribution which can be expressed as:

$$f(\hat{Q}) = \frac{1}{\hat{Q}\sqrt{\pi\eta}} \exp\left[- \frac{1}{2\eta} (\log \hat{Q} - \mu)^2 \right] \quad (12)$$

where

$$\mu = \frac{\sum^{n} \log \hat{Q}_i}{n} \quad (13)$$

$$\eta = \frac{\sum^{n} (\log \hat{Q}_i - \mu)^2}{n} \quad (14)$$

From Figures 53-55 it is seen that the data points are fit very well to the straight line. Hence, the crack growth rate is described by a two-parameter log-normal distribution.

3.6 TIME-TO-FAILURE

For the determination of the EIFS distribution, the crack growth rate over the crack size range of interest is given by Equation 1.

$$\frac{da(t)}{dt} = Q[a(t)]^b \quad (1)$$

Integrating Eq. 1 from t = 0 to t = time-to-failure (TTF), TTF can be found (Eq. 15) as a function of the crack size at t = 0, a(o), and that at t = TTF, a(TTF). Of course, a(o) is the EIFS and a(TTF) is the crack size at failure, or critical crack size, a_{crit}.

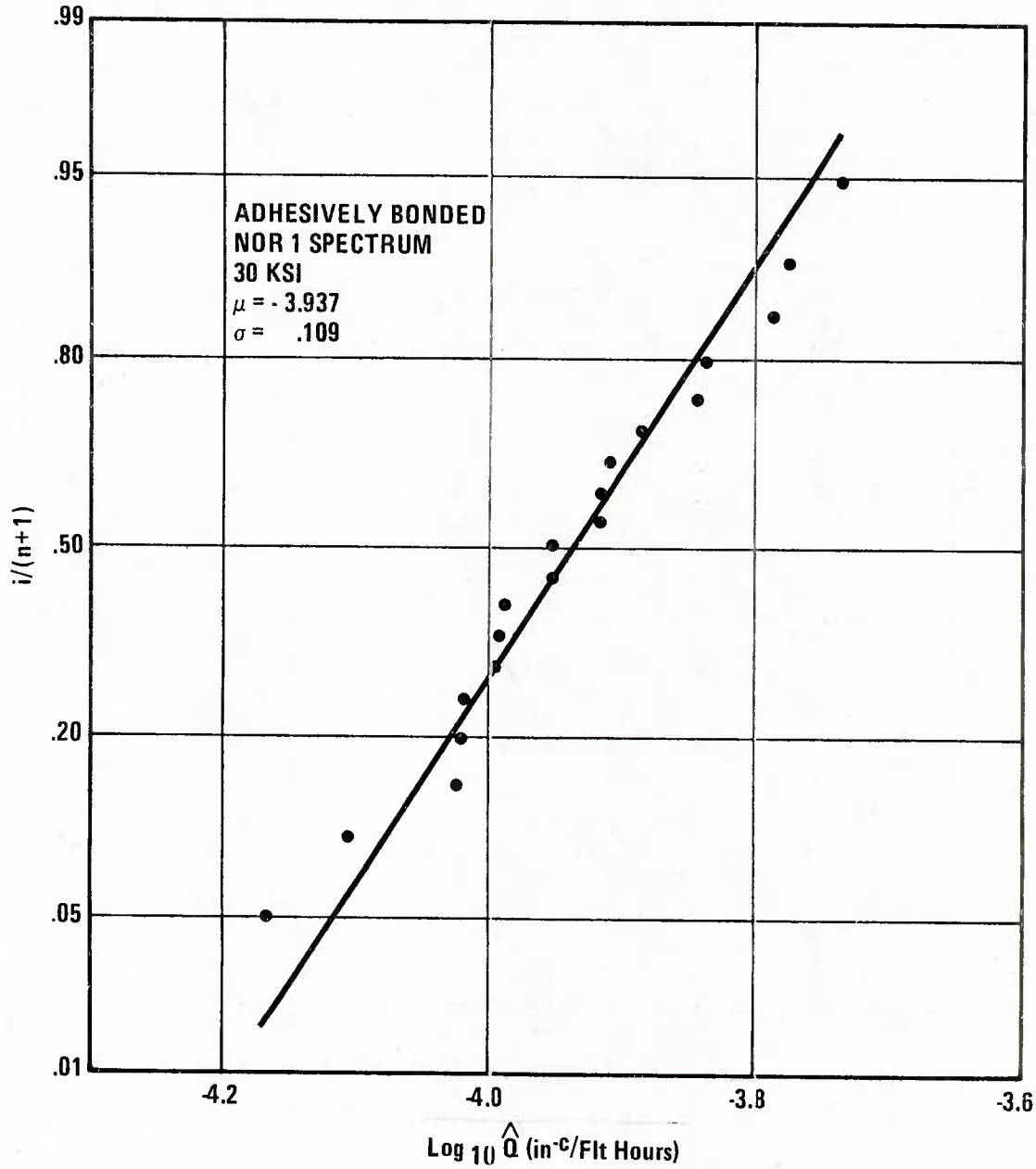

Figure 53. Q Distribution for Adhesively Bonded Specimens

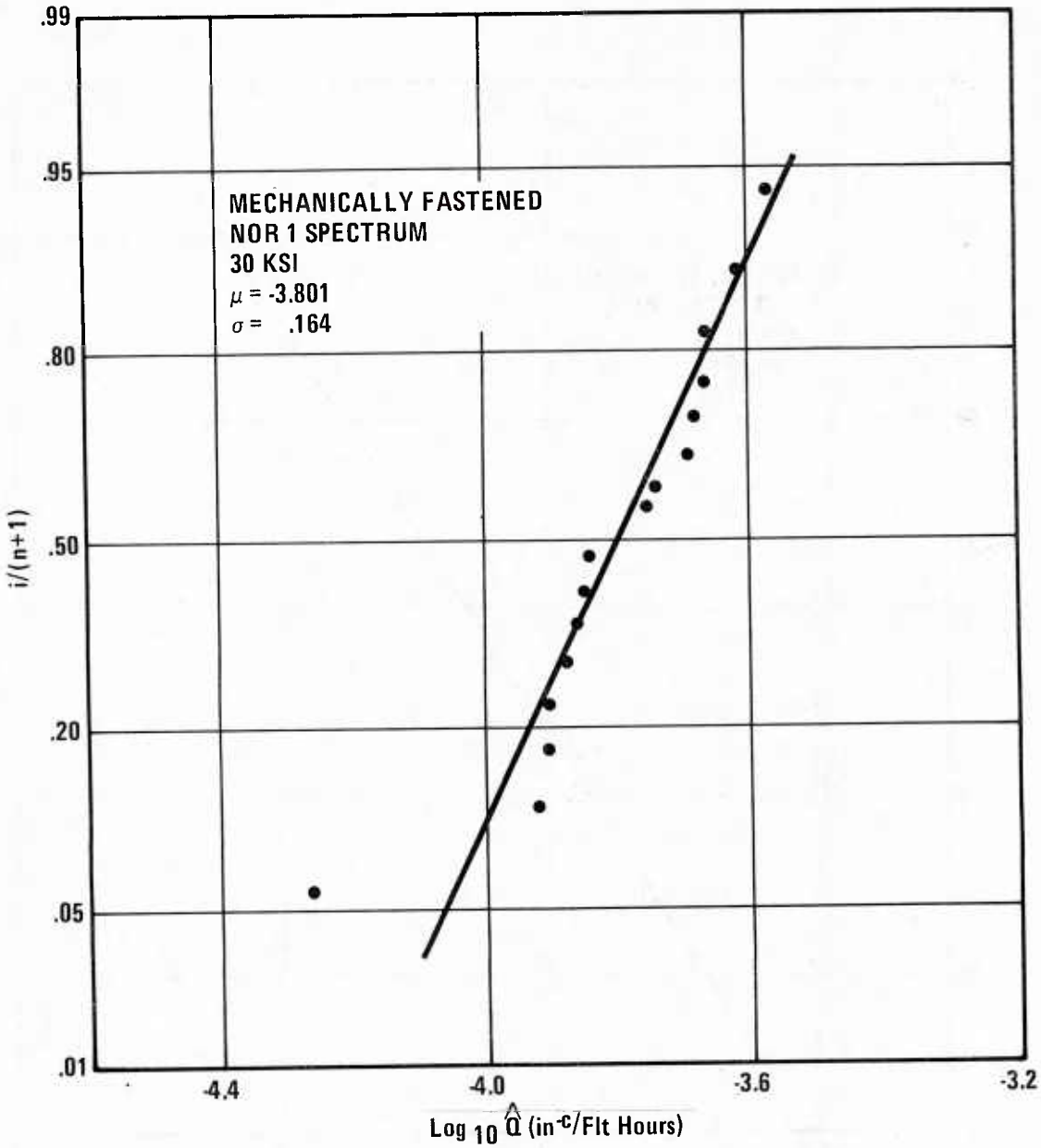

Figure 54. Q Distribution for Baseline Specimens

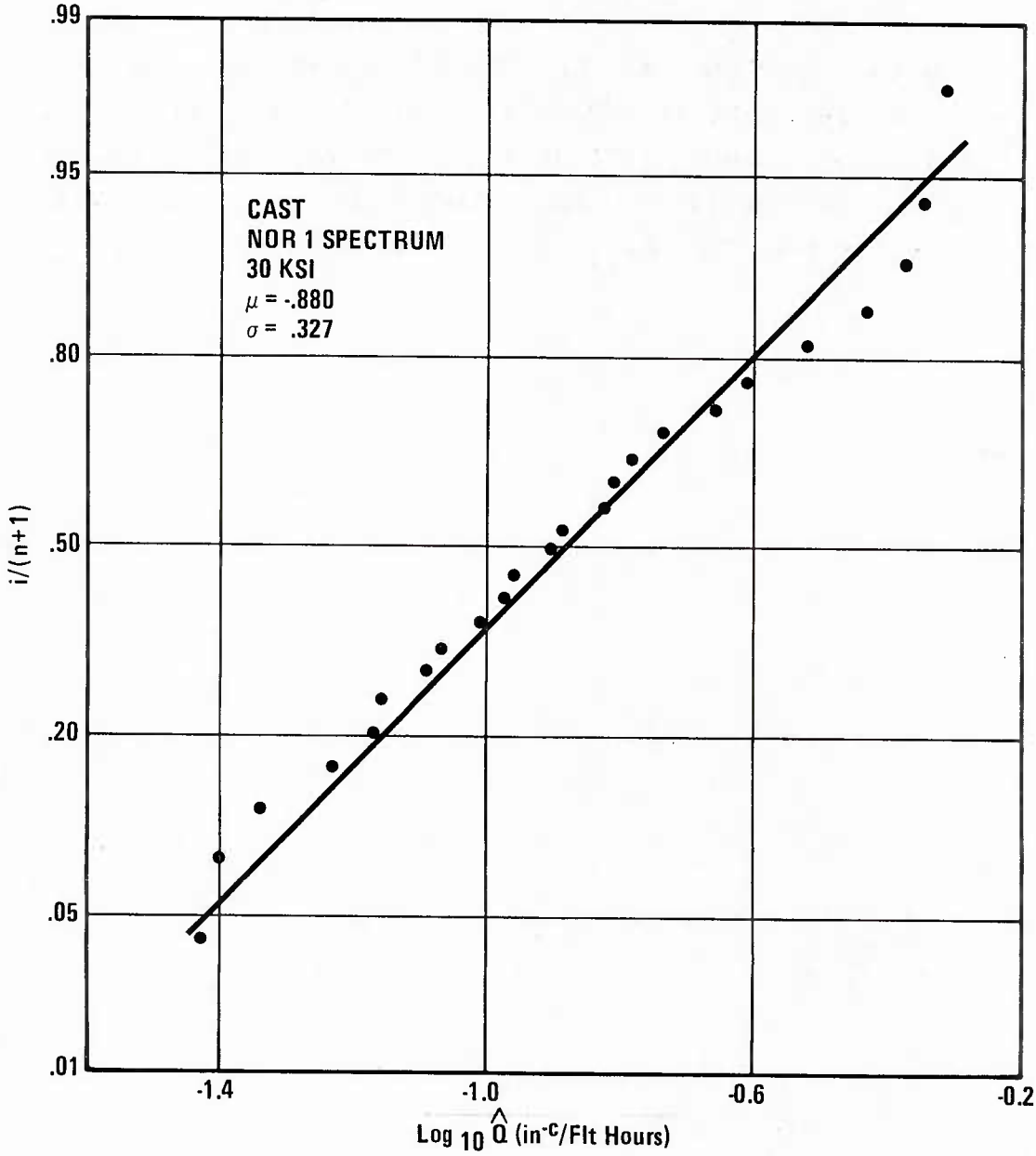

Figure 55. Q Distribution for Cast Specimens

$$TTF = \frac{1}{CQ}\left[a^{-c}(o) - a^{-c}(TTF)\right] \qquad (15)$$

Figure 56 shows the TTF distributions of adhesively bonded, baseline, and cast specimens for directly comparable test conditions. Each point in Figure 56 represents the TTF vs. i/(n+1) pair obtained from each specimen. The solid curves are the best fit $F_{TTF}(t)$ calculated using Eq. 6.

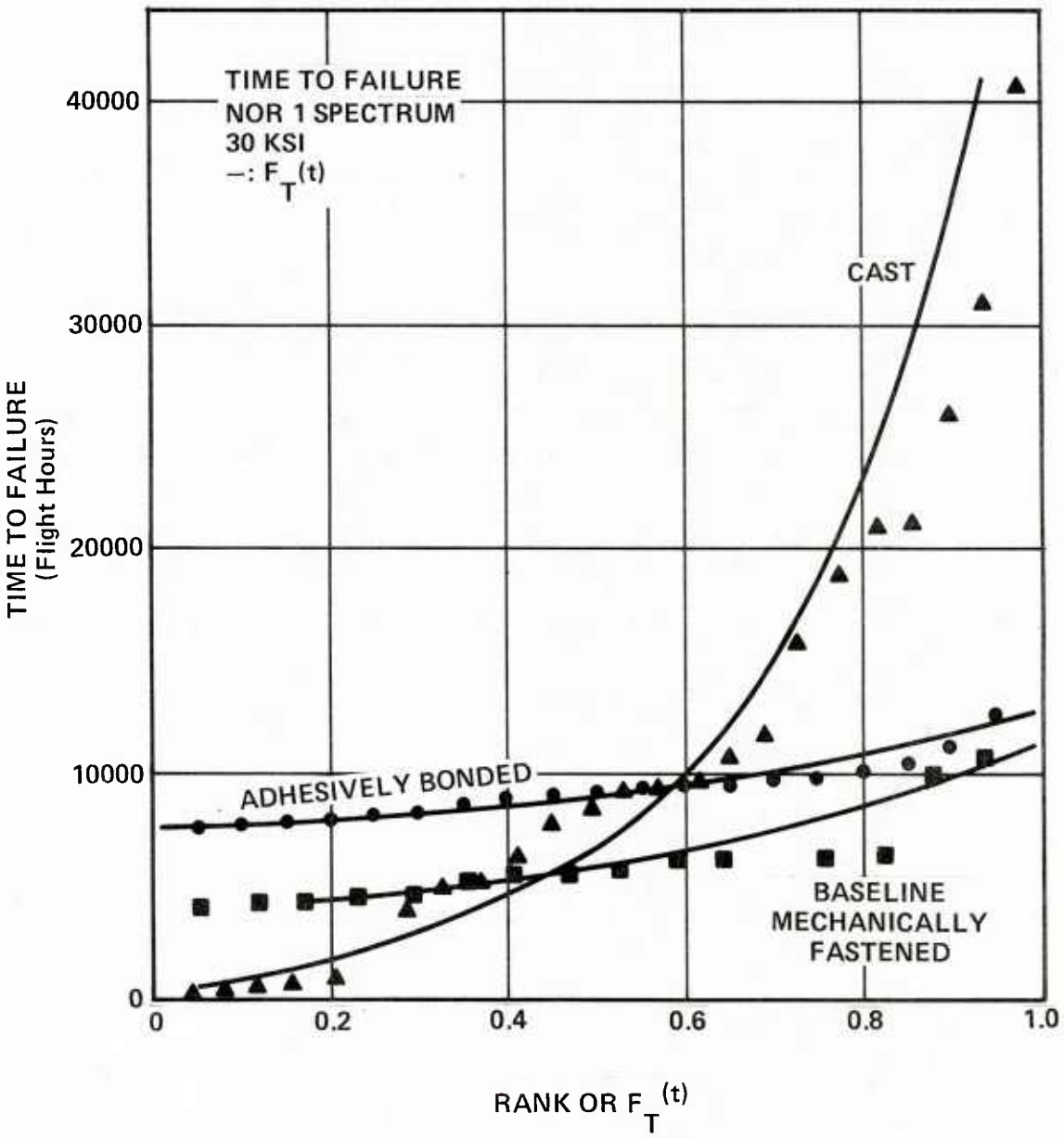

Figure 56. Comparison of Time-to-Failure in Adhesively Bonded, Baseline and Cast Specimens

SECTION IV

DISCUSSION

In Section III the IFQ model parameters for advanced joining concepts were presented. Also, the TTCI and EIFS distributions were examined for goodness-of-fit. In this section, IFQ and crack growth behavior of advanced joining concepts will be compared and discussed. Also, a methodology will be proposed to aid in comparing competing structural concepts during design.

4.1 DIRECT COMPARISON OF TEST RESULTS

To compare the EIFS of advanced joining concepts, the distribution of EIFS obtained from identical test conditions (NOR 1 spectrum, 30 ksi) is plotted for adhesively bonded, baseline, and cast specimens in Figure 57. Each data point in Figure 57 represents the calculated EIFS vs. i/(n+1) pair for a single specimen. The curves are the best fit distribution, $F_{a(o)}(x)$. $F_{a(o)}(x)$ was calculated as in Section III, using Equation 8 and Table 16.

Figure 57 shows that each joining concept possesses a quite different range of EIFS and average EIFS. The average EIFS and the range of the EIFS values are summarized in Table 17. As shown in Table 17, adhesively bonded specimens have the largest average EIFS and the widest range of EIFS values, while cast specimens have the smallest average EIFS and the narrowest range of EIFS values.

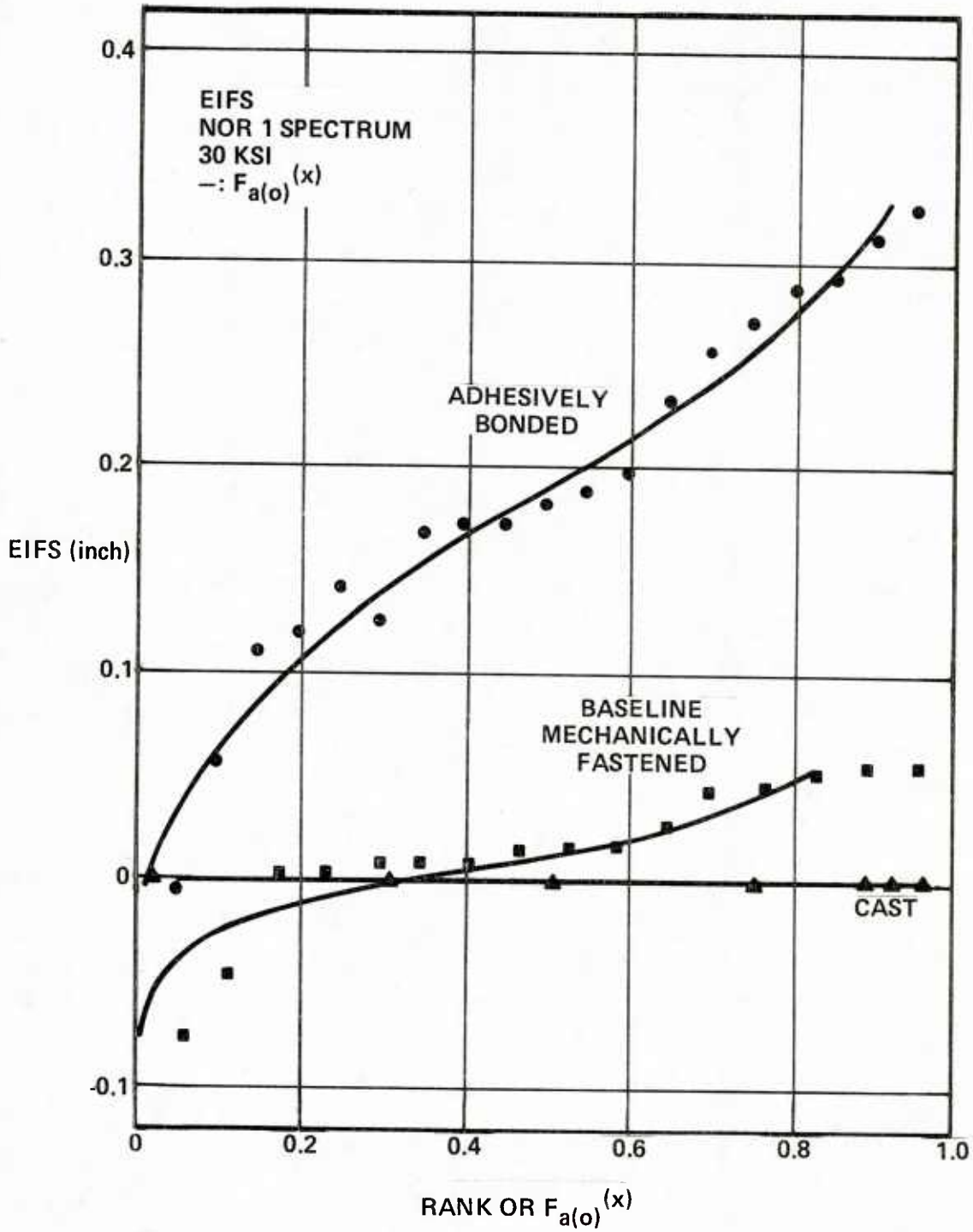

Figure 57. EIFS Comparison in Adhesively Bonded, Baseline, and Cast Specimens

Table 17 EIFS of Each Joining Concept (NOR 1, 30 KSI)

SPECIMEN	AVG EIFS (In.)	STD DEVIATION (In.)	RANGE OF EIFS (In.)
Adhesively Bonded	1.933×10^{-1}	8.739×10^{-2}	-2.591×10^{-3} to 3.281×10^{-1}
Baseline	2.276×10^{-2}	2.025×10^{-2}	-7.687×10^{-2} to 5.573×10^{-2}
Cast	1.020×10^{-7}	2.268×10^{-7}	4.820×10^{-10} to 1.790×10^{-6}

It may appear that cast specimens have the best IFQ compared with the other joining concepts. However, fatigue performance of materials depends on not only the EIFS but on fatigue crack growth behavior.

Equation 15 can also be applied to calculating the time required for an initial defect to become a fatigue crack of size a(t):

$$t = \frac{1}{CQ}\left[a^{-c}(0) - a^{-c}(t) \right] \tag{16}$$

Using Eq. 16 the crack growth behavior of the joining concepts can be determined in terms of an a(t) vs. t plot. However, as mentioned previously, each joining concept has a quite different range of EIFS and critical crack size. Hence, the normalized crack size, $a(t)/a_{crit}$ can be more conveniently used for the comparison of the crack growth behavior of the joining concepts.

Figure 58 shows the $a(t)/a_{crit}$ vs. t plot of each joining concept. For the determination of t in Figure 58 the mean EIFS (i.e. 50% rank EIFS) was used. Therefore, t in Figure 58 represents the mean-time to reach any crack size.

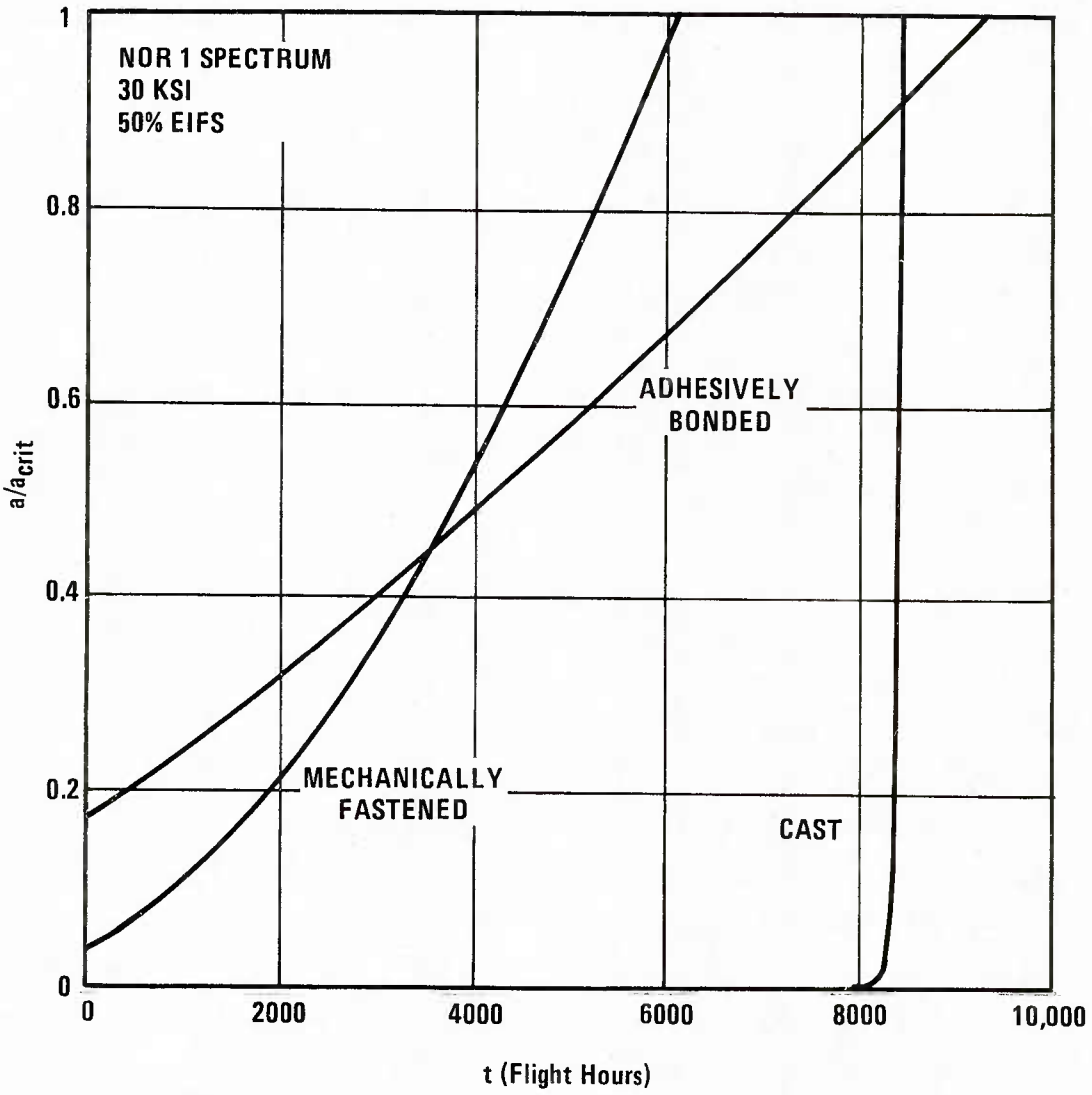

Figure 58. Comparison of Crack Growth Behavior in Adhesively Bonded, Baseline, and Cast Specimens

Note from figure 58 that cast specimens exhibit quite different crack growth behavior compared with adhesively-bonded and mechanically-fastened specimens. Cast specimens require a much longer mean time for the initiation of a crack, but once a crack is initiated, the crack grows relatively faster to critical size.

Also, note from Figure 58 that adhesively bonded specimens start with the largest initial defect but the time required to reach the critical crack size for adhesively bonded specimens is longer than that for other joining concepts.

For further information on the crack growth rate of the observed joining concepts, Figure 59 shows the log $d[a(t)/a_{crit}]/dt$ vs. $a(t)/a_{crit}$ plot of each joining concept. To determine the normalized crack growth rate (i.e. $d[a(t)/a_{crit}]/dt$) Eq. 11 was modified to:

$$\log \frac{d[a(t)/a_{crit}]}{dt} = b \log a(t) + \log Q - \log a_{crit} \qquad (17)$$

By using 95% range log $\hat{Q}$ values (i.e. mean log $\hat{Q} \pm 2\sigma$), the range of log $d[a(t)/a_{crit}]/dt$ was determined as shown in Figure 59.

Figure 59 shows that, at any normalized crack size, cast specimens have the fastest normalized crack growth rate, while adhesively bonded specimens have the slowest normalized crack growth rate. Also, the size of the 95%

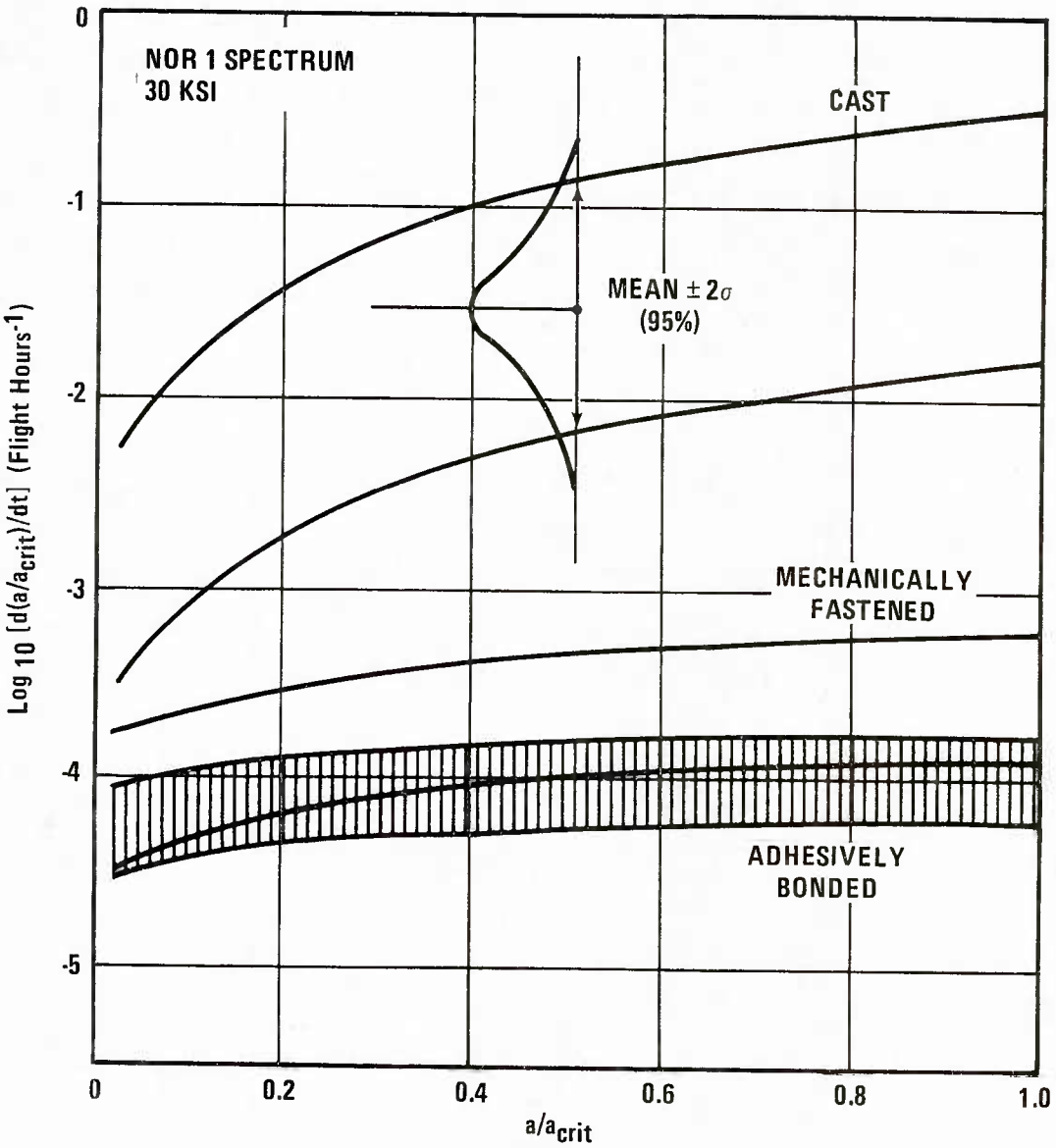

Figure 59. Comparison of Crack Growth Rate in Adhesively Bonded, Baseline, and Cast Specimen

range indicates that the normalized crack growth rate scatter is largest for castings and smallest for adhesively bonded specimens.

4.2 FLAW DISTRIBUTION AFTER SERVICE AND RELIABILITY CALCULATION

The previous section helps to show the importance of the interplay between the IFQ as quantified by the EIFS distribution and the crack growth rate. Figure 57 shows that castings have the smallest equivalent initial flaws of the three structural concepts, while Figure 59 shows castings also have the highest relative crack growth rate. These two elements must be combined in order to judge their relative importance, as in Figure 56.

The recommended method for properly considering both the EIFS distribution and the crack growth rate is to combine them to compute the flaw distribution after a desired service interval. This will be called the flaw distribution after service (FDAS). It can be easily computed by transforming Eqs. 8, 9, and 16 to obtain:

$$F_{a(T)}(x) = P[a(T) \leq x]$$

$$= \exp\left\{-\left[\frac{x^{-c} - a_o^{-c} + cQT(T-\epsilon)}{cQ\beta}\right]^{\alpha}\right\} \qquad (18)$$

where $F_{a(T)}(x)$ is the distribution of flaws after time T (i.e., the FDAS).

Equation 18 can be used to find the cumulative flaw distribution for any conditions. The parameters a_o, α, β, and ϵ for three structural concepts are given in Table 16. The parameter x can represent any flaw size of interest. The parameters Q and c (where c=b-1) describe crack growth, which is a function of geometry and loading. These are already known for the test conditions of this program and are given in Table 16. They can also be calculated using any valid crack growth prediction, such as a cycle-by-cycle computer anlaysis.

As an example, we might consider the probability that a 0.6-inch crack could exist in an adhesively bonded joint under NOR 1 spectrum conditions at 30 ksi after 4000 hours of service. Since the probability that a crack exceeds 0.6 inch is equal to $1-P[a(t) \leq 0.6]$, we can use Eq. 18 with x = 0.6 and T = 4000. The probability that a crack exceeds 0.6 inch is found to be 0.34. We can similarly compare the effect of using unscrimmed adhesive by substituting appropriate values from Table 16. The probability for unscrimmed adhesive is only 0.0002 , which shows tha advantage of unscrimmed FM-73 adhesive under these test conditions.

As another example, consider calculating the reliability for an application using A357 castings under the same loading conditions after 8000 flight hours. In this case, the information desired is the probability that a flaw is less than a_{crit}. Again Eq. 18 and values from Table 16 can be employed, with x = .194 in. and T = 8000.

The reliability for the above example (55%) is irrelevant. However, the method is important for obtaining quantitative, statistically based information for design

comparisons with relatively little effort. The parameters α, Q, β, and ϵ are fixed, since they were derived to be generic over all test conditions. (See Appendix A for details). Therefore these values can be obtained from Table 16 for any application. The value of a_o for these parameters is also given there. The crack growth parameters can be found from a crack growth analysis. It is only necessary to least squares fit the best line from the form given by Eq. 11 to the crack growth prediction. The parameters Q and b will then be known, and the product $Q\beta$ is constant for generic EIFS and is known from Table 16, so the proper value of β is determined uniquely. In this way, Eq. 18 can be used to find the flaw size distribution at any time, or for a reliability estimate for the intended application. This topic will be further explored at the conclusion of the following section.

4.3 STRESS AND SPECTRUM DEPENDENCE

An underlying assumption of analyses in this report is that the EIFS distribution is generic, that is, the same EIFS distribution can be used for different spectra and stress levels. This implies that for two test conditions, we must have

$$F_{a(o)}(x)_1 = F_{a(o)}(x)_2 \qquad (19)$$

Substituting Eq. 8, and noting that Eq. 19 must be true for all values of x, gives the conditions:

$$b_1 = b_2$$
$$\alpha_1 = \alpha_2 \qquad (20)$$
$$Q_1\beta_1 = Q_2\ \beta_2$$

See Appendix A for further details.

In Appendix A of the Phase I report for this program [7], data and rationale were presented to show that the conditions expressed above are indeed true for data generated in the Fastener Hole Quality program [4]. The excellent fit given by single EIFS distributions for combined data sets, shown in Figs. 48, 50, and 52, gives further support from the current program. Also, in Appendix A of Reference [7], it is shown that the relationship between test stress level, σ , and characteristic crack growth rate, Q, is given by

$$Q_i = A\ \sigma_i^{B} \qquad (21)$$

for a reasonable range of σ . Alternatively, since $Q\beta$ is constant, Eq. 21 can be used to find β for any stress level. Equation 21 provides the means for determining the effect of spectrum stress on structural performance.

Available data indicates [4,20] that B does not vary with changes in spectrum for a given material/structure. Since crack growth rate and Q_i do change for various spectra, A is postulated to be a characteristic measure of spectrum severity for a given material/structure. It is

beyond the scope of this program to ascertain whether this is generally true. However, the test plan carried out in this program does allow A and B to be determined. These are given in Table 18.

The exponent B is constant for a structural concept so that crack growth may be scaled for stress changes simply by using B from Table 18. For spectra different than those used in this program, crack growth predictions must be used to determine A. To minimize error, limited testing should be done for some known spectrum and stress level, to determine a valid Q - σ pair. A can be found from Eq. 21 if B in Table 18 is used. A crack growth analysis should be performed and the fit checked against the observed crack growth. Then a similar analysis can be performed for each new spectrum to determine A in Eq. 21. Eq. 21 then provides the basis for performing tradeoffs for varying stress levels.

We can now return to the calculation of reliability. Plugging critical crack sizes and other parameters found in Table 16 into Equation 18, reliability of each of the structural concepts may be calculated at any service time. Furthermore, the calculations may be repeated for any stress level by employing Eq. 21 and Table 18 to find appropriate values of Q.

This has been done and results plotted in Fig 60, for the NOR 1 spectrum at T = 16,000 flight hours. Relative rankings of the competing structural concepts are obviously sensitive to stress level. Since aircraft structural

Table 18 Parameters for use in Equation 21 to Determine Stress and Spectrum Dependence of Structural Performance

CONCEPT	SPECTRUM	A(1)	B
Adhesive Bonding, Scrimmed	NOR 1	3.15×10^{-12}	5.09
Adhesive Bonding, Unscrimmed	NOR 1	1.53×10^{-12}	5.09(2)
Mechanical Fastening, Sealant	NOR 1	5.26×10^{-10}	3.72
Mechanical Fastening, No Sealant	NOR 1	5.36×10^{-7}	3.72(2)
Monolithic Casting	NOR 1	1.01×10^{-12}	7.27
Monolithic Casting	GAR 2	1.46×10^{-12}	7.27(2)

(1) A given where σ expressed in ksi
(2) Assumed value

reliabilities less than 90 percent are generally of little interest, a closer look at the region of interest is shown in Fig 61. This indicates that at high reliabilities, castings can tolerate the least stress and adhesively bonded joints can tolerate the most stress, for the conditions stated. However, for 90 percent reliability, Figure 61 predicts that castings can actually be used at a slightly higher stress level than mechanically fastened 2124-T851 in the short transverse direction.

One additional item which might be considered in any statistically-based analysis is the confidence level

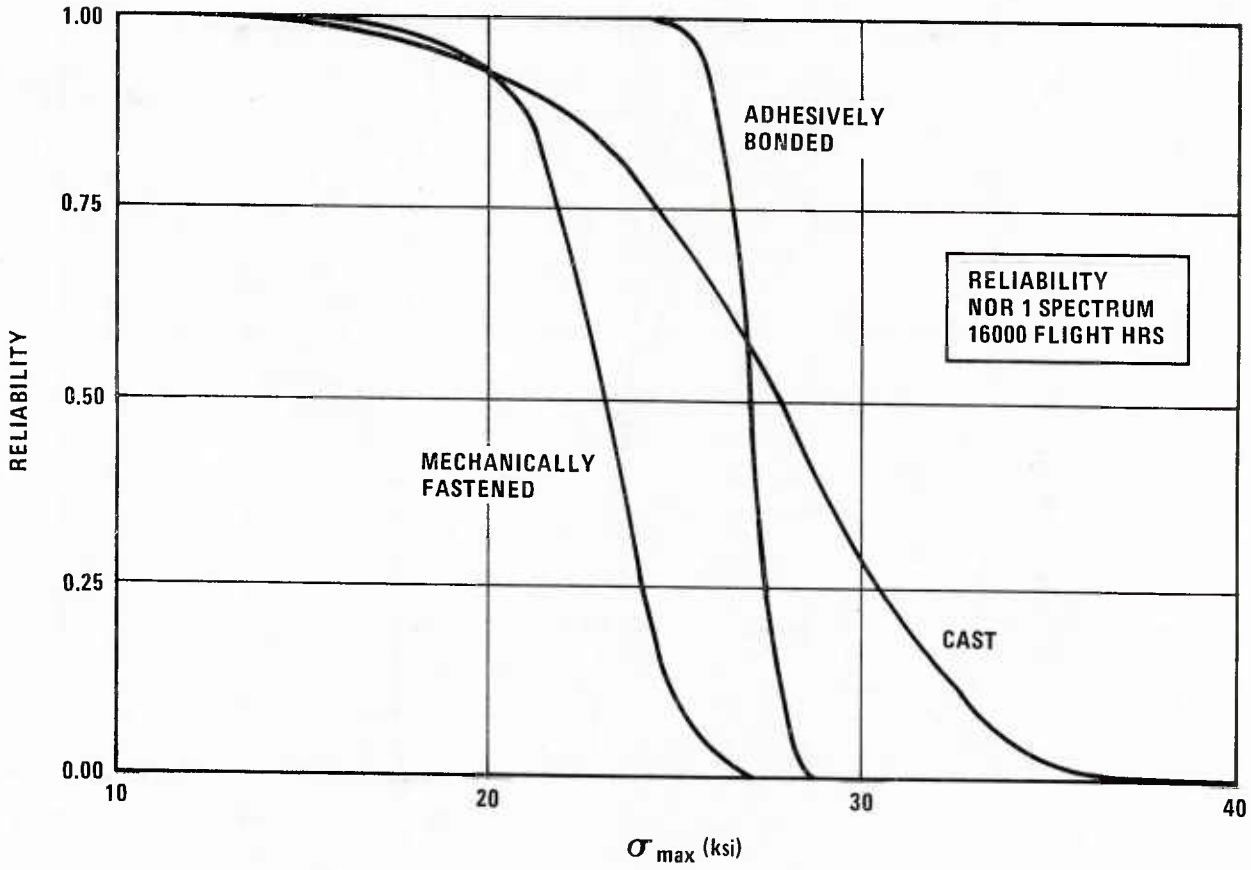

Figure 60. Comparison of Structural Reliability of Three Joining Concepts at 16,000 Flight Hours – NOR 1 Spectrum at 30 KSI

associated with estimates of distribution parameters. For $\alpha=0$, the prediction of structural performance will ultimately be based on statistical estimates of α (representing true life variability) and β (representing actual characteristic life). These estimates must be based on the 50% confidence (best fit) estimates which are obtained from the test data. 95% confidence estimates of $\hat{\alpha}$ and $\hat{\beta}$ must be lower than the 50% confidence limits, α and β . The

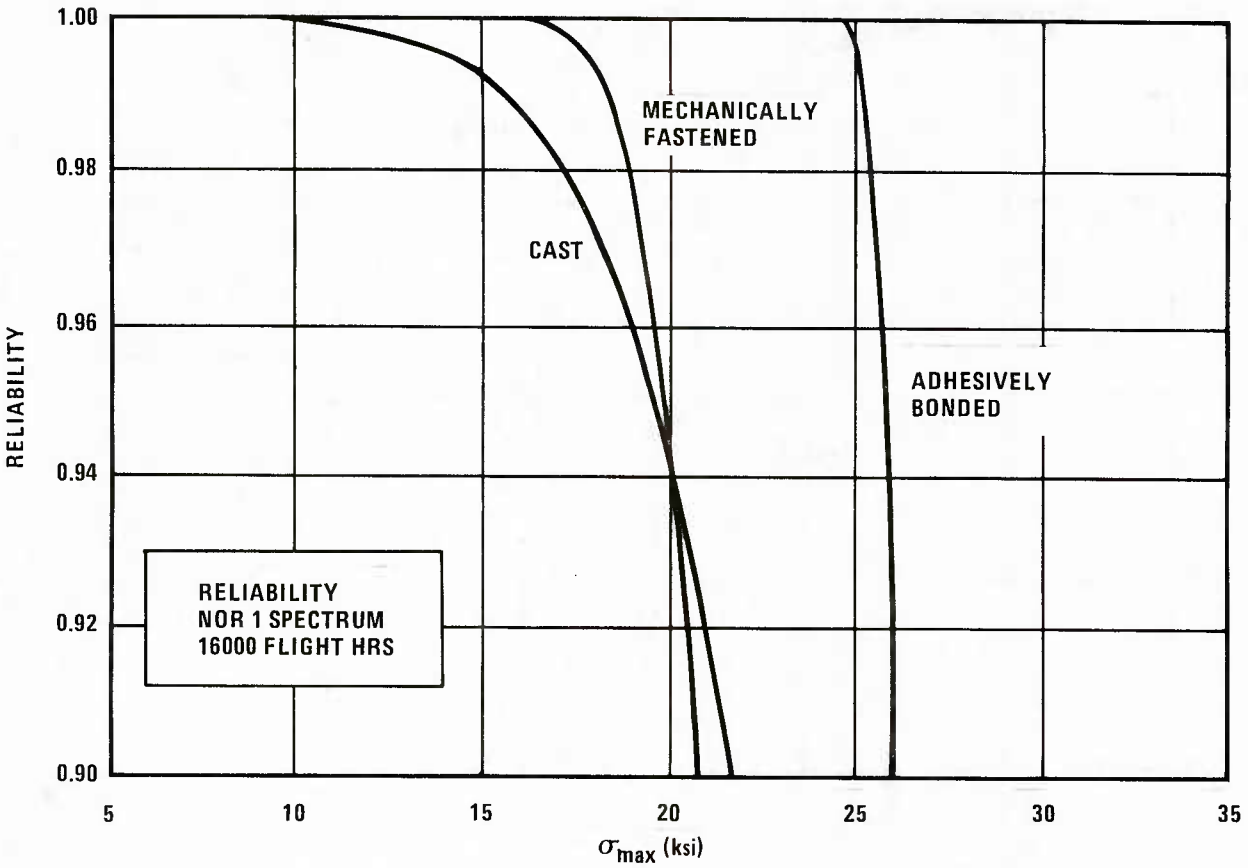

Figure 61. Comparison of Reliability Above 90 Percent for Three Joining Concepts

relationship between the two for the Weibull distribution can be represented

$$\hat{\alpha} = f \cdot \alpha$$
$$\hat{\beta} = g \cdot \beta \qquad (22)$$

The greater the number of specimens, the closer f and g are to unity, that is, the closer 95% confidence estimates are to the measured 50% confidence values. The values of f and g for various sizes of data sets have been extracted from Ref. [26] and summarized in Table 19.

Table 19 Factors for 90% and 95% Confidence in α and β

NUMBER OF SPECIMENS	10	20	40	50	100
f for 90% Confidence	63	.74	.83	.85	.89
g for 90% Confidence	.62	.73	.80	.82	.87
f for 95% Confidence	.55	.68	.78	.81	.87
g for 95% Confidence	.53	.65	.75	.78	.84

These factors can be used, along with the 50% confidence data presented in this report, to calculate 90% and 95% confidence estimates of $\hat{\alpha}$ and $\hat{\beta}$ for all joining concepts. Table 19 is also useful for planning the size of a sample for new applications of this methodology.

4.4 TRADEOFF METHODOLOGY FOR CRACK-GROWTH-CRITICAL STRUCTURE

Note that Figures 60 and 61 are calculated for a particular load history and service life for specific materials and structural concepts. No conclusions can be drawn from these figures for other materials, structural concepts, or joint geometries. Although not validated generally, the methodology does provide a means to extrapolate to other stress levels and spectra. This translates into the ability to predict structural performance of a given joining concept at many locations throughout the structure, or to conduct parametric weight studies by varying thickness, and therefore stress. Materials, manufacturing procedures, or design concepts other than those presented here, require coupon testing to establish baseline performance. Suggestions for conducting trade studies to compare structural performance of competing joining concepts follow.

Researchers at Lockheed have published a methodology for conducting weight-trade studies based on material properties and primary failure mode in a given structural component [27]. That methodology calculates relative structural efficiency by combining mechanical properties which control failure in each mode. For example, the relevant properties controlling the weight of structure which fails in simple tension are simply the tensile strength and the density of material. Similarly, the weight of a structural element which tends to buckle can be related to the elastic modulus and yield strength in compression, along with the material density. For fracture critical structural elements, the tendency has been to use density and fracture toughness (or sometimes constant amplitude crack growth rate at some stress intensity factor range) for characterizing structural weight. However, fracture toughness (or one point on a constant amplitude da/dN vs. ΔK curve) does not adequately determine the allowable stress for an element subject to complex spectrum fatigue loading. Instead, total spectrum crack growth and initial manufactured fatigue quality play a major role in determining structural life and allowable spectrum stress level.

We have suggested an alternative method of calculating crack sizes in a structure, which is statistically-based, is convenient, and which takes proper account of crack growth and IFQ. We propose that this method be used to estimate structural integrity and efficiency of crack-growth critical structure. The following elements we feel would provide a viable and accurate approach to estimating tradeoffs during design.

1) Select competing structural concepts. The design concepts must be defined in terms of preliminary designs in order to conduct the study.

2) Generate spectrum fatigue data for each joining concept. Data should be gathered for a relevant load history at two different stress levels.

3) Determine crack growth during testing. Fractography is highly recommended for its accuracy and very low manpower requirements. Other methods may be used if desired.

4) Analyze data as outlined in Appendix A or References [19 or 20] to obtain crack growth, and the TTCI and EIFS distribution parameters.

Note Steps 2 - 4 may be eliminated if data already exist. Sources of data include this report and References [20,28,29].

5) Predict crack growth. If using a cycle-by-cycle analysis it is recommended that observed data from step (3) be matched first to ensure accuracy of the analysis. New stress levels can be handled by Eq. 21.

6) Analytically grow the crack population forward, Eq. 18. This requires only that a service life goal be established and that the significant flaw size (e.g., critical crack size) and desired structural performance (e.g. reliability) be known.

7) Permute section thicknesses or other drivers to determine acceptable stresses (and weights) for the desired structural performance.

In this connection, note that Eqs. 18 and 21 imply that the allowable stress is given by solving:

$$F_{a(T)}(x) = \text{Desired reliability} = \exp\left[-\frac{a_{crit}^{-c} - a_o^{-c} + cA\sigma^B(T_{service} - \epsilon)}{cQ\beta}\right] \quad (23)$$

where all quantities except σ (including the product of $cQ\beta$) are known from Tables 16 and 18 or from testing. The allowable stress/density determines the appropriate weight fraction for fracture-critical structure in the failure mode type of weight-trade study.

4.5 GENERAL FIGURE-OF-MERIT

The foregoing section provides a method of determining the structural reliability for a given joining concept and service life. The weight of a structural concept is related to the service life and reliability by local section thickness and applied loading - that is, by stress. Therefore the methods presented in this report permit a designer to trade weight against life for competing structural concepts.

In actual practice, any aerospace structural design is the result of myriad considerations. These include such items as previous experience and confidence in the concept, philosophy of design, facilities available, sources of materials, ease and reliability of inspection, maintainability and supportability, and difficulty and confidence in design. Of course, performance goals and loading directly

influence the design. These all provide the context in which a design is selected.

In keeping with one of the objectives of this program, we have attempted to formalize a rational method for combining design selection considerations to produce a general figure-of-merit (FOM) for each of the joining concepts we have studied. We have been unable to completely reach this goal. It is difficult to quantify a tradeoff between dissimilar concepts such as pounds of weight or service hours against "experience" or "design philosophy". It is probably impossible to quantify a universal conversion factor between weight and maintainability.

We propose that a proper comparison can only be arrived at after certain tangible and intangible considerations are weighed by the designer or contractor to produce a list of acceptable design concepts. We suggest that cost is the most universally applicable normalizing parameter. Items such as facilities requirements, material sources, ease of inspection, ease of maintenance, weight, performance, and life can usually be expresssed in terms of cost. Methods to do this are available and beyond the scope of this program. Then, the most important items affecting design selection are cost, weight, and life. Of these, life requirements for a new design or redesign are usually fixed. Therefore the usual necessity is to trade weight-versus-cost, where cost includes not only material and labor, but facilities, maintenance, repair - in short, the lifecycle cost.

We have proposed an improved methodology for comparing the structural performance and efficiency of competing design concepts for fracture-critical structure. The method can be used to determine allowable spectrum stress level,

and therefore weight, for any joining concept, reliability and service life. Other aspects of the advanced joining concepts studied in this program cannot be so universally quantified.

The Phase I report for this program [7] includes considerable discussion of premium aluminum castings and adhesively bonded structure. Several references from relevant research are included. On the whole, cost savings available through use of monolithic aluminum castings are about 35 to 45 percent. These savings arise from lower material costs, greatly reduced machining and assembly costs, and additional savings due to reduction in parts count. However, the cost-saving potential is highly dependent on application, and may be zero, so general rules are difficult to formulate. The chief disadvantages of castings to date are limited strength, limited sources for some premium castings, the need for costly inspection, and low confidence in reliability. This program has provided data and a methodology which can go a long way to improve the last item in the list. Available cost savings via adhesive bonding have been estimated at up to 30 percent, but again, this would be application-dependent. Other benefits apply as well. Data from this program has shown excellent crack growth resistance. Also crack growth does not accelerate with crack length, producing great residual strength, even when a flaw is large. This, coupled with the inherent ease of inspection via ultrasonic techniques, provides excellent ability to ensure structural integrity through application of nondestructive inspections. However, strength is limited so that adhesive bonding of high-strength aluminum is limited to thicknesses of less than about 0.25 inch. Special fabrication facilities are also required. Finally, design using damage tolerance concepts

in fracture-critical adhesively bonded structure could be difficult.

SECTION V

CONCLUSIONS

The following conclusions are drawn from this program.

1. The initial fatigue quality model is found to be a very useful tool to predict the fatigue crack growth behavior of competing structural concepts.

2. The FM-73 adhesively bonded specimens used in this program had the largest equivalent initial flaw size, but they exhibited the slowest normalized crack growth rate in service, thereby requiring the longest time for an initial defect to reach the critical crack size among the concepts tested in this program. Adhesive bonding is recommended as the most promising advanced joining concept compared to mechanical fastening and monolithic aluminum castings.

3. Use of adhesives without scrim fibers can dramatically improve the structural performance and reliability of adhesively bonded structure.

4. Even though the A357 cast specimens used in this program possess the smallest equivalent initial flaw size, the normalized crack growth rate was much faster than the other joining concepts. Also, our cast specimens exhibited the most scatter in time-to-failure and crack growth rate data. A357 aluminum castings can be comparable in structural performance to conventional construction and usually have the lower cost.

5. Based on Fig. 57 and Tables 7-14, reasonable initial flaw types and sizes for the different structural concepts, based on the 90th percentile EIFS, would be:

   FM-73M Adhesive - a 0.30-inch central debond

   2024-T851 Baseline - a 0.050-inch fastener hole corner flaw

   A357-T6 Casting - a 0.001-inch fastener hole corner flaw

6. The EIFS distributions were found to be independent of test conditions. They can conveniently be used, along with crack growth rate estimates, to quantitatively determine and compare structural performance of joining concepts.

7. Defects in A357 castings were found to initiate fatigue cracks, and some were associated with early failures, but there was not a general correlation between defects and failure times.

8. None of the inspection techniques correlated well to EIFS or structural performance in any of the joining concepts. It was concluded that conventional NDI techniques cannot find the very small defects present in well-made components.

9. It is important to test representative test elements when obtaining IFQ data. As evidence, consider the dramatic shift in failure mode and flaw type when sealant was removed from the baseline specimens or when unscrimmed adhesive was tested.

10. Experimental data confirmed the analytical prediction that crack growth rate in adhesive bondlines would not depend on flaw size. However, it is very difficult to compute an appropriate value for strain energy release rate or stress intensity factor in an adhesive bond.

SECTION VI

RECOMMENDATIONS

1. The tradeoff methodology depends upon the availability of IFQ data, which requires several hundred manhours of testing and analysis per material/concept. A data base should be established for the most commonly used materials and joining concepts or for those with high potential for perforance or cost benefits.

2. Current Air Force damage tolerance specifications ensure that cracks which might be missed during inspection remain below the critical crack size throughout the life of the structure. These specifications essentially assure that a fully inspected airframe has the same reliability as the probability of detecting the assumed initial flaw size. Assurance is provided by deterministic crack growth analyses backed up by structural tests. Since an airframe with only 50 percent reliability stands an even chance of passing a structural test, the only economical way to assure high levels of reliability is through analysis based on statistically derived material properties (or inspection capability). We recommend the methods proposed in this program as an alternate basis for meeting durability and damage tolerance specifications. We feel these methods, based on element level testing, provide an effective compromise between the deterministic analyses and limited testing on the one hand, and very high costs associated with multiple structural tests, on the other.

3. We encourage consideration of adhesive bonding for joining crack-growth-critical structure.

4. Develop methods for handling and processing unscrimmed structural adhesives to improve strength and resistance to crack growth.

5. Develop methods to detect and to minimize causes of fast crack growth in premium aluminum castings. Mean time-to-failure of our A357 castings was actually longer than for 2124 plate, but scatter in crack growth rate was much larger in A357. If the most damaging portion of the scatter can be eliminated through processing or inspection improvements, low-cost structure could be built with much better performance and reliability.

6. More specific strategies should be developed to formalize intangible elements of design selection. This may amount to trying to document and transfer "experience". An effort to develop industry-wide aerospace design practice handbooks might be one approach.

7. We recommend keeping the initial flaw assumption at fastener holes as 0.050 inch for damage tolerence analysis in conventional construction. However, it appears new materials or classes of construction should be examined individually.

REFERENCES

1. MIL-STD-1530A (USAF), "Aircraft Structural Integrity Program," 11 December 1975.

2. MIL-A-83444 (USAF), "Airplane Damage Tolerance Requirements," 2 July 1974.

3. MIL-A-8866B (USAF), "Airplane Strength and Rigidity Reliability Requirements, Repeated Loads and Fatigue," 22 August 1975.

4. P. J. Noronha, S. P. Henslee, D. E. Gordon, Z. R. Wolanski, and B. G. W. Yee, "Fastener Hole Quality," Report AFFDL-TR-78-206, Vol. I, December 1978.

5. S. D. Manning, J. N Yang, M. Shinozuka, D. E. Gordon, S. M. Speaker, B. G. W. Yee, "Durability Methods Development - Phase II Summary," AFFDL-TR-79-3118, Vol. VII, August 1982.

6. W. R. Garver, "Spectrum Fatigue Testing of Mechanical Fasteners for Structural and Fuel Integrity," ERR-FW-2069, General Dynamics Report, April 1981.

7. W. R. Garver, "Initial Quality of Advanced Joining Concepts - Phase I," AFWAL-TR-83-3064, June 1983.

8. T. R. Brussat, S. T. Chiu, and S. Mostovoy, "Fracture Mechanics for Structural Adhesive Bonds - Final Report," AFML-TR-163, 1977.

9. T. R. Brussat, S. T. Chiu, and S. Mostovoy, "Fracture Mechanics for Structural Adhesive Bonds, Phase II, Final Technical Report," AFML-TR-163 Part II, 1978.

10. D. L. Potter, "Primary Adhesively Bonded Structure Technology (PABST), Design Handbook for Adhesive Bonding," AFFDL-TR-79-3129, Nov. 1979.

11. John Romanko and W. G. Knauss, "Fatigue Behavior of Adhesively Bonded Joints," Vol. I, General Dynamics, Fort Worth Division Report FZM-6889, January 1980, (Final Draft).

12. "Integrated Methodology for Adhesive Bonded Joint Life Predictions," Quarterly Progress Report No. 1, General Dynamics, Fort Worth Division Report FZM-6879, December 1979.

13. "Premium Castings," Product Manual, Premium Castings Division of Alcoa, Corona, CA, 1972.

14. Donald Goehler, "CAST Aluminum Structures Technology, Phase II, (CAST)," AFFDL-TR-78-7, January 1978.

15. C. E. Doyle, "Cast Aluminum Primary Structure: Detail Design Phase," General Dynamics, Fort Worth Division ERR-FW-1996, 22 December 1978.

16. J. M. Potter, W. R. Garver, K. M. Koepsel, and B. G. W. Yee, "Fatigue Crack Topology and Crack Growth," AGARD Report.

17. W. S. Johnson, and T. Spamer, "A User's Guide to CGR-GD, A Computerized Crack Growth Prediction Program," General Dynamics, Fort Worth Division Report FZS-241, November 1976.

18. S. Forness, "Fracture Mechanics Methodology Update," General Dynamics, Fort Worth Division ERR-FW-2219, May 1982.

19. S. D. Manning, J. N. Yang, M. Shinozuka, D. E. Gordon, S. M. Speaker, and B. G. W. Yee, "Durability Methods Development, Volume V," Air Force Flight Dynamics Laboratory, AFFDL-TR-79-3118, Vol. V, 1982.

20. S. D. Manning, J. N. Yang, and J. W. Norris "USAF Durability Design Handbook: Guidelines for the Analysis and Design of Durable Aircraft Structures," Air Force Flight Dynamics Laboratory, AFFDL-TR-99-3118, Vol. XI, February 1983.

21. D. A. Virkler, B. M. Hillberry, and P. K. Goel, "The Statistical Nature of Fatigue Crack Propagation," AFFDL-TR-78-43, April 1980.

22. J. Romanko, K. M. Liechti, W. G. Knauss, "Integrated Methodology for Adhesive Bonded Joint Life Predictions," Final Report, AFWAL-TR-82-4139, November 1982.

23. "Viscoelastic Stress Analysis Including Moisture Diffusion for Adhesively Bonded Joints," Semi-annual Progress Report No. 2 (April 1981 to September 1981), General Dynamics, Fort Worth Division Report FZM-6994, September 1981.

24. B. Dattaguru, R. A. Everett, J. D. Whitcomb, and W. S. Johnson, "Geometrically Nonlinear Analysis of Adhesively Bonded Joints," NASA Technical Memorandum 85462, September 1982.

25. W. S. Johnson, NASA Langley Research Center, FFB, Adhesive Bonded Systems, private communication, January 1981.

26. D. R. Thoman, L. J. Bain, and C. E. Amtle, "Maximum Likelihood Estimation, Exact Confidence Intervals for Reliability and Tolerance Limits in the Weibull Distribution," Technometrics, May 1970, Vol. 12, No. 2, pp. 363-371.

27. J. S. Ekvall, J. E. Rhodes, and G. G. Wald, "Methodology for Evaluating Weight Savings from Basic Material Properties", Design of Fatigue and Fracture Resistant Structures, ASTM STP 761, 1982, pp. 328-341.

28. P. J. Noronha, S. P. Henslee, D. E. Gordon, Z. R. Wolanski, and B. G. W. Yee, "Fastener Hole Quality," Report AFFDL-TR-78-206, Vol. II, December 1978.

29. S. M. Speaker and D. E. Gordon, "Durability Methods Development, Volume VIII - Test and Fractography Data", AFFDL-TR-79-3118, October 1982.

30. M. G. Salvadori and M. L. Baron, "Numerical Methods in Engineering", Prentice-Hall, Inc., NJ, 961.

31. R. H. Edwards, "Stress Concentrations Around Spheroidal Inclusions and Cavities," Journal of Applied Mechanics, Vol. 75, pp. 19-30, 1951.

APPENDIX A

EQUIVALENT INITIAL FLAW SIZE, AND DATA POOLING TECHNIQUES

A.1 EIFS Concept

One of the most important factors governing the structural performance of advanced structural concepts is the initial fatigue quality (IFQ). IFQ defines the initial manufactured state of a structural detail with respect to crack growth which is expected to occur in service. The IFQ for a group of replicate details can be presented by a distribution of equivalent initial flaw sizes (EIFS). Given that a crack occurs in a structure during service, the EIFS is the size of a hypothetical initial flaw which would result in the observed crack. The EIFS can be derived using fractography from fatigue test results. Crack growth observed after fatigue testing (fractography) is extrapolated backward to estimate EIFS. An EIFS distribution is obtained by fitting a statistical distribution to EIFS data sets.

An arbitrary crack size a_o can be selected such that it can be unambiguously observed. The time required for an initial defect to become a fatigue crack of size a_o is defined as the time-to-crack-initiation (TTCI). In general, the EIFS distribution is chosen so that the crack growth rate maps the EIFS distribution into the observed TTCI distribution. A conceptual description of the IFQ model is shown in Figure A1.

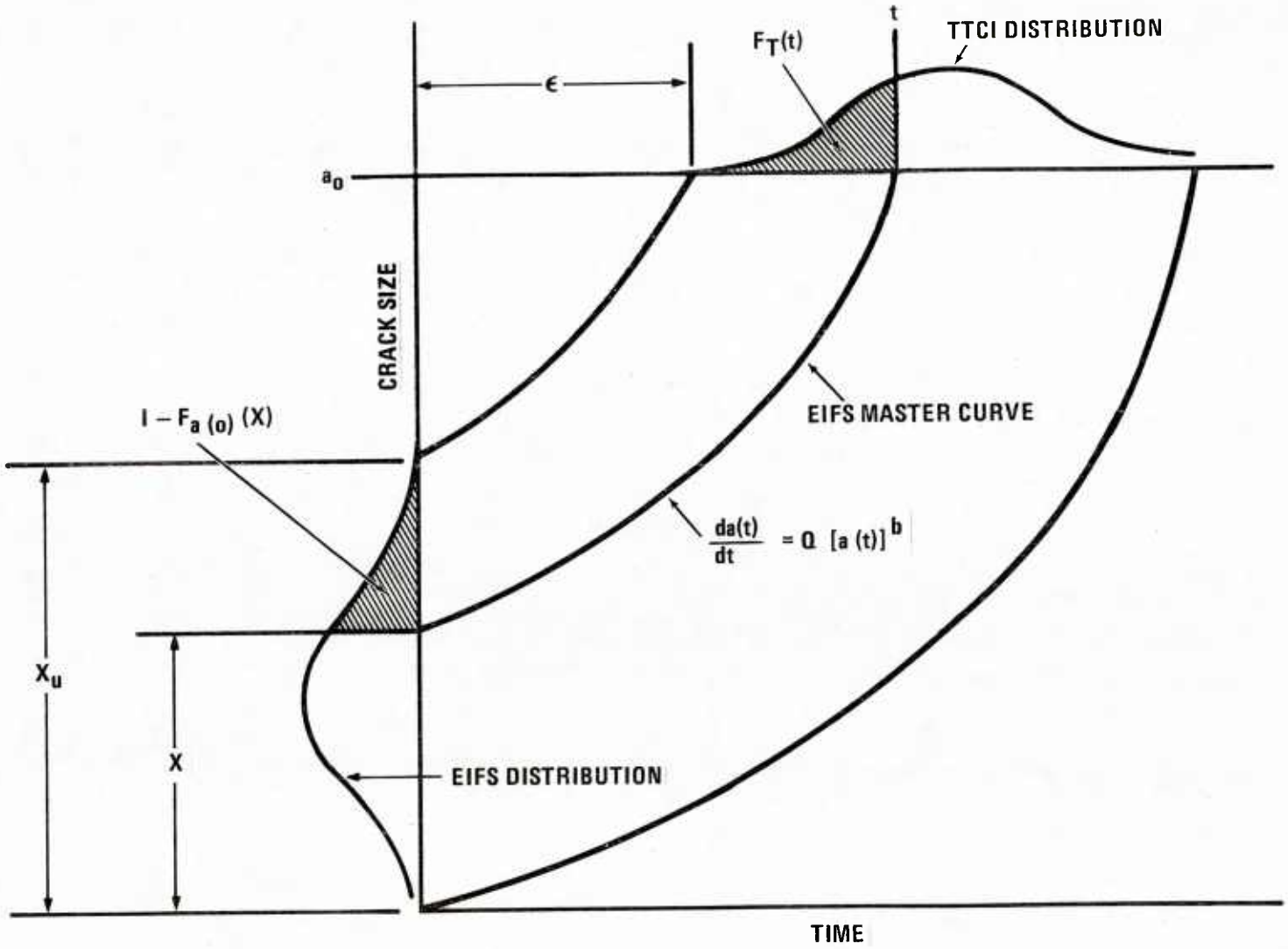

Figure A1. Conceptual Description of IFQ Model

The motivation for the EIFS concept is the hope that once the EIFS distribution is established, the fatigue crack population for any potential service load spectrum can be analytically predicted without further experimental tests. Intuitively, EIFS is an inherent property of such factors as the material, manufacturing/assembly techniques, and workmanship. An EIFS distribution should not depend on subsequent service, i.e., spectrum and load level. This implies that a set of identical test specimens, if divided into two or more groups and tested using different stress levels or spectra, should produce the same EIFS distribution. This is called a "generic" EIFS distribution.

It has long been noted that fatigue failure distributions can be fit by three-parameter Weibull distributions. Since failure in fracture critical structure corresponds to attainment of the critical crack size, it is reasonable to hope that this distributional form is appropriate for all crack sizes of interest. It has been found in this program, and in [19,20] that observed TTCI values for small crack sizes can usually be fit very well by a three-parameter Weibull distribution.

Therefore, a fractographically observed TTCI distribution can be expressed as:

$$F_T(t) = P[T \leq t] = 1 - \exp\left\{-\left[\frac{t-\varepsilon}{\beta}\right]^{\alpha}\right\} \quad ; \; t > \varepsilon \qquad (A1)$$

where T is a random variable indicating TTCI and $F_T(t)$ is just P[TTCI t]. The Weibull parameter α, is the shape parameter, β is the scale parameter, and ϵ is the lower bound of TTCI. The parameters α, β, ϵ, are determined from a best-fit of fractography data, according to conditions discussed further below.

The crack growth rate over the crack size range of interest is assumed to be expressed as:

$$\frac{da(t)}{dt} = Q[a(t)]^b \qquad (A2)$$

where a(t) is the crack size at time t, and Q and b are constants that are determined from the least square fit of all log da/dt vs. log a pairs of the sample.

Integrating Eq. A2 from t = 0 to t = T, the relationship between the crack size at t = 0, a(o) (i.e. EIFS), and that at t = T (i.e. a_o) is found to be:

$$\text{EIFS} = a(0) = \frac{a_0}{\left(1+a_0^c\ cQT\right)^{1/c}} \qquad (A3)$$

where c = b - 1.

Combining Eq. A1 and A3, one may obtain the EIFS distribution as:

$$F_{a(o)}(x) = \exp\left\{-\left[\frac{x^{-c} - x_u^{-c}}{cQ\ \beta}\right]^{\alpha}\right\} \quad ; \ 0 < x \leq x_u \qquad (A4)$$

$$= 1 \quad ; \ x \geq x_u$$

where $F_{a(o)}(x)$ is just P[EIFS < x] and where x_u is the upper bound of the EIFS which is defined as :

$$x_u = [a_0^{-c} + CQ\epsilon]^{-1/c} \qquad \text{(A5)}$$

Therefore, the EIFS distribution can be determined from Eq. A4, if the parameters Q, c(=b-1), α, β, and ϵ are properly calibrated based on the fractographic data.

As mentioned previously, EIFS is intuitively a generic property of such factors as the material, manufacturing/assembly techniques, and workmanship and should be independent of load spectrum and stress level. Eq. A4 shows that the necessary conditions to ensure that the EIFS distribution is generic among two or more data sets are:

$$\begin{aligned} b_1 &= b_2 = \ldots = b_n \\ \alpha_1 &= \alpha_2 = \ldots = \alpha_n \\ Q_1\beta_1 &= Q_2\beta_2 = \ldots = Q_n\beta_n \end{aligned} \qquad \text{(A6)}$$

Accordingly, we recommend that any sample of identically prepared test elements be randomly split into at least two groups. These should be tested at different stress levels. If possible, a third group tested with a different spectrum is desirable. Then all fractography is least squares fit subject to the conditions given in Eq. A6. Adequate fits to the data have been found so far using this procedure, and this procedure ensures that the EIFS is as generic as can be among the conditions tested. Testing at

two stress levels also reveals the dependence of crack growth on stress level, which is useful for performing trade studies.

A.2 Procedures for Calibrating IFQ Model Parameters

For the calibration of IFQ model parameters, data pooling procedures are required. In general, a pooled data set represents a set of identical test specimens and contains a number of individual data sets. An individual data set obtained from a certain test condition consists of a number of individual test specimens.

For this program, five pooled data sets were studied as presented in Table A1.

Table A1. Pooled Data Sets In This Program

POOLED DATA SET	INDIVIDUAL DATA SET		NO. OF SPECIMENS
Adhesively Bonded (Scrimmed)	NOR 1 NOR 1	24 KSI 30 KSI	19 19
Adhesively Bonded (Unscrimmed)	NOR 1	30 KSI	20
Mechanically Fastened (Sealant)	NOR 1 NOR 1	24 KSI 30 KSI	19 16
Mechanically Fastened (No Sealant)	NOR 1	24 KSI	10
Cast	NOR 1 GAR 1 GAR 1	30 KSI 28 KSI 34 KSI	50 20 20

To avoid confusions arising from data pooling procedures, IFQ model parameters are designated as follows:

p_i: parameter P representing an individual specimen

P_I: parameter P representing an individual data set

P*: parameter P representing a pooled data set

The following procedures were used to pool the data:

1. First, the crack growth information of each individual specimen was obtained in terms of a vs. t or da/dt vs. a from fractographic (or other crack growth) data.

2. A crack size range-of-interest for crack growth analysis was selected for each pooled data set:

	A_{min} (inch)		A_{max} (inch)
ADHESIVELY BONDED (SCRIMMED):	0.010	to	0.500
ADHESIVELY BONDED (UNSCRIMMED):	0.010	to	0.500
MECHANICALLY FASTENED (SEALANT):	0.001	to	0.500
MECHANICALLY FASTENED (NO SEALANT):	0.001	to	0.500
CAST:	0.001	to	0.500

3. The crack growth parameters for each individual specimen, Q_i and b_i, were determined by a least squares fit using the following equation transformed from Eq. A2.

$$\log \frac{da}{dt} = b \log a + \log Q \qquad \text{(A7)}$$

4. As specified in Eq. A6, the b_i value of each individual specimen in a pooled data set is supposed to be identical to satisfy the generic property of the EIFS distribution. Thus, a single b* value for each pooled data set was determined from the pooled fractographic data in a least squares sense using Eq. A7.

5. Based on the b* value obtained, the Q_i value was determined for each individual specimen.

6. For the determination of TTCI, an arbitrary reference crack size, a_o, was assumed for each pooled data set in the range.

7. Using the a_o, Q_i and b* vaues, TTCI for each individual specimen was determined by a three-point Lagrangian interpolation [30].

8. An arbitrary lower bound of TTCI, ϵ_I, was assumed for each individual data set. As will be seen later, the selected ϵ_I results in an upper bound of EIFS, x_u.

9. Eq. A1 was transformed into the following least squares fit form:

$$\log \left\{ -\ln \left[1-F_T(t) \right] \right\} = \alpha \log (t-\varepsilon) - \alpha \log \beta \qquad \text{(A8)}$$

It is seen from Eq. A8 that $-\ln [1-F_T(t)]$ vs. $(t - \epsilon)$ will be plotted as a straight line on log-log scale paper.

10. The cumulative distribution of TTCI was estimated by ranking the obtained TTCI-ϵ values in ascending order

using the following equation:

$$F_T(t) = \frac{r}{n+1} \tag{A9}$$

where r is the rank of TTCI- ϵ of the specimen in the individual data set, and n is the number of specimens in the individual data set.

11. Combining E.q A8 and A9, the Weibull distribution parameters for each individual data set, x_I and ϵ_I were determined from the pairs of the specimens in the data set by using the least squares fit.

12. From the $\hat{Q}_i$ and β_I parameters, the product $\hat{Q}_i \beta_I$ was obtained for each individual specimen.

13. As specified in Eq. A6, the $\hat{Q}_i \beta_I$ value of each specimen in a pooled data set is supposed to be identical. Thus, the $(\hat{Q}_i \beta_I)^*$ value for each pooled data set was determined by averaging the $\hat{Q}_i \beta_I$ values.

14. From the $(\hat{Q}_i \beta_I)^*$ value, the Q_I was determined for each individual data set:

$$Q_I = \frac{(\hat{Q}_i \beta_I)^*}{\beta_I} = \frac{\Sigma \hat{Q}_i \beta_I}{n \beta_I} \tag{A10}$$

15. As specified in Eq. A7, the α_I value of each individual data set in a pooled data set is supposed to be identical. Hence, in order to determine the α^* value for a pooled data set, Eq. Al was transformed into the following least squares fit form:

$$\log \left\{ -\ln [\, 1-F_T(t)] \right\} = \alpha \log \left[\frac{t-\varepsilon}{\beta} \right] \tag{A11}$$

The $(TTCI-\epsilon)/\beta_I$ value for each specimen was computed and then ranked in the pooled data set. The α^* value was determined for each pooled data set from the $-\ln [1 - F_T(t)]$ vs. $(TTCI-\epsilon)/\beta_I$ pairs of the specimens in the pooled data set by using a least squares fit and calculating the slope.

16. Using Eq. A5, Q_I, and b^*, the x_u value for each individual data set was determined from the assumed ϵ_I value. However, the x_u value of each individual data set in a pooled data set should be identical to satisfy the generic property of the distribution and should be in the range:

$$\log [-\ln F_{a(o)}(x)] = \alpha \log (x^{-c} - x_u^{-c}) - \alpha \log CQ\beta \qquad \text{(A12)}$$

Therefore, ϵ_I must be selected to satisfy the above conditions.

17. The EIFS for each individual specimen was determined from Eq. A3, using the Q_I, b^*, x_u, and TTCI values.

18. The goodness-of-fit of the obtained EIFS values was examined for each pooled data set, by calculating the squared error:

$$\sum^{n} (F_{a(o)}(x) - EIFS)^2 \qquad \text{(A13)}$$

where $F_{a(o)}(x)$ is given by Eq. 4.

19. To optimize the goodness-of-fit of the EIFS distribution, the steps 7-18 were repeated for a number of different sets of a_o and x_u values.

APPENDIX B

FRACTOGRAPHY DATA

ADHESIVELY BONDED TEST ELEMENTS (SCRIMMED)
NOR 1 Spectrum
24 ksi Max. Spectrum Stress
Data Set AB124

spec. (#)	t (flt hrs)	a (in)
1	4218.75	0.297500
2	4218.75	0.247500
3	4218.75	0.445000
	8437.50	0.707500
	1317.0	1.31000
4	4218.75	0.267500
	8437.50	0.397500
	13500.0	0.540000
5	4218.75	0.227500
	8437.50	0.402500
	13500.0	0.520000
	17718.8	0.675000
6	4218.75	0.325000
	8437.50	0.530000
	13500.0	0.692500
	17718.8	0.827500
	21937.5	1.04250
7	4218.75	0.287500
	8437.50	0.452500
	13500.0	0.595000
	17718.8	0.685000
	21937.5	0.855000
8	4218.75	0.162500
	8437.50	0.327500
	13500.0	0.422500
	17718.8	0.485000
	21937.5	0.587500
	27000.0	0.640000
9	4218.75	0.315000
	8437.50	0.485000
	13500.0	0.600000
	17718.8	0.800000
	21937.5	0.967500
	27000.0	1.18700
10	4218.75	0.327500
	8437.50	0.482500
	13500.0	0.660000
	17718.8	0.827500
	21937.5	1.02000
	27000.0	1.27500
11	4218.75	0.407500
	8437.50	0.552500
	13500.0	0.690000
	17718.8	0.780000
	21937.5	0.897500
	27000.0	1.08700

spec. (#)	t (flt hrs)	a (in)
12	4218.75	0.240000
	8437.50	0.372500
	13500.0	0.515000
	17718.8	0.645000
	21937.5	0.735000
	27000.0	0.925000
13	4218.75	0.245000
	8437.50	0.400000
	13500.0	0.582000
	17718.8	0.702000
	21937.5	0.740000
	27000.0	0.770000
14	4218.75	0.820000E-01
	8437.50	0.292000
	13500.0	0.355000
	16664.1	0.455000
	20882.8	0.557000
	25101.6	0.698000
	27000.0	0.753000
15	8437.50	0.145000
	13500.0	0.335000
	16664.1	0.410000
	20882.8	0.527000
	25101.6	0.585000
	27000.0	0.672000
16	1054.69	0.300000
	3164.06	0.340000
	11601.6	0.545000
	15609.4	0.600000
	24046.9	0.710000
	27000.0	0.790000
17	4218.75	0.280000
	8437.50	0.460000
	13500.0	0.637500
	17718.8	0.855000
	21937.5	0.980000
	27000.0	1.40500
18	8437.50	0.505000
	16664.1	0.625000
	25101.6	0.745000
19	1054.69	0.360000
	5273.44	0.510000
	9492.19	0.610000
	13500.0	0.690000
	17718.8	0.780000
	21937.5	0.880000
	27000.0	1.02000
	31218.8	1.19000

ADHESIVELY BONDED TEST ELEMENTS (SCRIMMED)
NOR 1 Spectrum
30 ksi Max. Spectrum Stress
Data Set AB130

spec. (#)	t (flt hrs)	a (in)
1	1054.69	0.307500
	2109.37	0.457500
	3164.06	0.565000
2	1054.69	0.367500
	2109.37	0.540000
	3164.06	0.715000
	4218.75	0.887500
3	1054.69	0.315000
	2109.37	0.477500
	3164.06	0.577500
	4218.75	0.757500
	5273.44	0.922500
4	1054.69	0.292500
	2109.37	0.425000
	3164.06	0.570000
	4218.75	0.765000
	5273.44	0.930000
5	2109.37	0.400000
	3164.06	0.465000
	4218.75	0.560000
	5273.44	0.667500
	6328.12	0.792500
6	2109.37	0.487500
	4218.75	0.702500
7	4218.75	0.622500
8	1054.69	0.305000
	2109.37	0.367500
	3164.06	0.475000
	4218.75	0.572500
	5273.44	0.757500
	6328.12	0.835000
	7382.81	1.03250
9	1054.69	0.240000
	2109.37	0.350000
	3164.06	0.450000
	4218.75	0.530000
	5273.44	0.610000
	6328.12	0.720000
	7382.81	0.800000
10	1054.69	0.120000
	2109.37	0.200000
	3164.06	0.340000
	4218.75	0.420000
	5273.44	0.490000
	6328.12	0.630000
	7382.81	0.740000
	8437.50	0.930000
11	1054.69	0.110000
	2109.37	0.230000
	3164.06	0.350000
	4218.75	0.480000
	5273.44	0.540000
	6328.12	0.620000
	7382.81	0.715000
	8437.50	1.02000

spec. (#)	t (flt hrs)	a (in)
12	1054.69	0.400000
	2109.37	0.510000
	3164.06	0.590000
	4218.75	0.670000
	5273.44	0.740000
	6328.12	0.820000
	7382.81	0.890000
	8437.50	1.02000
	9492.19	1.15000
13	1054.69	0.267500
	2109.37	0.380000
	3164.06	0.450000
	4218.75	0.555000
	5273.44	0.667500
	6328.12	0.740000
	7382.81	0.832500
	8437.50	0.970000
	9492.19	1.19200
14	1054.69	0.245000
	2109.37	0.360000
	3164.06	0.435000
	4218.75	0.487500
	5273.44	0.550000
	6328.12	0.620000
	7382.81	0.732500
	8437.50	0.857000
	9492.19	0.930000
	10546.9	1.10000
15	1054.69	0.275000
	2109.37	0.415000
	3164.06	0.475000
	4218.75	0.560000
	5273.44	0.627500
	6328.12	0.720000
	7382.81	0.780000
	8437.50	0.867000
	9492.19	0.972500
	10546.9	1.08000
16	1054.69	0.172500
	2109.37	0.322500
	3164.06	0.400000
	4218.75	0.532500
	5273.44	0.612500
	6328.12	0.680000
	7382.81	0.765000
	8437.50	0.945000
	9492.19	1.07700
17	1054.69	0.272500
	2109.37	0.300000
	3164.06	0.407500
	4218.75	0.510000
	5273.44	0.570000
	6328.12	0.597500
	7382.81	0.707500
	8437.50	0.760000
	9492.19	0.827500
	10546.9	0.985000
18	1054.69	0.137500
	2109.37	0.215000
	3164.06	0.270000
	4218.75	0.360000
	5273.44	0.405000
	6328.12	0.472500
	7382.81	0.540000
	8437.50	0.587500
	9492.19	0.730000
	10546.9	0.902500
19	1054.69	0.350000
	6328.12	0.642500
	10546.9	0.840000
	14554.7	1.17250

ADHESIVELY BONDED TEST ELEMENTS (UNSCRIMMED)
NOR 1 Spectrum
30 ksi Max. Spectrum Stress
Data Set UB130

spec. (#)	t (flt hrs)	a (in)
1	4218.75	0.194000
	8437.50	0.356000
	13500.0	0.512000
	17718.8	0.987000
	21937.5	1.13700
2	4218.75	0.144000
	8437.50	0.300000
	10546.9	0.369000
	13500.0	0.600000
	15609.4	0.650000
	17718.8	0.700000
	19828.1	0.793000
	21937.5	0.907500
	24046.9	1.06300
	26156.3	1.16300
3	4218.75	0.243000
4	4218.75	0.294000
5	4218.75	0.367000
6	4218.75	0.219000
7	4218.75	0.237000
8	4218.75	0.162000
	8437.50	0.362000
9	2109.37	0.125000
	3164.06	0.206000
	4218.75	0.256000
	6328.12	0.343000
	8437.50	0.394000
10	4218.75	0.363000
	8437.50	0.606000
	13500.0	0.787000
11	4218.75	0.111000
	8437.50	0.331000
	12656.3	0.471000
	13500.0	0.572000
12	4218.75	0.137000
	8437.50	0.575000
	13500.0	0.962000
13	4218.75	0.262000
	8437.50	0.489000
	13500.0	0.766000
14	4218.75	0.212500
	8437.50	0.350000
	13500.0	0.512000
15	4218.75	0.206000
	8437.50	0.381000
	13500.0	0.606000
	17718.8	0.857000
16	4218.75	0.209000
	8437.50	0.419000
	13500.0	0.604000
	17718.8	0.862000
17	4218.75	0.252000
	8437.50	0.485000
	13500.0	0.622000
	17718.8	0.869000
18	4218.75	0.281000
	8437.50	0.450000
	13500.0	0.672000
	17718.8	0.950000

MECHANICALLY FASTENED TEST ELEMENTS (SEALANT)
NOR 1 Spectrum
24 ksi Max. Spectrum Stress
Data Set B24B

spec. (#)	t (flt hrs)	a (in)
1	1054.69	0.340000E-01
	2109.37	0.565000E-01
	3164.06	0.839000E-01
	4218.75	0.107200
	5273.44	0.133500
	6328.12	0.168700
	7382.81	0.216500
	8437.50	0.260600
	9270.70	0.392200
2	1054.69	0.289000E-01
	2109.37	0.511000E-01
	3164.06	0.751000E-01
	4218.75	0.945000E-01
	5273.44	0.132600
	6328.12	0.164000
	7382.81	0.204600
	8437.50	0.257400
	9376.17	0.367600
3	1054.69	0.235000E-01
	2109.37	0.446000E-01
	3164.06	0.638000E-01
	4218.75	0.810000E-01
	5273.44	0.102800
	6328.12	0.129800
	7382.81	0.158200
	8437.50	0.189400
	9492.19	0.236000
	10546.9	0.305800
	10852.7	0.382700
4	3164.06	0.296000E-01
	4218.75	0.494000E-01
	5273.44	0.834000E-01
	6328.12	0.120000
	7382.81	0.149600
	8437.50	0.190300
	9492.19	0.230300
	10546.9	0.298700
	11105.9	0.383200
5	1054.69	0.205000E-01
	2109.37	0.360000E-01
	3164.06	0.552000E-01
	4218.75	0.767000E-01
	5273.44	0.105000
	6328.12	0.126100
	7382.81	0.147700
	8437.50	0.175200
	9492.19	0.218400
6	1054.69	0.321000E-01
	2109.37	0.499000E-01
	3164.06	0.714000E-01
	4218.75	0.901000E-01
	5273.44	0.111200
	6328.12	0.139600
	7382.81	0.171500
	8437.50	0.204800
	9492.19	0.268800
	10546.9	0.352100
	11380.1	0.400600
7	1054.69	0.347000E-01
	2109.37	0.479000E-01
	3164.06	0.614000E-01
	4218.75	0.889000E-01
	5273.44	0.109400
	6328.12	0.129600
	7382.81	0.151100
	8437.50	0.175100
	9492.19	0.210900
	10546.9	0.261800
	11591.0	0.343200

spec. (#)	t (flt hrs)	a (in)	spec. (#)	t (flt hrs)	a (in)
8	1054.69	0.389000E-01	11	3164.06	0.398000E-01
	2109.37	0.620000E-01		4218.75	0.526000E-01
	3164.06	0.760000E-01		5273.44	0.724000E-01
	4218.75	0.964000E-01		6328.12	0.907000E-01
	5273.44	0.119400		7382.81	0.106700
	6328.12	0.137500		8437.50	0.125800
	7382.81	0.154500		9492.19	0.142300
	8437.50	0.179800		10546.9	0.172300
	9492.19	0.214600		11601.6	0.194800
	10546.9	0.249700		13500.0	0.248000
	11591.0	0.310100		14554.7	0.291600
				15293.0	0.363200
9	1054.69	0.108000E-01			
	2109.37	0.174000E-01	12	1054.69	0.256000E-01
	3164.06	0.277000E-01		2109.37	0.430000E-01
	4218.75	0.450000E-01		3164.06	0.652000E-01
	5273.44	0.672000E-01		4218.75	0.864000E-01
	6328.12	0.851000E-01		5273.44	0.100200
	7382.81	0.100800		6328.12	0.110000
	8437.50	0.124900		7382.81	0.123000
	9492.19	0.152500		8437.50	0.135000
	10546.9	0.187600		9492.19	0.147600
	11601.6	0.240300		10546.9	0.159300
	12645.7	0.333600		11601.6	0.175700
				12656.3	0.204200
				13500.0	0.262800
10	1054.69	0.437000E-01		14554.7	0.330100
	2109.37	0.609000E-01		15609.4	0.417600
	3164.06	0.769000E-01		16231.6	0.458000
	4218.75	0.926000E-01			
	5273.44	0.110700			
	6328.12	0.129600			
	7382.81	0.148200			
	8437.50	0.162400			
	9492.19	0.176100			
	10546.9	0.196100			
	11601.6	0.210400			
	12656.3	0.233700			
	13500.0	0.294100			
	14554.7	0.374800			
	15177.0	0.423900			

spec. (#)	t (flt hrs)	a (in)	spec. (#)	t (flt hrs)	a (in)
13	1054.69	0.294000E-01	15	2109.37	0.547000E-01
	2109.37	0.421000E-01		3164.06	0.707000E-01
	3164.06	0.528000E-01		4218.75	0.826000E-01
	4218.75	0.669000E-01		5273.44	0.103200
	5273.44	0.892000E-01		6328.12	0.122200
	6328.12	0.103900		7382.81	0.151300
	7382.81	0.122100		8437.50	0.170800
	8437.50	0.137200		9492.19	0.193700
	9492.19	0.150900		10546.9	0.207800
	10546.9	0.165100		11601.6	0.237100
	11601.6	0.184100		12656.3	0.269800
	12656.3	0.204200		13500.0	0.289800
	13500.0	0.220800		14554.7	0.306300
	14554.7	0.243000		15609.4	0.321200
	15609.4	0.270100		16664.1	0.358400
	16664.1	0.311400		17718.8	0.383000
	17391.8	0.377600		18393.8	0.406200
14	1054.69	0.650000E-02	16	7382.81	0.504000E-01
	2109.37	0.101000E-01		8437.50	0.661000E-01
	3164.06	0.191000E-01		9492.19	0.848000E-01
	4218.75	0.279000E-01		10546.9	0.990000E-01
	5273.44	0.394000E-01		11601.6	0.125500
	6328.12	0.530000E-01		12656.3	0.143500
	7382.81	0.666000E-01		13500.0	0.155600
	8437.50	0.864000E-01		14554.7	0.169600
	9492.19	0.997000E-01		15609.4	0.199000
	10546.9	0.124600		16664.1	0.237900
	11601.6	0.147600		17718.8	0.279500
	13500.0	0.186200		18552.0	0.340900
	14554.7	0.228800			
	15609.4	0.271900			
	16664.1	0.308400			
	17718.8	0.374200			

spec. (#)	t (flt hrs)	a (in)
17	1054.69	0.243000E-01
	2109.37	0.402000E-01
	3164.06	0.517000E-01
	4218.75	0.660000E-01
	5273.44	0.788000E-01
	6328.12	0.849000E-01
	7382.81	0.966000E-01
	8437.50	0.110900
	9492.19	0.121500
	10546.9	0.135800
	11601.6	0.150800
	13500.0	0.177300
	14554.7	0.198200
	15609.4	0.242300
	16664.1	0.270600
	17718.8	0.317000
	18773.4	0.336000
	18963.3	0.349800
18	1054.69	0.333000E-01
	2109.37	0.567000E-01
	3164.06	0.806000E-01
	4218.75	0.923000E-01
	5273.44	0.119700
	6328.12	0.137700
	7382.81	0.154400
	8437.50	0.170100
	9492.19	0.185100
	10546.9	0.207900
	11601.6	0.223300
	12656.3	0.241100
	14554.7	0.270100
	15609.4	0.299000
	16664.1	0.326700
	17718.8	0.360500
	18773.4	0.399500
	19828.1	0.436500
	20882.8	0.469600
	21842.6	0.607300
19	24036.3	0.373000

MECHANICALLY FASTENED TEST ELEMENTS (SEALANT)
NOR 1 Spectrum
30 ksi Max. Spectrum Stress
Data Set B30B

spec. (#)	t (flt hrs)	a (in)
1	1054.69	0.826000E-01
	2109.37	0.133400
	3153.52	0.229700
2	1054.69	0.746000E-01
	2109.37	0.143900
	3164.06	0.209300
	3891.80	0.321800
3	1054.69	0.578000E-01
	2109.37	0.101700
	3164.06	0.186000
	3997.27	0.300100
4	1054.69	0.236000E-01
	2109.37	0.596000E-01
	3164.06	0.190700
	4208.20	0.359300
5	1054.69	0.541000E-01
	2109.37	0.102600
	3164.06	0.161200
	4218.75	0.221200
	4419.14	0.284100
6	1054.69	0.791000E-01
	2109.37	0.137700
	3164.06	0.230600
	4218.75	0.292000
	4608.98	0.370000
7	1054.69	0.383000E-01
	2109.37	0.775000E-01
	3164.06	0.127200
	4218.75	0.188600
	4841.02	0.263300
8	1054.69	0.544000E-01
	2109.37	0.995000E-01
	3164.06	0.152100
	4218.75	0.198200
	5252.34	0.280200
9	1054.69	0.686000E-01
	2109.37	0.108700
	3164.06	0.149900
	4218.75	0.198000
	5262.89	0.287300
10	1054.69	0.374000E-01
	2109.37	0.645000E-01
	3164.06	0.108200
	4218.75	0.160700
	5262.89	0.240000
11	1054.69	0.252000E-01
	2109.37	0.562000E-01
	3164.06	0.107000
	4218.75	0.156700
	5273.44	0.253700
	5473.83	0.306200

spec. (#)	t (flt hrs)	a (in)
12	1054.69	0.401000E-01
	2109.37	0.960000E-01
	3164.06	0.135400
	4218.75	0.168300
	5273.44	0.206900
	6317.58	0.279400
13	1054.69	0.538000E-01
	2109.37	0.865000E-01
	3164.06	0.130900
	4218.75	0.173200
	5273.44	0.222900
	6317.58	0.302800
14	4218.75	0.209000E-01
	5273.44	0.402000E-01
	6328.12	0.682000E-01
	7382.81	0.116000
	8437.50	0.178900
	9481.64	0.292500
15	1054.69	0.257000E-01
	2109.37	0.736000E-01
	3164.06	0.897000E-01
	4218.75	0.102300
	5273.44	0.124800
	6328.12	0.139000
	7382.81	0.157600
	8437.50	0.176000
	9492.19	0.197100
	10546.9	0.216800
	11601.6	0.246000
	12656.3	0.270100
	13531.6	0.287500
16	1054.69	0.257000E-01
	2109.37	0.736000E-01
	3164.06	0.897000E-01
	4218.75	0.102300
	5273.44	0.124800
	6328.12	0.139000
	7382.81	0.157600
	8437.50	0.176000
	9492.19	0.197100
	10546.9	0.216800
	11601.6	0.246000
	12656.3	0.270100
	13531.6	0.287500

MECHANICALLY FASTENED TEST ELEMENTS (NO SEALANT)
NOR 1 Spectrum
24 ksi Max. Spectrum Stress
Data Set BNS24B

spec. (#)	da/dt (in/flt hr)	a (in)
1	0.495703E-03	0.194000E-01
	0.580078E-03	0.292000E-01
	0.590625E-03	0.433000E-01
	0.822656E-03	0.649000E-01
	0.907031E-03	0.757000E-01
	0.111797E-02	0.844000E-01
	0.949219E-03	0.942000E-01
	0.100195E-02	0.103400
	19002.3*	0.120000
2	0.852187E-02	0.440800
	0.542109E-02	0.374700
	0.395508E-02	0.330200
	0.353320E-02	0.294700
	0.306914E-02	0.263400
	0.265781E-02	0.236300
	0.288984E-02	0.210000
	0.362812E-02	0.179100
	0.303750E-02	0.147500
	0.158203E-02	0.125600
	0.165586E-02	0.110200
	0.137109E-02	0.959000E-01
	0.156094E-02	0.820000E-01
	0.183516E-02	0.659000E-01
	0.141328E-02	0.505000E-01
	0.123398E-02	0.379000E-01
	22452.2*	0.500000
3	0.580078E-03	0.259000E-01
	0.885937E-03	0.828000E-01
	0.147656E-02	0.110600
	0.158203E-02	0.133000
	0.161367E-02	0.153300
	0.232031E-02	0.164100
	0.305859E-02	0.224200
	28040.9*	0.300000
4	0.527344E-03	0.217000E-01
	0.111797E-02	0.556000E-01
	0.153984E-02	0.794000E-01
	0.158203E-02	0.125400
	0.198281E-02	0.163000
	0.239414E-02	0.179000
	0.232031E-02	0.194200
	0.245742E-02	0.221200
	0.280547E-02	0.266900
	28040.9*	0.270000
5	0.580078E-03	0.136000E-01
	0.432422E-03	0.140000E-01
	0.569531E-03	0.189000E-01
	0.622266E-03	0.267000E-01
	0.109687E-02	0.435000E-01
	0.107578E-02	0.511000E-01
	0.122344E-02	0.598000E-01
	0.127617E-02	0.911000E-01
	0.155039E-02	0.141700
	0.197227E-02	0.154800
	0.333281E-02	0.237100
	0.295313E-02	0.250500
	0.569531E-02	0.286900
	28163.3*	0.370000
6	0.274219E-03	0.387000E-01
	0.328008E-03	0.428000E-01
	0.537891E-03	0.482000E-01
	0.527344E-03	0.557000E-01
	0.107578E-02	0.835000E-01
	0.114961E-02	0.938000E-01
	0.103359E-02	0.101600
	0.580078E-03	0.113400
	0.200391E-02	0.200200
	0.197227E-02	0.288100
	0.358594E-02	0.335100
	32051.9*	0.350000

* t
(flt hrs)

spec. (#)	da/dt (in/flt hr)	a (in)
7	0.548437E-03	0.292000E-01
	0.717188E-03	0.346000E-01
	0.854297E-03	0.421000E-01
	0.949219E-03	0.506000E-01
	0.105469E-02	0.613000E-01
	0.131836E-02	0.796000E-01
	0.129727E-02	0.121800
	0.205664E-02	0.139500
	0.214102E-02	0.188000
	0.284766E-02	0.256000
	34897.5*	0.400000
8	0.421875E-03	0.343000E-01
	0.596953E-03	0.737000E-01
	0.129727E-02	0.118600
	0.100195E-02	0.127800
	0.139219E-02	0.147300
	0.155039E-02	0.160500
	0.237305E-02	0.211900
	0.247852E-02	0.245200
	0.295313E-02	0.287400
	37534.2*	0.440000
9	0.386016E-03	0.640000E-02
	0.392344E-03	0.153000E-01
	0.379688E-03	0.202000E-01
	0.696094E-03	0.342000E-01
	0.675000E-03	0.459000E-01
	0.590625E-03	0.658000E-01
	0.537891E-03	0.717000E-01
	0.738281E-03	0.772000E-01
	0.133945E-02	0.104100
	0.126563E-02	0.143200
	39116.2*	0.240000
10	0.274219E-03	0.128000E-01
	0.114961E-03	0.686000E-01
	0.812109E-03	0.885000E-01
	0.184570E-02	0.122800
	0.137109E-02	0.181200
	0.221484E-01	0.237600
	40278.5*	0.340000

* t (flt hrs)

CAST TEST ELEMENTS
NOR 1 Spectrum
30 ksi Max. Spectrum Stress
Data Set CB130

spec. (#)	da/dt (in/flt hr)	a (in)
1	0.131836E-02	0.209000E-01
	0.131836E-02	0.137500
	0.351211E-02	0.160400
	2094.60*	0.170000
2	0.512578E-02	0.120900
	0.686602E-02	0.640000E-01
	0.332227E-02	0.157000E-01
	3150.30*	0.160000
3	0.255234E-01	0.143300
	0.579023E-02	0.699000E-01
	0.273164E-02	0.295000E-01
	0.175078E-02	0.830000E-02
	3784.20*	0.250000
4	0.165586E-01	0.203800
	0.902812E-02	0.833000E-01
	0.427148E-02	0.202000E-01
	4205.04*	0.281600
5	0.899648E-02	0.101600
	0.290039E-02	0.456000E-01
	0.239414E-02	0.205000E-01
	0.970313E-03	0.460000E-02
	4208.20*	0.143900
6	0.142383E-01	0.152000
	0.352266E-02	0.681000E-01
	0.248906E-02	0.396000E-01
	0.293203E-02	0.139000E-01
	4208.20*	0.219300
7	0.595898E-02	0.908000E-01
	0.340664E-02	0.466000E-01
	0.265781E-02	0.172000E-01
	0.558984E-03	0.260000E-02
	4208.20*	0.118800
8	0.995625E-02	0.129200
	0.450352E-02	0.658000E-01
	0.283711E-02	0.310000E-01
	0.142383E-02	0.108000E-01
	0.421875E-03	0.210000E-02
	5157.42*	0.171300
9	0.485156E-02	0.148000
	0.337500E-02	0.110000
	0.379688E-02	0.760000E-01
	0.411328E-02	0.380000E-01
	0.200391E-02	0.900000E-02
	5252.34*	0.171900
10	0.421875E-03	0.620000E-02
	0.168750E-02	0.840000E-02
	0.135000E-02	0.145000E-01
	0.105469E-02	0.452000E-01
	0.189844E-02	0.580000E-01
	0.147656E-02	0.334000E-01
	0.126563E-02	0.408000E-01
	0.200391E-02	0.599000E-01
	0.168750E-02	0.682000E-01
	0.158203E-02	0.704000E-01
	0.189844E-02	0.829000E-01
	5259.70*	0.112800
11	0.420820E-02	0.185800
	0.454570E-02	0.144300
	0.298477E-02	0.108600
	0.378633E-02	0.765000E-01
	5252.34*	0.205800
12	0.807891E-03	0.104000E-01
	0.168750E-02	0.157000E-01
	0.210937E-02	0.185000E-01
	0.179297E-02	0.247000E-01
	0.223594E-02	0.307000E-01
	0.337500E-02	0.111700
	0.253125E-02	0.438000E-01
	0.253125E-02	0.117000
	0.210937E-02	0.690000E-01
	0.149766E-02	0.793000E-01
	0.210937E-02	0.143300
	5259.70*	0.329500

* t
(flt hrs)

spec. (#)	da/dt (in/flt hr)	a (in)
13	0.316406E-03	0.540000E-02
	0.632813E-03	0.690000E-02
	0.738281E-03	0.940000E-02
	0.126563E-02	0.135000E-01
	0.302695E-02	0.593000E-01
	0.298477E-02	0.842000E-01
	0.274219E-02	0.949000E-01
	0.237305E-02	0.112200
	0.189844E-02	0.668000E-01
	0.193008E-02	0.439000E-01
	0.263672E-02	0.739000E-01
	5259.70 *	0.171100
14	0.129727E-01	0.168600
	0.359648E-02	0.905000E-01
	0.287930E-02	0.598000E-01
	0.214102E-02	0.360000E-01
	0.273164E-02	0.129000E-01
	5262.89 *	0.229700
15	0.685547E-03	0.680000E-02
	0.791016E-03	0.850000E-02
	0.263672E-02	0.455000E-01
	0.474609E-03	0.400000E-02
	0.351211E-02	0.783000E-01
	0.179297E-02	0.681000E-01
	0.105469E-02	0.537000E-01
	0.596953E-03	0.242000E-01
	0.337500E-02	0.107700
	6317.50 *	0.156300
16	0.121289E-02	0.206000E-01
	0.116016E-02	0.176000E-01
	0.126563E-02	0.200000E-01
	0.342773E-02	0.855000E-01
	0.290039E-02	0.605000E-01
	0.274219E-03	0.530000E-02
	0.474609E-03	0.810000E-02
	0.116016E-02	0.169000E-01
	0.295313E-02	0.712000E-01
	6317.50 *	0.110000
17	0.303750E-02	0.100900
	0.211992E-02	0.765000E-01
	0.202500E-02	0.569000E-01
	0.146602E-02	0.403000E-01
	0.160312E-02	0.258000E-01
	0.191953E-02	0.910000E-02
	6317.58 *	0.115200

spec. (#)	da/dt (in/flt hr)	a (in)
18	0.109898E-01	0.847000E-01
	0.699258E-02	0.568000E-01
	0.499922E-02	0.400000E-01
	0.343828E-02	0.285000E-01
	0.257344E-02	0.193000E-01
	0.149766E-02	0.710000E-02
	6317.58 *	0.103200
19	0.843750E-03	0.169000E-01
	0.949219E-03	0.259000E-01
	0.896484E-03	0.356000E-01
	0.189844E-02	0.707000E-01
	0.149766E-02	0.100900
	0.316406E-02	0.108600
	0.179297E-02	0.118900
	0.193008E-02	0.980000E-01
	0.168750E-02	0.730000E-01
	0.580078E-03	0.552000E-01
	0.843750E-03	0.220000E-02
	7369.10 *	0.120000
20	0.379688E-03	0.156000E-01
	0.131836E-02	0.271000E-01
	0.105469E-02	0.388000E-01
	0.421875E-03	0.734000E-01
	0.791016E-03	0.109900
	0.421875E-03	0.705000E-01
	0.738281E-03	0.444000E-01
	0.632813E-03	0.674000E-01
	0.738281E-03	0.439000E-01
	0.527344E-03	0.208000E-01
	0.738281E-03	0.689000E-01
	0.632813E-03	0.709000E-01
	0.632813E-03	0.769000E-01
	7361.72 *	0.126200
21	0.175078E-02	0.101200
	0.189844E-02	0.107700
	0.280547E-02	0.117800
	0.984023E-03	0.442000E-01
	0.632813E-03	0.222000E-01
	0.158203E-02	0.372000E-01
	0.158203E-02	0.974000E-01
	7836.33 *	0.161600

* t
(flt hrs)

spec. (#)	da/dt (in/flt hr)	a (in)
22	0.129727E-02	0.209000E-01
	0.105469E-02	0.159000E-01
	0.137109E-02	0.579000E-01
	0.126563E-02	0.554000E-01
	0.184570E-02	0.817000E-01
	0.129727E-02	0.332000E-01
	0.147656E-02	0.791000E-01
	0.165586E-02	0.816000E-01
	0.351211E-02	0.198600
	8423.80*	0.220000
23	0.706641E-03	0.424000E-01
	0.100195E-02	0.500000E-01
	0.791016E-03	0.659000E-01
	0.142383E-02	0.819000E-01
	0.210937E-02	0.203600
	0.263672E-02	0.164100
	0.274219E-02	0.156800
	0.158203E-02	0.994000E-01
	0.491484E-03	0.390000E-02
	0.527344E-03	0.678000E-01
	0.263672E-02	0.111400
	0.949219E-03	0.840000E-02
	8426.95*	0.207700
24	0.647578E-02	0.198600
	0.429258E-02	0.147800
	0.335391E-02	0.111600
	0.298477E-02	0.815000E-01
	0.273164E-02	0.544000E-01
	0.125508E-02	0.355000E-01
	0.157148E-02	0.221000E-01
	0.155039E-02	0.730000E-02
	8416.41*	0.229000
25	0.491484E-03	0.680000E-02
	0.949219E-03	0.890000E-02
	0.126563E-02	0.139000E-01
	0.137109E-02	0.198000E-01
	0.158203E-02	0.249000E-01
	0.189844E-02	0.308000E-01
	0.195117E-02	0.640000E-01
	0.245742E-02	0.151100
	0.263672E-02	0.160600
	8426.95*	0.202500
26	0.316406E-03	0.209000E-01
	0.345938E-03	0.271000E-01
	0.348047E-03	0.388000E-01
	0.596953E-03	0.579000E-01
	0.843750E-03	0.113000
	0.137109E-02	0.129500
	0.864844E-03	0.979000E-01
	0.696094E-03	0.717000E-01
	32262.9*	0.190000
27	0.237305E-02	0.434000E-01
	0.369141E-02	0.544000E-01
	0.949219E-03	0.177000E-01
	0.105469E-02	0.104000E-01
	40500.0*	0.600000E-01
28	0.119180E-02	0.203000E-01
	0.667617E-02	0.169500
	0.116016E-02	0.330000E-01
	0.105469E-02	0.737000E-01
	0.147656E-02	0.498000E-01
	9481.64*	0.240000
29	0.864844E-03	0.149000E-01
	0.152930E-02	0.314000E-01
	0.158203E-02	0.672000E-01
	0.168750E-02	0.785000E-01
	0.200391E-02	0.901000E-01
	0.237305E-02	0.157600
	0.527344E-03	0.450000E-02
	0.116016E-02	0.960000E-02
	0.175078E-02	0.125800
	9481.64*	0.162700
30	0.500977E-03	0.760000E-02
	0.464062E-03	0.120000E-01
	0.527344E-03	0.286000E-01
	0.606445E-03	0.397000E-01
	0.843750E-03	0.487000E-01
	0.149766E-02	0.120600
	0.210937E-02	0.110500
	0.158203E-02	0.533000E-01
	0.949219E-03	0.648000E-01
	0.237305E-02	0.831000E-01
	9471.09*	0.144300

* t (flt hrs)

spec. (#)	da/dt (in/flt hr)	a (in)
31	0.122344E-02	0.227000E-01
	0.101883E-02	0.318000E-01
	0.158203E-02	0.454000E-01
	0.200391E-02	0.767000E-01
	0.232031E-02	0.885000E-01
	9481.64 *	0.180000
32	0.590625E-03	0.113000E-01
	0.984023E-03	0.203000E-01
	0.611719E-03	0.379000E-01
	0.152930E-02	0.448000E-01
	0.147656E-02	0.100600
	0.179297E-02	0.552000E-01
	9479.53 *	0.170000
33	0.738281E-03	0.156000E-01
	0.896484E-03	0.351000E-01
	0.791016E-03	0.417000E-01
	0.843750E-03	0.640000E-01
	0.263672E-02	0.863000E-01
	0.369141E-03	0.114000E-01
	0.580078E-03	0.775000E-01
	0.131836E-02	0.950000E-01
	0.210937E-02	0.111000
	0.791016E-03	0.588000E-01
	10536.3 *	0.126700
34	0.794180E-02	0.138500
	0.227812E-02	0.908000E-01
	0.215156E-02	0.698000E-01
	0.152930E-02	0.523000E-01
	0.156094E-02	0.377000E-01
	0.706641E-03	0.269000E-01
	0.601172E-03	0.207000E-01
	0.442969E-03	0.158000E-01
	0.675000E-03	0.105000E-01
	0.769922E-03	0.360000E-02
	10525.8 *	0.175400
35	0.500977E-03	0.360000E-02
	0.118125E-02	0.128000E-01
	0.274219E-02	0.756000E-01
	0.395508E-02	0.137400
	11588.9 *	0.220000

* t (flt hrs)

spec. (#)	da/dt (in/flt hr)	a (in)
36	0.224648E-02	0.115200
	0.183516E-02	0.960000E-01
	0.210937E-02	0.773000E-01
	0.174023E-02	0.590000E-01
	0.106523E-02	0.457000E-01
	0.113906E-02	0.353000E-01
	0.938672E-03	0.254000E-01
	0.116016E-03	0.155000E-01
	11591.0 *	0.125800
37	0.907031E-02	0.210600
	0.324844E-02	0.152600
	0.295313E-02	0.123200
	0.249961E-02	0.973000E-01
	0.222539E-02	0.749000E-01
	0.101250E-02	0.596000E-01
	0.119180E-02	0.491000E-01
	0.843750E-03	0.395000E-01
	0.138164E-02	0.289000E-01
	0.854297E-03	0.183000E-01
	0.150820E-02	0.710000E-02
	11591.0 *	0.253200
38	0.653906E-03	0.170000E-01
	0.643359E-03	0.231000E-01
	0.949219E-03	0.890000E-01
	0.117070E-02	0.102300
	0.351211E-03	0.870000E-02
	0.685547E-03	0.237000E-01
	0.168750E-02	0.129400
	0.949219E-03	0.401000E-01
	15493.4 *	0.288100
39	0.119180E-01	0.305700
	0.279492E-02	0.236200
	0.292148E-02	0.209100
	0.288984E-02	0.181600
	0.400781E-02	0.148900
	0.165586E-02	0.122000
	0.160312E-02	0.106600
	0.112852E-02	0.936000E-01
	0.801562E-03	0.845000E-01
	0.126563E-02	0.747000E-01
	0.108633E-02	0.635000E-01
	0.153984E-02	0.511000E-01
	0.151875E-02	0.366000E-01
	0.116016E-02	0.239000E-01
	0.780469E-03	0.147000E-01
	0.116016E-02	0.550000E-02
	17708.2 *	0.361900

spec. (#)	da/dt (in/flt hr)	a (in)
40	0.413437E-02	0.220900
	0.397617E-02	0.182400
	0.271055E-02	0.150700
	0.210937E-02	0.127900
	0.175078E-02	0.102900
	0.186680E-02	0.791000E-01
	0.142383E-02	0.635000E-01
	0.114961E-02	0.513000E-01
	18762.9 *	0.240500
41	0.448242E-03	0.251000E-01
	0.421875E-03	0.307000E-01
	0.400781E-03	0.373000E-01
	0.474609E-03	0.521000E-01
	0.685547E-03	0.602000E-01
	0.949219E-03	0.108900
	0.168750E-02	0.118600
	0.184570E-02	0.126600
	0.158203E-02	0.132900
	0.126563E-02	0.723000E-01
	19712.1*	0.199500
42	0.179297E-03	0.390000E-02
	0.527344E-03	0.234000E-01
	0.400781E-03	0.980000E-02
	0.769922E-03	0.334000E-01
	0.878555E-03	0.496000E-01
	0.105469E-02	0.586000E-01
	0.527344E-03	0.728000E-01
	0.491484E-02	0.162100
	0.245742E-02	0.184400
	0.280547E-02	0.215700
	0.896484E-03	0.109200
	0.791016E-03	0.826000E-01
	0.168750E-02	0.132500
	20862.0 *	0.232000
43	0.217266E-02	0.144000
	0.780469E-03	0.130100
	0.959766E-03	0.121800
	0.685547E-03	0.114000
	0.864844E-03	0.106700
	0.885937E-03	0.984000E-01
	0.864844E-03	0.901000E-01
	0.210937E-02	0.777000E-01
	0.101250E-02	0.647000E-01
	0.748828E-03	0.563000E-01
	0.938672E-03	0.483000E-01
	0.706641E-03	0.347000E-01
	0.611719E-03	0.410000E-01
	0.611719E-03	0.285000E-01
	20872.3*	0.154200
44	0.659180E-02	0.140400
	0.171914E-02	0.101000
	0.843750E-03	0.888000E-01
	0.100195E-02	0.800000E-01
	0.126563E-02	0.693000E-01
	0.109687E-02	0.581000E-01
	0.833203E-03	0.489000E-01
	0.614883E-03	0.397000E-01
	0.991406E-03	0.298000E-01
	0.105469E-02	0.201000E-01
	20882.8 *	0.171700
45	0.491484E-03	0.342000E-01
	0.913359E-02	0.151000E-01
	0.738281E-03	0.824000E-01
	0.110742E-02	0.120800
	0.221484E-02	0.240300
	0.225703E-02	0.250800
	0.197227E-02	0.239100
	0.147656E-02	0.133400
	0.949219E-03	0.114900
	0.632813E-03	0.978000E-01
	0.400781E-03	0.445000E-01
	22654.7 *	0.253200
46	0.227813E-03	0.690000E-02
	0.369141E-03	0.233000E-01
	0.438750E-03	0.372000E-01
	0.456680E-03	0.459000E-01
	0.843750E-03	0.105500
	0.170859E-02	0.201500
	0.263672E-02	0.243100
	0.210937E-02	0.234100
	0.274219E-02	0.186600
	0.667617E-03	0.883000E-01
	0.474609E-03	0.717000E-01
	26135.2*	0.372400

* t (flt hrs)

spec. (#)	da/dt (in/flt hr)	a (in)
47	0.421875E-03	0.426000E-01
	0.158203E-02	0.593000E-01
	0.411328E-03	0.333000E-01
	0.495703E-03	0.531000E-01
	0.158203E-02	0.755000E-01
	0.601172E-03	0.184000E-01
	0.843750E-03	0.128900
	26145.7 *	0.230000
48	0.305859E-03	0.257000E-01
	0.305859E-03	0.231000E-01
	0.305859E-03	0.202000E-01
	0.189844E-03	0.170000E-01
	0.295312E-03	0.141000E-01
	0.232031E-03	0.116000E-01
	0.263672E-03	0.800000E-02
	30997.3 *	0.269000E-01

* t
(flt hrs)

CAST TEST ELEMENTS
GAR Spectrum
28 ksi Max. Spectrum Stress
Data Set CGAR 28

spec. (#)	da/dt (in/flt hr)	a (in)
1	6350.00 *	0.210000
2	7025.00 *	0.260000
3	7723.00 *	0.310000
4	8723.00 *	0.140000
5	9780.00 *	0.265000
6	0.450000E-05	0.141000E-01
	0.600000E-05	0.193000E-01
	0.105000E-04	0.113100
	0.102000E-04	0.637000E-01
	0.155000E-04	0.979000E-01
	0.190000E-04	0.161300
	0.280000E-04	0.198200
	0.162000E-04	0.123500
	10039.0 *	0.290000
7	10780.0 *	0.300000
8	10847.0 *	0.200000
9	0.230000E-05	0.126000E-01
	0.330000E-05	0.178000E-01
	0.475000E-05	0.225000E-01
	0.550000E-05	0.249000E-01
	0.700000E-05	0.348000E-01
	0.116000E-05	0.750000E-02
	0.350000E-05	0.326000E-01
	0.120000E-04	0.470000E-01
	0.105000E-04	0.541000E-01
	0.105000E-04	0.179500
	11471.0 *	0.250000
10	12780.0 *	0.250000

* t (flt hrs)

CAST TEST ELEMENTS
GAR Spectrum
34 ksi Max. Spectrum Stress
Data Set CGAR 34

spec. (#)	da/dt (in/flt hr)	a (in)
1	1063.10 *	0.235000
2	0.831000E-03	0.209000
	0.391000E-03	0.155000
	0.372000E-03	0.118000
	1281.80 *	0.200000
3	1352.60 *	0.190000
4	1749.60*	0.100000
5	0.117000E-04	0.510000E-02
	0.316000E-04	0.457000E-01
	0.970000E-04	0.891000E-01
	0.112000E-04	0.295000E-01
	0.102000E-03	0.654000E-01
	1934.30 *	0.175000
6	0.146000E-04	0.340000E-01
	0.470000E-04	0.754000E-01
	0.110000E-04	0.226000E-01
	0.180000E-04	0.345000E-01
	1934.00*	0.130000
7	2063.10*	0.220000
8	0.132000E-04	0.700000E-02
	0.130000E-04	0.123000E-01
	0.290000E-04	0.237000E-01
	0.123000E-04	0.320000E-02
	0.916000E-05	0.117000E-01
	2471.00 *	0.190000

spec. (#)	da/dt (in/flt hr)	a (in)
9	0.132000E-04	0.222000E-01
	0.143000E-04	0.302000E-01
	0.430000E-04	0.431000E-01
	0.540000E-04	0.723000E-01
	0.120000E-04	0.204000E-01
	2655.00*	0.200000
10	2736.00 *	0.100000
11	0.225000E-04	0.278000E-01
	0.340000E-04	0.488000E-01
	0.820000E-05	0.295000E-01
	0.373000E-04	0.634000E-01
	2749.00 *	0.140000
12	0.140000E-05	0.120000E-02
	0.180000E-04	0.670000E-02
	0.353000E-04	0.264000E-01
	0.306000E-04	0.307000E-01
	0.387000E-04	0.353000E-01
	0.250000E-04	0.405000E-01
	2999.00 *	0.190000
13	3063.00 *	0.320000
14	0.380000E-05	0.260000E-02
	0.425000E-05	0.520000E-02
	0.625000E-05	0.890000E-02
	0.900000E-05	0.173000E-01
	4000.00 *	0.700000E-01

* t
(flt hrs)

spec. (#)	t (flt hrs)	a (in)
15	0.500000E-05	0.142000E-01
	0.485000E-05	0.239000E-01
	0.200000E-05	0.411000E-01
	4000.00 *	0.120000
16	0.560000E-05	0.111000E-01
	0.153000E-04	0.218000E-01
	0.250000E-04	0.719000E-01
	0.148000E-04	0.258000E-01
	0.306000E-04	0.431000E-01
	0.600000E-04	0.132000
	4471.00 *	0.170000
17	4780.00 *	0.130000
18	0.633000E-05	0.118000E-01
	0.933000E-05	0.254000E-01
	0.145000E-04	0.370000E-01
	0.177000E-04	0.449000E-01
	0.310000E-04	0.862000E-01
	5185.00 *	0.250000
19	0.147000E-04	0.242000E-01
	0.172000E-04	0.436000E-01
	0.367000E-04	0.778000E-01
	0.957000E-05	0.610000E-02
	0.500000E-05	0.330000E-02
	0.281000E-04	0.763000E-01
	0.390000E-04	0.110400
	0.425000E-05	0.840000E-02
	5934.00 *	0.200000
20	0.875000E-05	0.311000E-01
	0.136000E-04	0.452000E-01
	0.100000E-04	0.294000E-01
	0.366000E-05	0.550000E-02
	0.151000E-04	0.524000E-01
	0.200000E-04	0.770000E-01
	0.340000E-04	0.142500
	0.140000E-04	0.937000E-01
	6749.00 *	0.250000

* t (flt hrs)

APPENDIX C

FAILURE TIME, CRACK GROWTH RATE, AND MICROSTRUCTURE OF A357 ALUMINUM CASTINGS

Figure 56 in Section 3.5 shows a very large scatter in failure time for A357 aluminum castings compared to the other joining concepts under identical test conditions. As discussed in Section 3.1.3, the earliest failures were related to defects very near the drilled hole which acted as a crack starter. However, we did not get a very strong correlation to casting defects seen on the fracture surface, since there were some specimens with many defects which had long fatigue lives, while other test elements failed relatively quickly with no apparent reason. We therefore undertook a small investigation to see if there might be any other factors which could help to explain the large scatter in failure times, especially to explain the early failures.

Data from the CB130 set of specimens (50 castings) are plotted in Figure C1. Data are plotted on a Weibull probability scale with circled points representing three specimens which failed relatively early (specimen numbers 110, 134 and 147) and three specimens which failed relatively late (specimens 5, 16 and 117). Shown in Figure C2 are the crack growth rates of these same six test elements, with the "early" failures plotted as circles and the "late" failures plotted as triangles. It is easy to see that the sampled test elements which took a long time to fail also had lower spectrum crack growth rates - as much as one order of magnitude at the smaller crack sizes. We conclude the natural scatter in crack growth rate in the A357 cast aluminum specimens might have been at least partially responsible for the scatter in total failure time.

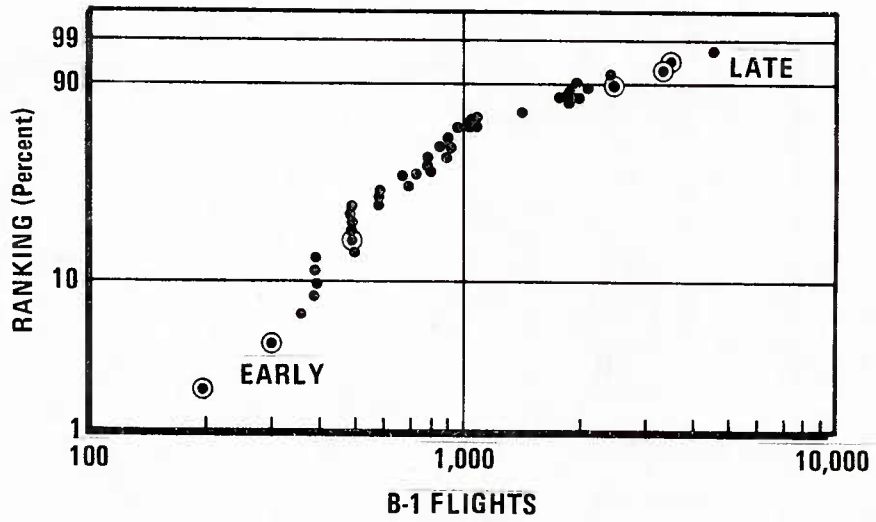

Figure C1 Weibull Failure Distribution for CB130 A357 Cast Test Elements

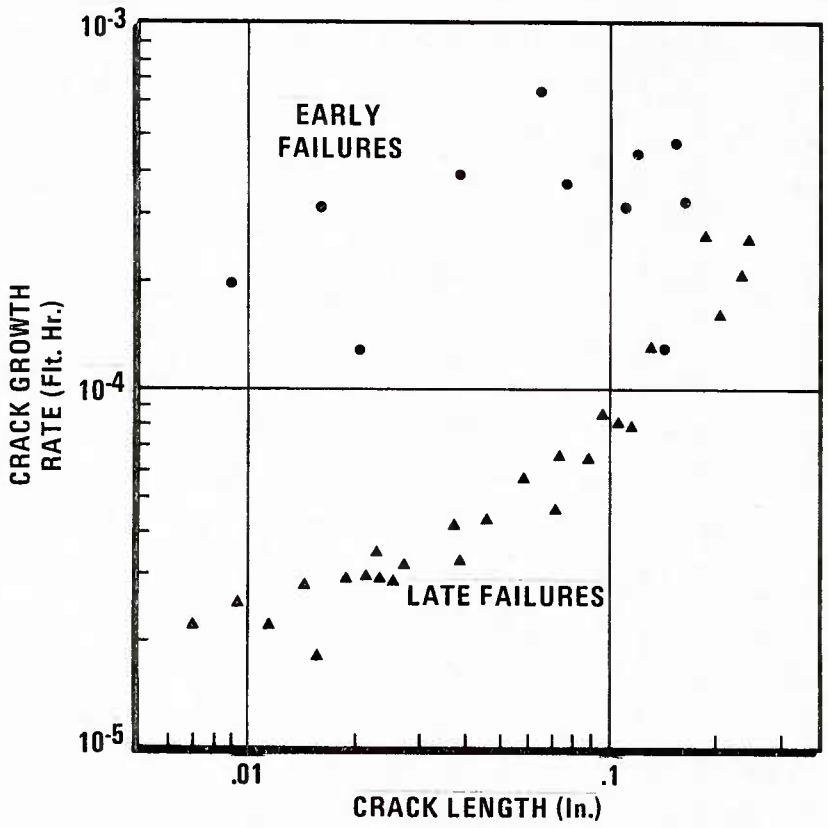

Figure C2 Spectrum Crack Growth Rate Comparison of "Early" and "Late" A357 Failures

Researchers at Boeing have used computer automated image analysis of micrographs to predict ductility in A357 castings, during performance of Contract F33615-80-3209, "Manufacturing Methodology Improvement for Casting Ductility." Ductility of A357 casting was found in that program to depend on yield strength or hardness, and microstructural features such as dendrite cell size or area, percentage of porosity, and aspect ratio (length to breadth) of the silicon eutectic particles outlining the dendrite cells. Samples of each of the six specimens used in plotting Figure C2 were mounted and polished and sent to Boeing for microstructural analysis. Results are given in Table C1. A plot of the silicon eutectic aspect ratio against failure time is given in Figure C3. It appears there may be an inverse correlation between failure time and the aspect ratio of the hard silicon-rich phase. This could be rationalized by noting that the local stress at the tip of a hard ellipsoidal particle increases as the ratio of major axis to minor axis increases [31]. Therefore we expect the local stresses at the tips of particles to be higher for particles with high aspect ratios for a given applied stress. This could lead to faster crack growth in castings with particles having a high average aspect ratio. We recommend this as a topic for further research.

Table C1 Microstructural Measurements from A357 Cast Aluminum Samples Tested at 30 KSI, NOR 1 Spectrum (CB 130)

Group	Specimen Number	Failure Time (Flt. Hrs)	Dendrite Cell Count (0.0001 In^2)	Particle Aspect Ratio	Porosity (Percent)	Estimated Ductility (Percent)
Early Failures	110	2,094	22.8	1.953	0.270	2.9
	134	3,150	26.4	1.860	0.122	4.7
	147	5,262	24.2	1.854	0.424	2.9
Late Failures	5	26,143	32.4	1.651	0.061	8.0
	16	30,996	25.7	1.672	0.404	3.8
	117	32,260	25.6	1.720	0.337	3.9

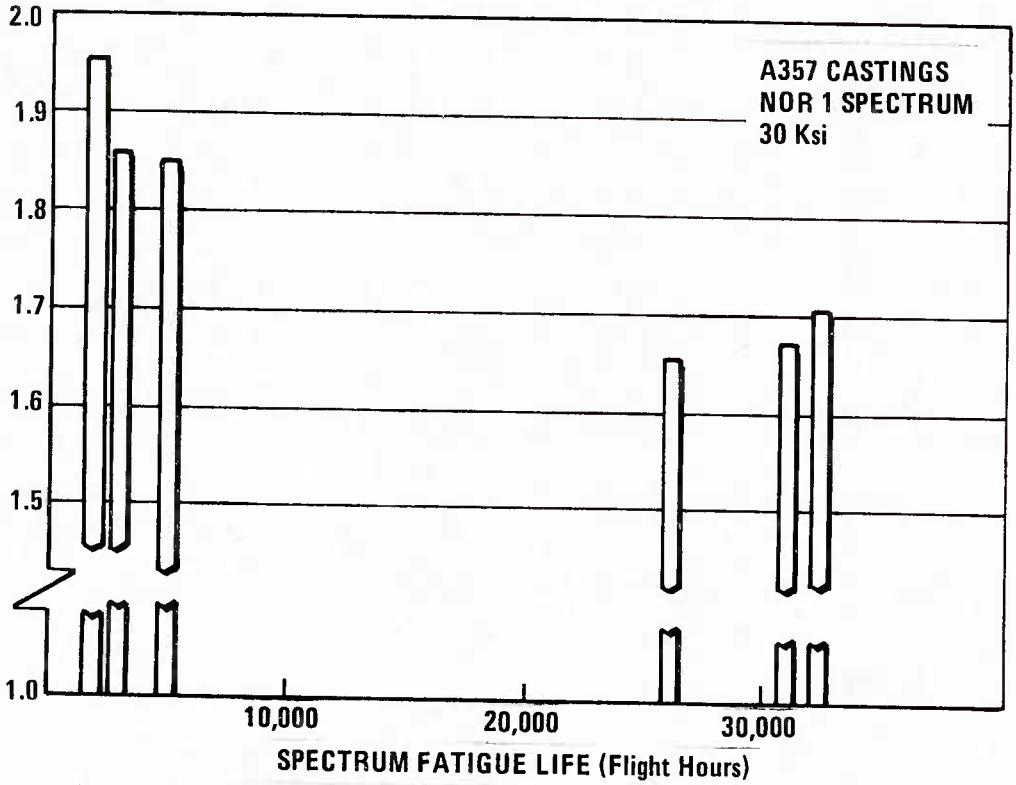

Figure C3 Silicon Particle Aspect Ratio and Failure Times in A357 Samples

LIST OF SYMBOLS

SYMBOL	DESCRIPTION
a	Crack Length
a_o	Crack Length at t = TTCI
a(o)	EIFS
a_{crit}	a(TTF), Critical Crack Size
b	Crack Growth Parameter
c	= b-1
EIFS	Equivalent Initial Flaw Size
$F_{a(o)}(x)$	= P[a(o) < x]
$F_T(t)$	= P[T < t]
FDAS	= Flaw Distribution After Service
i	Subscript Representing an Individual Specimen
I	Subscript Representing an Individual Data Set
IFQ	Initial Fatigue Quality
P[]	Probability
Q	Crack Growth Parameter
Q_i	Q for Specimen Using Pooled b
Q_I	Q Obtained from Pooled Data Set
t	Time
T	A Random Variable Indicating TTCI
TTCI	Time to Crack Initiation
TTF	Time to Failure
x	A Random Variable indicating EIFS

LIST OF SYMBOLS (Continued)

SYMBOL	DESCRIPTION
x_u	Upper bound of EIFS
α	Shape Parameter of TTCI Distribution
β	Scale Parameter of TTCI Distribution
ϵ	Lower Bound of TTCI Distribution
*	Superscript Representing a Pooled Data Set

U219246